博士論文

Source area identification and source estimation of alkenes in the Tokyo Bay coastal area, Japan

東京湾岸地域におけるアルケン発生源地域及び発生源推定

国立大学法人　横浜国立大学大学院

環境情報学府

福﨑　有希子

Yukiko Fukusaki

2021 年 3 月

Table of Content

List of Abbreviations and Acronyms

AMeDAS	Automated Meteorological Data Acquisition System
CPF	Conditional Probability Function
FID	Flame Ionization Detector
GC	Gas Chromatgraphy
JMA	Japan Meteorological Agency
LPG	Liquefied Petroleum Gas
MS	Mass Spectrometer
NMHC	Non-Methane Hydrocarbons
NO	Nitric Oxide
NO_2	Nitrogen Dioxide
NOx	Nitrogen Oxides
Ox	Photochemical Oxidants
PMF	Positive Matrix Factorization
PRTR	Pollutant Release and Transfer Register
TMI	Tokyo Metropolitan Research Institute for Environmental Protection
VOCs	Volatile Organic Compounds
YEI	Yokohama Environmental Science Research Institute

Abstract of thesis

Photochemical smog arises from the accumulation of photochemical oxidants (Ox), the major component of which is ozone (O_3). O_3 also plays a role in climate change as a greenhouse gas. Consequently, short- and long-term O_3 reduction is required both to prevent photochemical smog and to combat climate change. Ox compounds are generated via the photochemical reaction of volatile organic compounds (VOCs) with OH radicals. In the South Kanto region of Japan, previous research has found that aromatics (such as 1,3,5-trimethylbenzene and m,p-xylene) and alkenes (such as ethylene and propylene) significantly contribute to the formation of photochemical reactions. The sources of major aromatics (such as 1,3,5-trimethylbenzene and m,p-xylene) have been clarified by the Pollutant Release and Transfer Register (PRTR) system in Japan. However, the major alkene species are not listed in the PRTR system. This study aims to identify alkene source areas and to estimate the major alkene source in the Tokyo Bay coastal area.

First of all, we categorized the fifty-four days on which photochemical smog warnings were issued in Tokyo, Chiba, Kawasaki, and/or Yokohama into three groups (SS, LSS, and LSW days) and validated VOC-sensitivity in the South Kanto region. Ox levels tended to increase due to increasing NMHC concentrations, suggesting VOC-sensitivity in the South Kanto region. Furthermore, we extracted the atmospheric environmental monitoring stations where NMHC concentrations most frequently exceeded 0.40 ppm C during the fifty-four days under investigation, with the result that the Honmoku, Daishi, Higashikoujiya, and Ichihara stations were identified. These stations were located at or next to major petrochemical industrial facilities in the Tokyo Bay coastal area. Conditional Probability Function (CPF) analysis made clear that the major VOC sources

were found in directions that were to the W, ESE, SE, and WSW of the Honmoku, Daishi, Higashikoujiya, and Ichihara stations, respectively.

Secondly, we tested the validity of the method combining VOC concentration ratios to total VOC concentrations with the prevailing wind direction using a small number of VOC datasets as a means of source area identification. More specifically, VOC concentration ratios according to the 16 wind directions to total VOC concentrations were compared to the distance-weighted emissions using data from the PRTR database. Since VOC concentrations in the Tokyo Bay coastal area are affected by industrial sources, the VOC concentration ratios according to the 16 wind directions are expected to be proportional to emission ratios of these industrial sources according to the 16 wind directions. The results showed a very similar outcome. Since a certain outcome was obtained even with the small number of samples, it appears that VOC concentrations in the Tokyo Bay coastal area were affected by local industrial sources and wind direction. From this result, it is demonstrated that the method of using VOC concentration ratios (according to the 16 wind directions to total VOC concentrations) was useful for VOC source area identification. Alkene concentration ratios were calculated according to the 16 wind directions in order to identify alkene source areas. The wind direction with highest alkene concentration ratio agreed with the location of the block with facilities treating 1,3-butadiene at all sampling sites except for the Central Breakwater Landfill Joint Office. From the above result, it seems likely that the main alkene source was located on the same block as the facilities treating 1,3-butadiene.

Finally, the source apportionment of VOCs using positive matrix factorization (PMF) was conducted, and the major alkene sources in the Tokyo Bay coastal area were estimated in

comparison to alkene concentration ratios with factor contributions according to the 16 wind directions. PMF analysis resolved six factors that were identified as liquefied petroleum gas (LPG) + industry, aged air masses, fuel evaporation, the petrochemical industry, aromatics, and solvent usage. The correlation between the contribution for the petrochemical industry and the alkene concentration ratio was 0.95, 0.74, and 0.74 at the Ushioda, Yokohama Port Symbol Tower, and Honmoku sites, respectively. Furthermore, the contribution ratios for the petrochemical industry according to the 16 wind directions were most consistent with the alkene concentration ratios according to the 16 wind directions. This corresponded to the location of petrochemical industrial complex in the Kawasaki coastal area and indicated that the petrochemical industry was the main alkene source in this area. The source contributions showed significant spatial variations across sampling sites. The contribution ratio for the petrochemical industry at each sampling site tended to gradually decrease with increasing distance from the Kawasaki coastal area to the Ushioda (18.9%), Yokohama Port Symbol Tower (16.3%), and Honmoku (16.2%) sites. At the Honmoku site, which is adjacent to petroleum refinery, fuel evaporation was the major source of VOCs. The local LPG + industry effect was overwhelmingly dominant at the Higashikoujiya site. The petrochemical industry was the most significant contributor to ozone production according to a comparison of the OH radical loss rate (L^{OH}) value of the sources. It was estimated that Ox concentrations could be reduced by up to about 30% by controlling emissions from the petrochemical industry. The L^{OH} values for the petrochemical complex in the Kawasaki coastal area and refinery around the Honmoku site were 45 and 3.5, respectively, suggesting that the photochemical reactivity for petrochemical complex was more than 10 times higher than that for refinery. Moreover, considering the main aromatic sources, it was shown that the petrochemical

complex accounted for 67% of the total L^{OH} for the main industrial VOC sources. The above results indicate that it is crucial to control the level of alkenes emitted by the petrochemical industry to effectively reduce levels of photochemical oxidants.

Chapter 1

Introduction

Introduction

1.1 Background and objectives

The accumulation of photochemical oxidants (Ox) causes photochemical smog, which adversely influences human health and vegetation. A major component of photochemical oxidants is ozone. Ozone (O_3) is classified into two types: stratospheric and tropospheric O_3. Stratospheric O_3 exists at the stratosphere 20–50 km above the Earth's surface and plays a role in absorbing harmful ultraviolet rays. On the other hand, tropospheric O_3 exists in the troposphere (0–10 km above the Earth's surface) and not only adversely influences human health but also contributes to climate change as a greenhouse gas. Therefore, short- and long-term O_3 reduction measures are required to combat photochemical smog and climate change. The Japanese government has set environmental standards in order to achieve O_3 reductions. Concerning VOCs, the VOC emission control system was implemented in 2006 because it was expected that the non-issue rate of photochemical smog warnings would increase to about 90% nationwide as a result of reducing VOC emissions by about 30%. Consequently, VOC emissions were reduced by more than 40% nationwide in 2010 compared to 2000. In contrast, Ox environmental standards are not being met. In Yokohama City, Ox did not meet environmental standards at any of the monitoring stations for 30 consecutive years prior to 2019. In recent years, a new Ox indicator has been put forth. The new Ox measure is the moving average value of the 99th percentile value per year of the maximum value (during 8 hours of the day) for the past 3 years, including the current year. It is an indicator to evaluate how the highest concentration levels have shifted over a long period of time, by focusing on days when the Ox concentration was high in given year. Figure 1-1 shows

the year-to-year variation of the new Ox indicator in Yokohama City. The trend is almost flat, although there are some fluctuations.

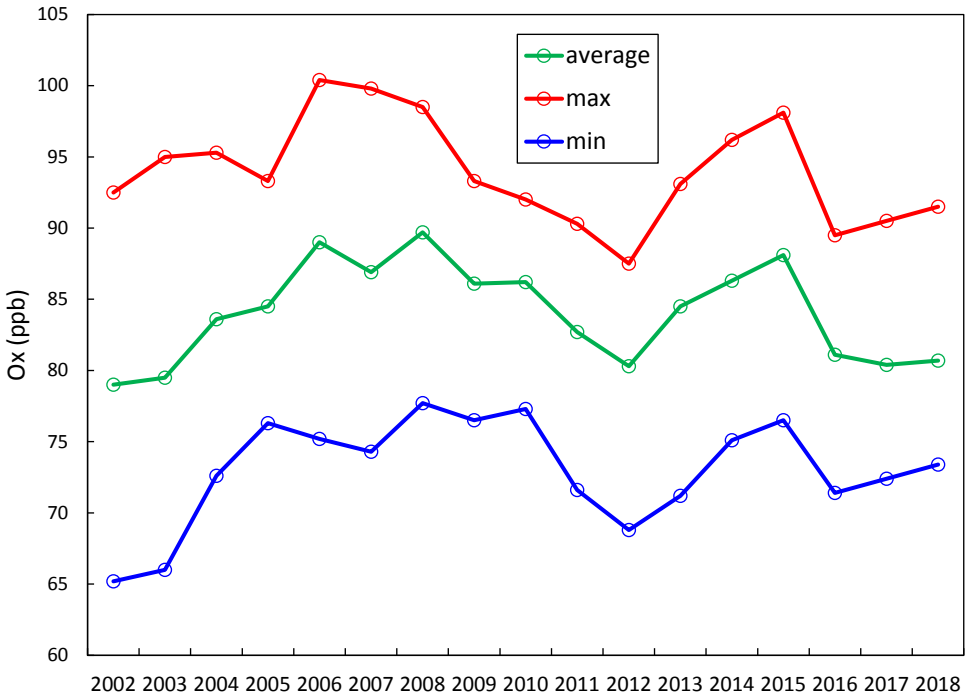

Figure 1-1. Variation of the new Ox indicator.

O_3 is generated via photochemical reactions of VOC and NOx emitted from facilities, vehicles, etc. In general, O_3 levels in air are kept constant due to equilibrium reactions with NO and NO_2 (Figure 1-2).

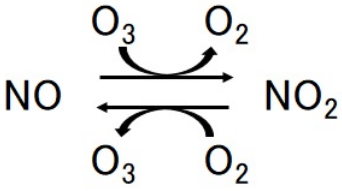

Figure 1-2. Equilibrium reactions with NO and NO_2.

However, in the presence of VOCs, RO_2 radicals (which are formed via the oxidization of VOCs) oxidize NO in place of O_3, whereas O_3 increases via the reverse reaction of NO_2 and O_2. This is the mechanism by which O_3 concentrations increase (Figure 1-3).

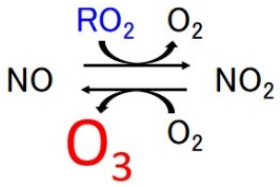

Figure 1-3. Mechanism of increasing O_3 concentrations.

The oxidization of VOCs is initiated by OH radicals, which are regenerated, resulting in a replicating cycle. This reaction cycle is called the HOx (= OH + HO_2) cycle (Figure 1-4).

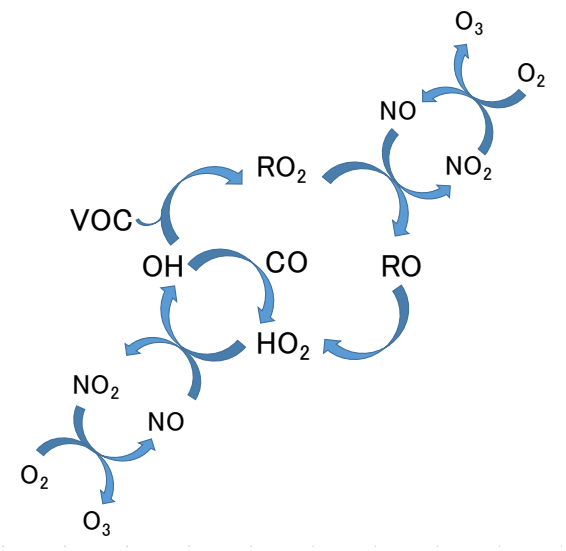

Figure 1-4. The HOx cycle.

It is important to control this reaction in order to suppress O_3 production. However, O_3 concentration is not simply proportional to the concentrations of VOCs and/or NOx, making it complex to control O_3 production. Figure 1-5 shows the HOx cycle including HOx radical loss reaction. Although HOx cycle include other reaction (formation of peroxyacyl nitrates and so on), only HOx cycle shown in Figure 1-5 is considered due to simplification in this study.

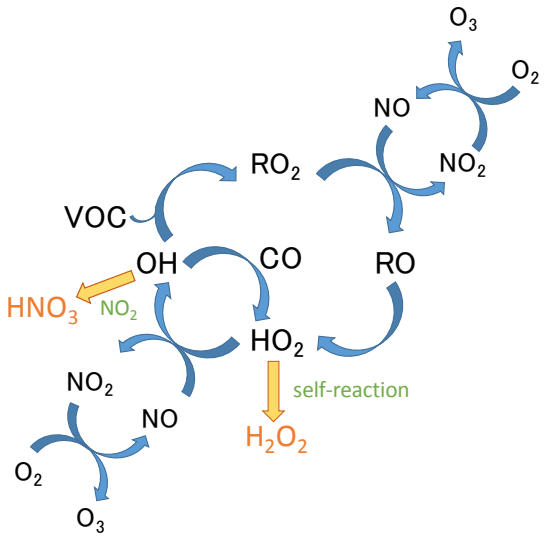

Figure 1-5. The HOx cycle including the HOx loss process.

If the NOx concentration is high, the HOx cycle accelerates, whereas the accompanying loss of the OH radical shortens the lifetimes of the OH radical and NOx. If the NOx concentration is low, the HOx cycle speed is slow, whereas the lifetimes of the OH radical and NOx are extended because the OH radical loss reaction is not facilitated. Therefore, O_3 concentration is not simply proportional to NOx concentration. Which of the two reductions, VOCs versus NOx, is more effective in mitigating the O_3 levels depends on the region. The domain where O_3 concentration declines due to the reduction of NOx is

called NOx-sensitive, whereas the domain where O_3 concentration declines due to the reduction of VOC is called VOC-sensitive. It has been speculated that regulation of VOCs is effective for reducing Ox in metropolitan areas such as Tokyo and Yokohama because of high NOx concentrations. In VOC-sensitive domain, the reaction of VOCs with OH radical is most significant as rate-determining step in HOx cycle.

There are various categories of VOCs such as alkanes, alkenes, aromatics and so on, and each VOC species has different photochemical reactivity. It is important to intensively reduce VOC species with high photochemical reactivity for the effective mitigation of Ox. In Saitama Prefecture, with the highest frequency of photochemical smog warnings, the concentrations of ethylene, propylene, 1-butene, toluene, xylene, and ethylbenzene (all of which are associated with high photochemical reactivity) increased upwind and decreased downwind in the daytime. This suggests that high Ox concentrations downwind were the result of high VOC levels upwind in the daytime when sea breezes blew (Takeuchi et al., 2012).

Ox production is affected by not only precursors such as VOCs and NOx but also by meteorological conditions. In the Kanto region, Ox concentration tends to increase in the summer. It is affected by the sea breeze, which is the dominant summertime meteorological system in this region. The studies focusing attention on days on which the sea breeze developed in Tokyo and its suburban area reported that NMHC and NOx concentrations increased in Tokyo's 23 wards in the early morning before onset of the sea breeze, resulting in increasing Ox levels (Yoshikado, 2015; Yoshikado, 2016).

We conducted VOC investigations at Tokyo and Yokohama in the summer of 2014–2015 in order to identify VOC species that significantly contribute to the photochemical

reaction in the South Kanto region (Fukusaki et al., 2018). The air samples were collected every hour at multiple points moving from the upwind direction to the downwind direction. VOC species that largely contribute to the photochemical reaction were identified by the significant correlation between changes in VOC and Ox concentrations before and after advection of air masses. The results indicated that aromatics (such as xylene and trimethylbenzene) and alkenes (such as ethylene and propylene) most significantly contributed to photochemical reactions in the South Kanto region. It is conceivable that the sources of these species exist in the upwind area or that these species are accumulated in Tokyo Bay by the land breeze at night and/or dawn and then carried to the inland area by the sea breeze during the day. It is crucial to identify the sources of these species to facilitate measures for controlling the Ox production. The major sources of aromatics have been registered in the Pollutant Release and Transfer Register (PRTR) database in Japan; however, major alkene species such as ethylene are not included. The source locations and emission levels of 1,3,5-trimethylbenzene and xylene from the PRTR data are shown in Figure 1-6.

The major sources of aromatic species are the painting industry, especially for ships and vehicles. The emission standard levels of total VOC have been set according to the type and scale of facilities by the Air Pollution Control Act. Furthermore, the emission standard levels for benzene, toluene, xylene, trichloroethylene, tetrachloroethylene, dichloromethane, formaldehyde, and phenol are set by an ordinance in the City of Yokohama. The designated VOC emission facilities which are subject to the Air Pollution Control Act and the ordinance have addressed emission measures such as introducing combustion treatment equipment. However, concerning alkenes, the major sources have

not been identified and it has not been well-known whether the emission measures have been addressed or not.

Previous studies outside of Japan have shown that the major source of alkenes (including ethylene and propylene) was the petrochemical industry (Roberts et al., 2004; Zheng et al., 2020). In aircraft measurements in Houston (Ryerson et al., 2003), alkenes strongly dominated the total OH reactivity, especially with ethylene and propylene constituting >70% of the measured total directly over the source areas. Above the Ship Channel where petrochemical complexes were clustered, the contribution from alkenes was >80%. Moreover, anthropogenic emissions of ethylene and propylene and the aldehyde photoproducts derived from these species dominated initial VOC reactivity of petrochemical plumes for the first 50 km of transport (first 2-3 hours after emission). Because alkenes are rapidly consumed, initial reaction rates of alkenes with OH radicals due to emissions from the facilities significantly affect the rate of O_3 formation and background O_3 levels. Additionally, aldehydes formed by photochemical reaction of alkenes further promote O_3 formation, because aldehydes have high OH reactivity and photolysis of formaldehyde becomes an important free radical source. The Tokyo Bay coastal area is home to 6 of the 15 petrochemical complexes existing in Japan. Therefore, if major sources of alkenes exist in the Tokyo Bay coastal area, it is speculated that the anthropogenic emissions of alkenes significantly contribute to O_3 levels over a wide area of the Kanto region downwind. This study aims to identify the alkene source areas and to determine the major alkene source in the Tokyo Bay coastal area.

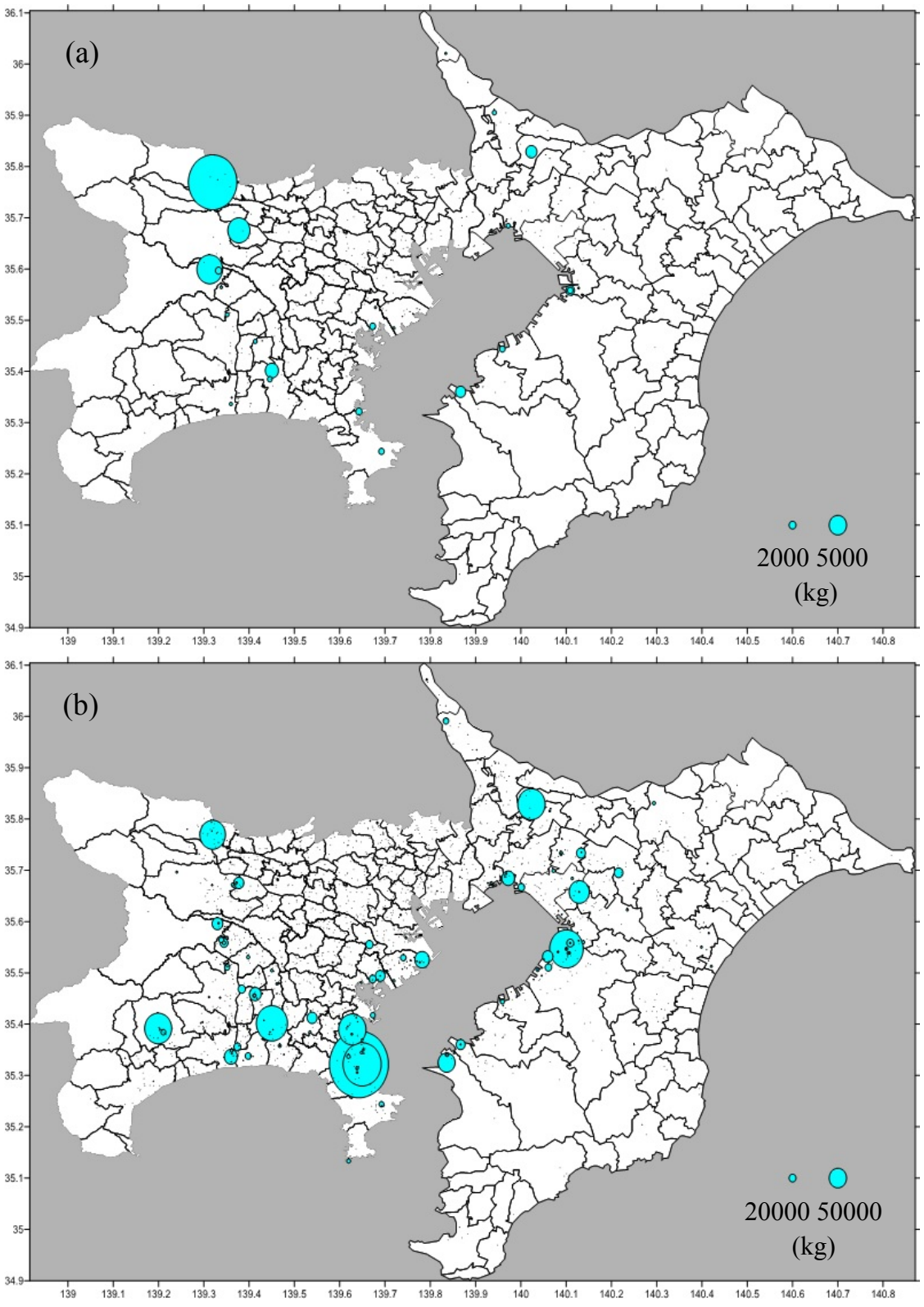

Figure 1-6. The source locations and emissions of (a) 1,3,5-trimethylbenzene and (b) xylene by 2016 PRTR data.

1.2 Composition of thesis

This thesis consists of three chapters which involve: (1) the analysis of high Ox level phenomena in the South Kanto region of Japan, (2) the source area identification of alkenes using alkene concentration ratios according to the 16 wind directions in the Tokyo Bay coastal area, and (3) source estimation of alkenes in the Tokyo Bay coastal area. The goals of the three chapters are as follows: (1) the validation of the VOC-sensitivity in Yokohama and Tokyo and the major source area identification of NMHC, (2) testing the validity of the method combining VOC concentration ratios to total VOC concentration with the prevailing wind direction using a small number of VOC datasets as a means of source area identification and the major source area identification of alkenes, and (3) source estimation of alkenes using positive matrix factorization (PMF) analysis.

First, we classified fifty-four days on which the photochemical smog warnings were issued in Tokyo, Chiba, Kawasaki, and/or Yokohama into three groups (SS, LSS, and LSW days) according to sea-breeze patterns and validated VOC-sensitivity in the South Kanto region. In addition, the atmospheric environmental monitoring stations where NMHC concentrations exceeded 0.40 ppm C were more frequently extracted from all atmospheric environmental monitoring stations in Tokyo, Kanagawa, and Chiba. The locations of major NMHC sources were estimated by Conditional Probability Function (CPF) analysis at these monitoring stations. Secondly, we tested the validity of the method combining VOC concentration ratios to total VOC concentrations according to the 16 wind directions with the prevailing wind direction as a means of source area identification of VOCs, and the major alkene source area was identified. Finally, the source apportionment of VOCs was conducted by PMF analysis, and the major alkene sources

in the Tokyo Bay coastal area were estimated in comparison to alkene concentration ratios with factor contributions according to the 16 wind directions.

References

Fukusaki, Y., Ishikura, A., Hoshi, J., Komori, A., Shimura, T., Ueno, H., 2018. Simultaneous survey of volatile organic compounds in Yokohama and Tokyo in summer. J. Jpn. Soc. Atmos. Environ. 53, 13-24 [in Japanese].

Roberts, P.T., Brown, S.G., Reid, S.B., Buhr, M.P., Funk, T.H., Stiefer, P.S., 2004. Emission Inventory Evaluation and Reconciliation in the Houston-Galveston Area. STI-903640-2490-FR.

Ryerson, T. B., Trainer, M., Angevine, W. M., Brock, C. A., Dissly, R. W., Fehsenfeld, F. C., Frost, G. J., Goldan, P. D., Holloway, J. S., Hubler, G., Jakoubek, R. O., Kuster, W. C., Neuman, J. A., Nicks Jr., D. K., Parrish, D. D., Roberts, J. M., Sueper, D. T., 2003. Effect of petrochemical industrial emissions of reactive alkenes and NOx on tropospheric ozone formation in Houston, Texas. J. Geophy. Res. 108, 1-24.

Takeuchi, T., Matsumoto, R., Karaushi, M., 2012. Characteristics of the regional and temporal concentration variation in volatile organic compounds and relationship with photochemical oxidant in Saitama prefecture. J. Jpn. Soc. Atmos. Environ. 47, 127-134 [in Japanese].

Yoshikado, H., 2015. Summertime behavior of the precursors (non-methane hydrocarbons and nitrogen oxides) related with high concentrations of ozone in the Tokyo metropolitan area. J. Jpn. Soc. Atmos. Environ. 50, 44-51 [in Japanese].

Yoshikado, H., 2016. How much did the VOC emission control executed since 2016 affect the high levels of local ozone formation-details of exclusion of meteorological effect-. J. Jpn. Soc. Atmos. Environ. 51, 230-237 [in Japanese].

Zheng, H., Kong, S., Yan, Y., Chen, N., Yao, L., Liu, X., Wu, F., Cheng, Y., Niu, Z., Zheng, S., Zeng, X., Yan, Q., Wu, J., Zheng, M., Liu, D., Zhao, D., Qi, S., 2020. Compositions, sources and health risks of ambient volatile organic compounds (VOCs) at a petrochemical industrial park along the Yangtze River. Sci. Total. Environ. 703, 135505. https://doi.org/10.1016/j.scitotenv.2019.135505.

Chapter 2

Analysis of high Ox phenomena in the South Kanto region of Japan

Analysis of high Ox phenomena in the South Kanto region of Japan

2.1 Introduction

Photochemical air pollution in the summer in the Kanto region is affected by local sea-land breezes. In the summer, a significant sea breeze is formed in the Kanto region by integrating a heat low originating at Nagano Prefecture with local sea breezes. This massive sea breeze carries air pollutants in the Tokyo Bay coastal area to inland and mountainous areas (Endo et al., 2013). The Ox level gradually rises due to photochemical reactions along with the inflow of air pollutants to the inland area. The formation of a local sea-land breeze is affected by the synoptic scale wind, which depends on pressure patterns. The sea breeze in the Kanto region is roughly categorized into the following two types: southeasterly and southwesterly winds. The southwesterly wind blows if the predominant Pacific high extends from the east of Japan to the south of the Kanto region. The result is that the Ox level does not rise in the South Kanto region because the sea breeze does not penetrate to the inland area, whereas the Ox level rises in the North Kanto region due to inflow of the sea breeze with polluted air masses (Figure 2-1). The southeasterly sea breeze blows if the Pacific high does not prevail. The result is that the Ox level increased in the South Kanto region due to the inflow of the sea breeze with polluted air masses, whereas Ox level does not rise in the North Kanto region because the sea breeze does not penetrate into this region (Figure 2-2).

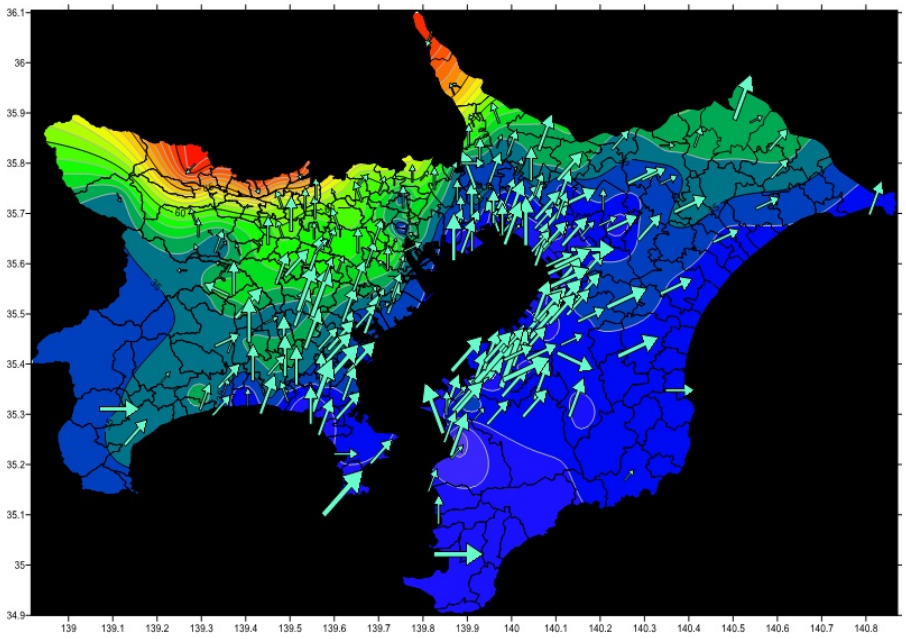

Figure 2-1. Ox concentration distribution and wind vectors under prevailing southwesterly winds (1300 LT, August 30, 2013).

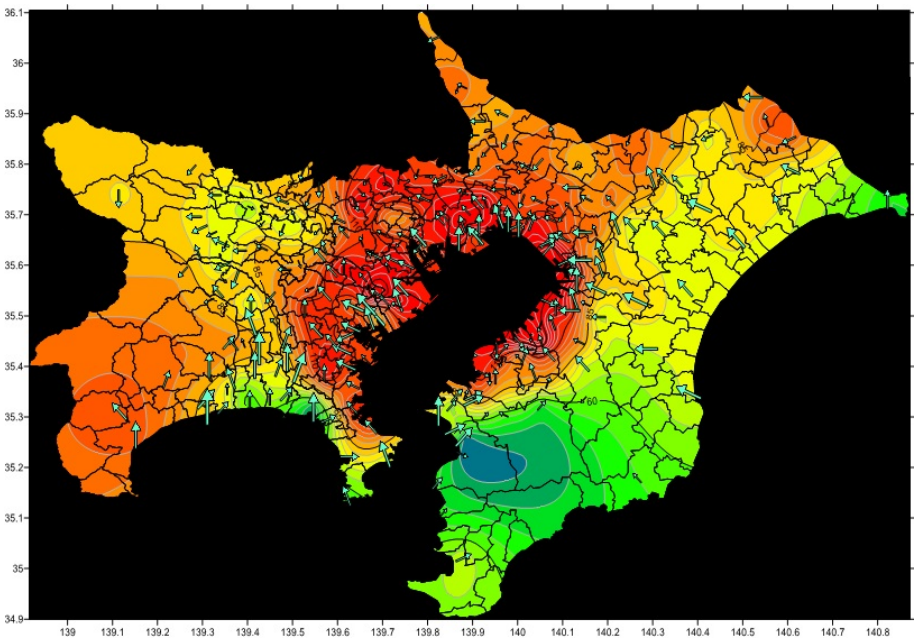

Figure 2-2. Ox concentration distribution and wind vectors under prevailing southeasterly winds (1200 LT, July 26, 2014).

Several studies on high Ox phenomena focusing on meteorological conditions have been performed. Iida (2005) categorized 32 days on which photochemical smog warnings were issued at Tokyo, Chiba, Saitama, and Kanagawa into 8 patterns according to the wind at 850 hPa, with the result that the Ox level exceeded 120 ppb throughout the South Kanto region when the wind direction at 850 hPa was northwest and the Pacific high extended to the southeast or south of the Kanto region. In addition, Inoue (2008) estimated that the appearance of high Ox levels was caused by temperatures exceeding 30°C, formation of an inversion layer, and wind convergence on the ground in Chiba Prefecture in 2008. Yoshikado (2015, 2016) reported that Ox levels increased when NMHC and NOx concentrations increased in Tokyo's 23 wards in the early morning before the onset of the sea breeze. These studies have mainly examined the relationship between meteorological conditions and Ox levels without discussion of NMHC and NOx sources. However, these studies imply that the sea breeze from Tokyo Bay contributes to the Ox level, as the main NMHC and/or NOx sources originate in the Tokyo Bay coastal area. It is speculated that the accumulation of NMHC (due to the development of land-sea breezes and the weak inflow of the sea breeze) causes the photochemical smog in the South Kanto region. In this study, the fifty-four days on which the photochemical smog warnings were issued in Tokyo, Chiba, Kawasaki, and/or Yokohama are categorized into three groups according to the sea-breeze patterns. VOC-sensitivity in the South Kanto region is validated through comparison of the number of hours on which Ox, NMHC and NOx concentration exceeded the criteria, and finally, the location of major NMHC source is estimated by Conditional Probability Function (CPF) analysis for NMHC concentrations at the monitoring stations.

2.2 Methods

The fifty-four days when the photochemical smog warning was issued in Tokyo, Chiba, Kawasaki, and/or Yokohama (during July and August between 2012 and 2015) were the focus of this analysis. The data used for analysis is Ox, NOx, NMHC, wind direction, and wind speed between the fifty-four days at 157 atmospheric environmental monitoring stations in Tokyo, Kanagawa, and Chiba. Automated Meteorological Data Acquisition System (AMeDAS) data from the Japan Meteorological Agency (JMA) for wind direction and wind speed at Tokyo, Nerima, and Yokohama were also employed for classification of sea-breeze days. The atmospheric environmental monitoring stations in Tokyo, Kanagawa, and Chiba were classified into coastal and inland areas in Figure 2-3.

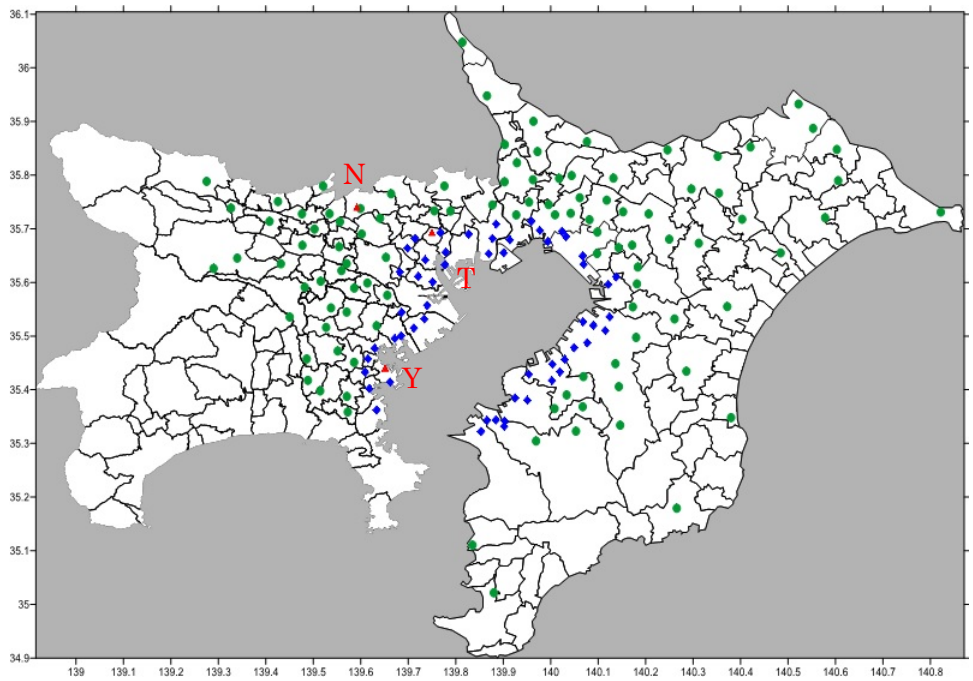

Figure 2-3. The targeted atmospheric environmental monitoring stations (blue (◇): coastal areas, green (○): inland areas); AMeDAS stations (red (△), Y: Yokohama, T: Tokyo, and N: Nerima).

The fifty-four days investigated in this study were classified as days on which the sea breeze developed in Yokohama, Tokyo, and its suburban areas (SE days, below) according to the following conditions for Yokohama and Tokyo: Southeasterly wind during the daytime; wind direction in the hours between 0800 and 1700 LT was E to S, clockwise. The remaining days were classified as days on which southwesterly winds developed in the South Kanto region (SW days, below). Furthermore, SB days was classified as days on which the land-sea breeze developed in Yokohama, Tokyo, and its suburban areas (LS days, below) according to the following conditions for Tokyo:

1) Land breeze or calm at dawn; wind direction between 0400 and 0700 LT was WSW and ENE clockwise, or calm with wind speeds of 1.0 m s^{-1} for 2 consecutive hours.
2) Southeasterly wind during the daytime; wind direction between 0800 and 1700 LT was ESE to SSW clockwise with wind speeds of 2 m s^{-1} or greater for 2 consecutive hours.

The remaining SE days were classified as days on which the prevailing sea breeze developed (SS days, below). Finally, LS days were classified as the days on which the sea breeze easily penetrates to the inland area (LSS days, below) according to the following conditions for Nerima: Southeasterly wind during the daytime; wind direction between 0900 and 1700 LT was ESE to SSW clockwise with wind speeds of 2 m s^{-1} or greater for 2 consecutive hours. The remaining LS days were classified as days without inflow of the sea breeze to the inland area (LSW days, below). LSW days are compared

with SS days primarily in this study.

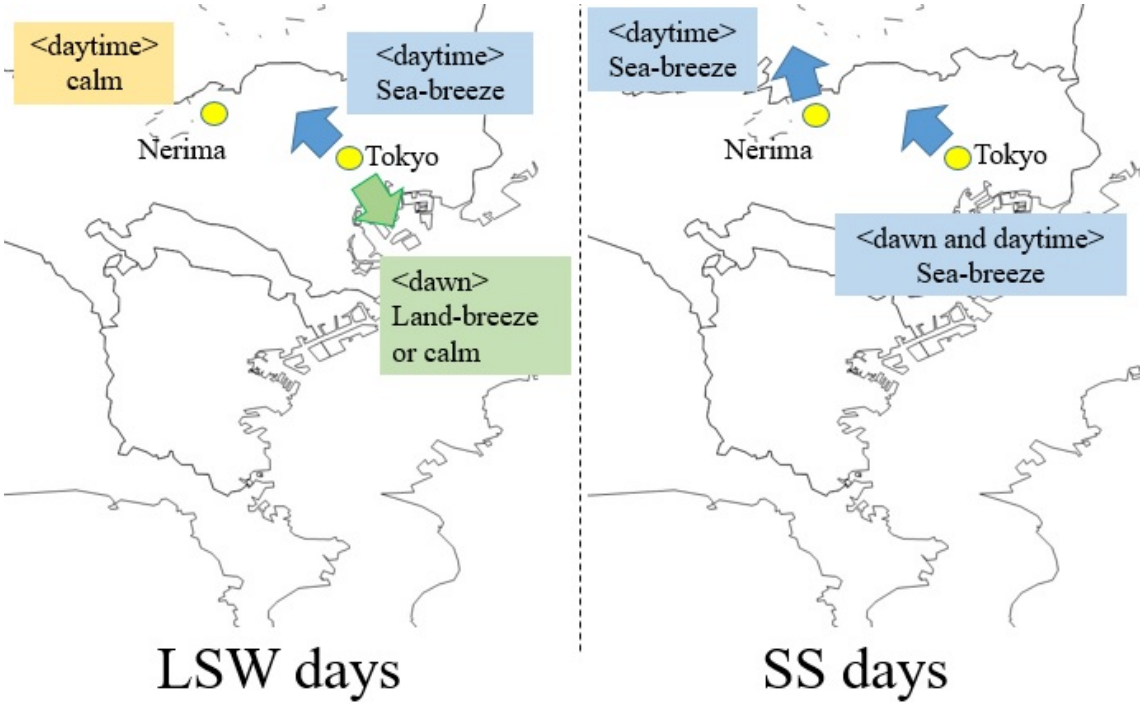

Figure 2-4. Wind direction at Tokyo and Nerima at LSW and SS days.

The number of hours on which the concentrations for Ox, NMHC, and NOx exceed the criteria were compared between eight areas according to the SS, LSS, and LSW days. The criteria for Ox, NMHC, and NOx were set as 120 ppb, 0.40 ppm C, and 60 ppb, respectively. The reason for this is that the hourly standard of the Ox level for the photochemical smog warnings is 120 ppb, and the upper environmental standard for NOx is 60 ppb. The explanation for the NMHC criteria is discussed below in section 2.3.2.1.

In the analysis of NMHC concentration differences, a high Ox day was defined as the days during July and August (between 2012 and 2015) on which Ox concentrations

exceeded 120 ppb at the Yokohama commercial high school and the Tsuzuki ward general government building in the City of Yokohama (both are atmospheric environmental monitoring stations). In contrast, a low Ox day was a day on which the Ox concentration was below 60 ppb. The reason for these criteria is that the hourly standard for the Ox level for the photochemical smog warnings is 120 ppb, while the environmental standard for Ox levels is 60 ppb. The nearly 35,000 data entries for NMHC, wind direction, and wind speed between 2012 and 2015 were employed for CPF analysis at each monitoring station. CPF analysis is the method estimating the location of major source, by dividing the number of hours when NMHC concentration exceeded the criterion to total number of hours, as a following equation:

$$\mathrm{CPF} = {}^{m_{\Delta\theta}}/_{n_{\Delta\theta}}$$

where $m_{\Delta\theta}$ is the number which winds blow from $\Delta\theta$ direction when NMHC concentration exceeded the criterion and $n_{\Delta\theta}$ is total number which winds blow from $\Delta\theta$ direction. The threshold criterion was set as the upper 10th percentile to define the directionality of the sources clearly. Wind direction was split into 16 sectors ($\Delta\theta = 22.5°$).

2.3 Results and discussion

2.3.1 Comparison of Ox, NOx, and NMHC concentrations on each of the SS, LSS, and LSW days

The conditions described in section 2.2 resulted in 10 SS days, 6 LSS days, and 36 LSW days (Figure 2-5).

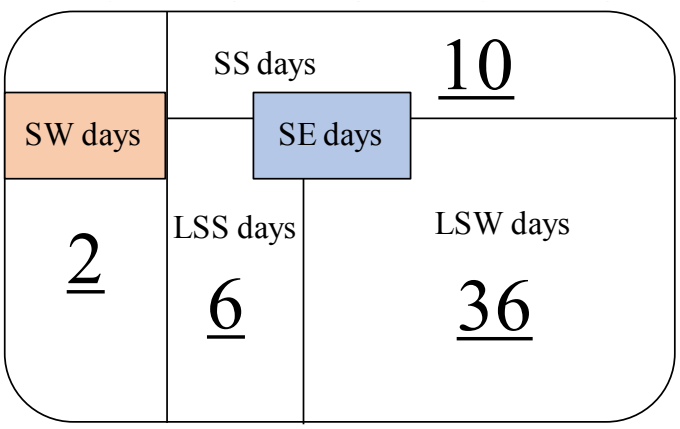

Figure 2-5. Number of days in the groups defined in this study.

This result indicates that the Ox level easily exceeds 120 ppb during the development of the land-sea breeze and the weak inflow of the sea breeze.

Figure 2-6 shows the number of hours during which the concentrations of Ox, NMHC, and NOx exceeded the criteria at each of eight areas for a single monitoring station.

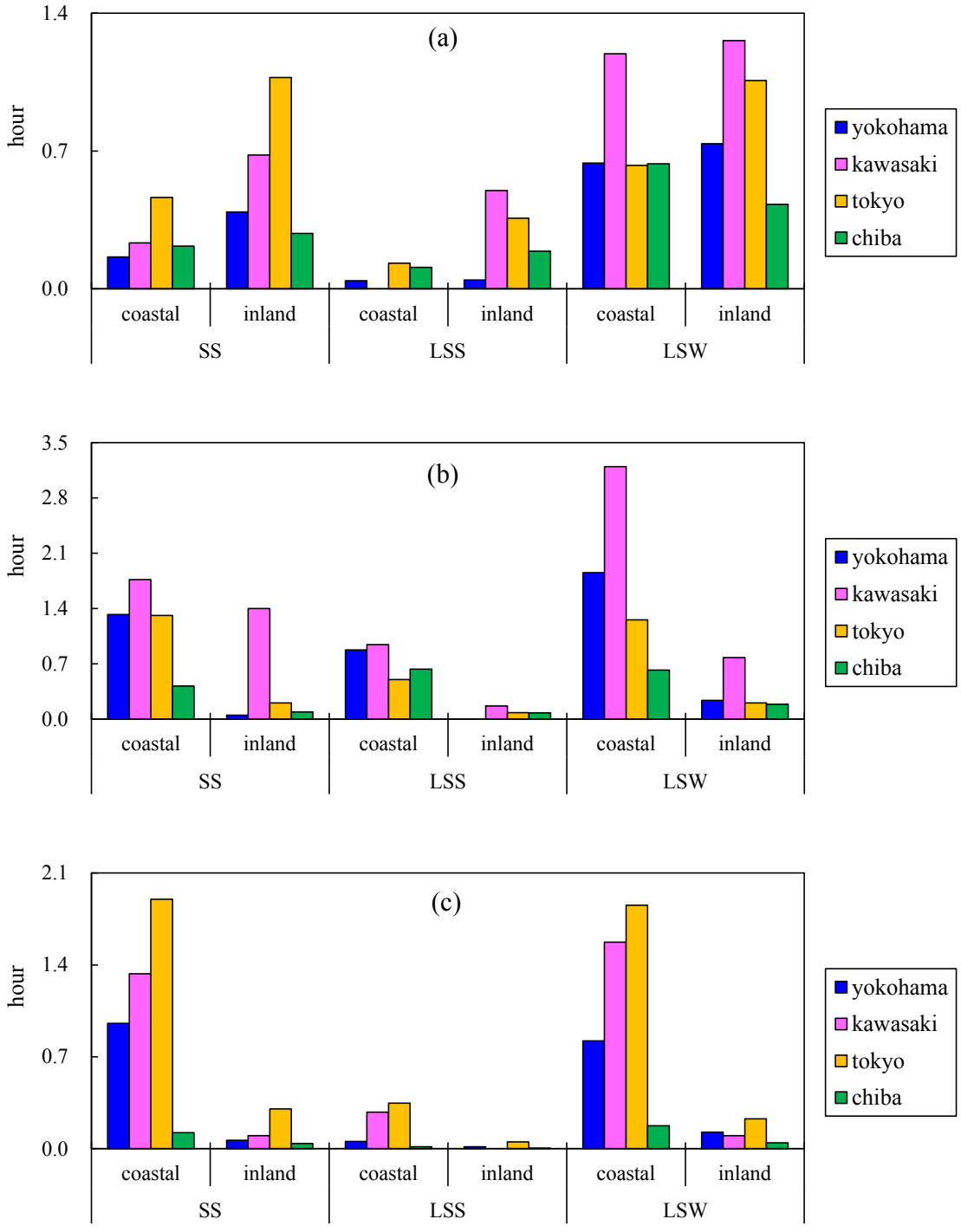

Figure 2-6. The number of hours during which the concentrations of (a) Ox, (b) NMHC, and (c) NOx exceeded the criteria at each of eight areas for a single monitoring station.

The Ox level most frequently exceeded 120 ppb at the Kawasaki inland area on LSW days (1.26 h), followed by the Kawasaki coastal area on LSW days (1.19 h). The NMHC level most frequently exceeded 0.40 ppm C at the Kawasaki coastal area on LSW days (3.19 h), followed by the Yokohama coastal area on LSW days (1.85 h). It was noteworthy that NMHC concentrations increased significantly to 3.19 at the Kawasaki coastal area on LSW days. The NOx level most frequently exceeded 60 ppb at the Tokyo coastal area on SS days (1.90 h), followed by the Tokyo coastal area on LSW days (1.85 h). In comparing SS days with LSW days at all areas excluding the Tokyo area and the Kawasaki inland area, the number of hours for Ox and NMHC on LSW days was higher than on SS days. In Kawasaki inland area, the number of hours for NMHC on SS days was higher than on LSW days. This reason is that NMHC in the inland area on SS days contributed to Ox levels downwind due to the sea-breeze penetrating or was not high photochemical reactivity. On SS and LSS days, the number of hours for Ox in the inland area was higher than that in the coastal area, suggesting that Ox levels tended to rise in the inland area because the sea breeze penetrated to the inland area. The number of hours for NOx on LSW days was nearly equal to that on SS days. This suggests the possibility that the increase in Ox comes from the increase in NMHC as a result of VOC-sensitive processes. The reason for the lack of any difference between LSW and SS days in the Tokyo area is that there are no major NMHC sources in this region.

2.3.2 Characteristics of NMHC concentrations under high Ox levels

2.3.2.1 Determination of criteria for NMHC concentrations

The differences in NMHC concentrations according to Ox levels were examined. The

average NMHC concentrations at six atmospheric environmental monitoring stations located in the Tokyo Bay coastal area (Daiba, Takanawa, Higashikoujiya, Ushioda, Namamugi, and Honmoku) were calculated for high Ox and low Ox days. The average NMHC concentration on high Ox days was 0.30 ppm C, whereas the average NMHC concentration on low Ox days was 0.15 ppm C. It was found that the NMHC concentration on high Ox days was about twice than that on low Ox days. Therefore, 0.40 ppm C was set as the criterion for high NMHC concentration.

2.3.2.2 Extraction of the atmospheric environmental monitoring stations where NMHC concentrations exceeded the criteria more frequently

We extracted the monitoring stations where NMHC concentration exceeded 0.40 ppm C more frequently during the fifty-four days of our study. The distribution of the number of hours on which NMHC concentration exceeded 0.40 ppm C is shown in Figure 2-7.

The top four monitoring stations extracted were Honmoku (202 hours), Daishi (122 hours), Higashikoujiya (318 hours), and Ichihara (175 hours). These monitoring stations accorded quite well with locations of petrochemical industrial facilities (Figure 2-8).

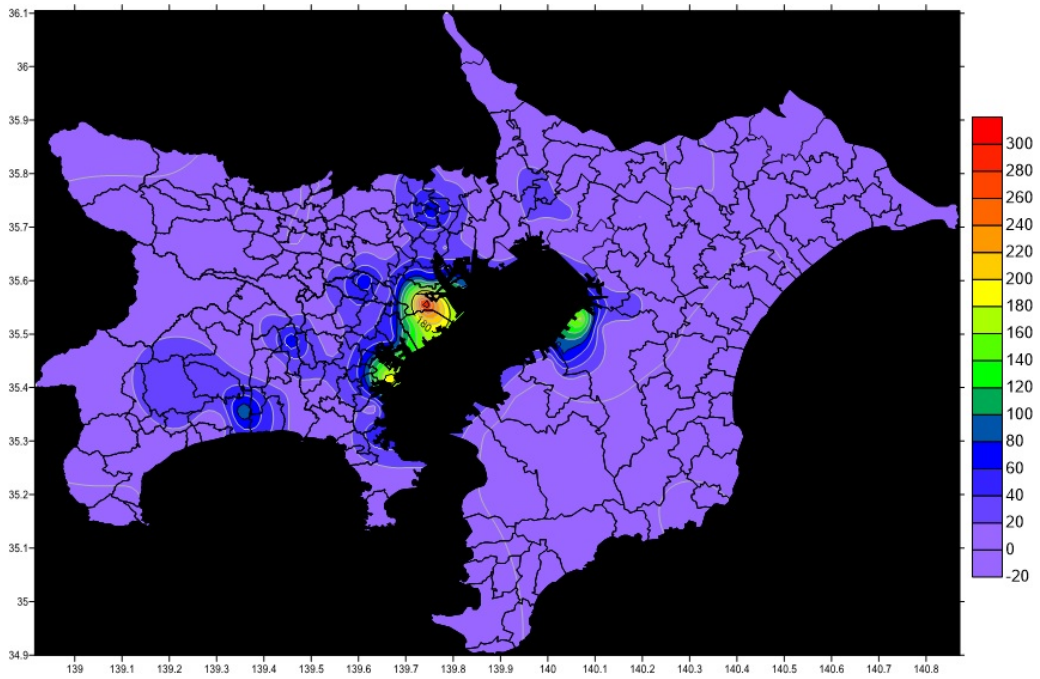

Figure 2-7. Frequency distribution of high NMHC concentration.

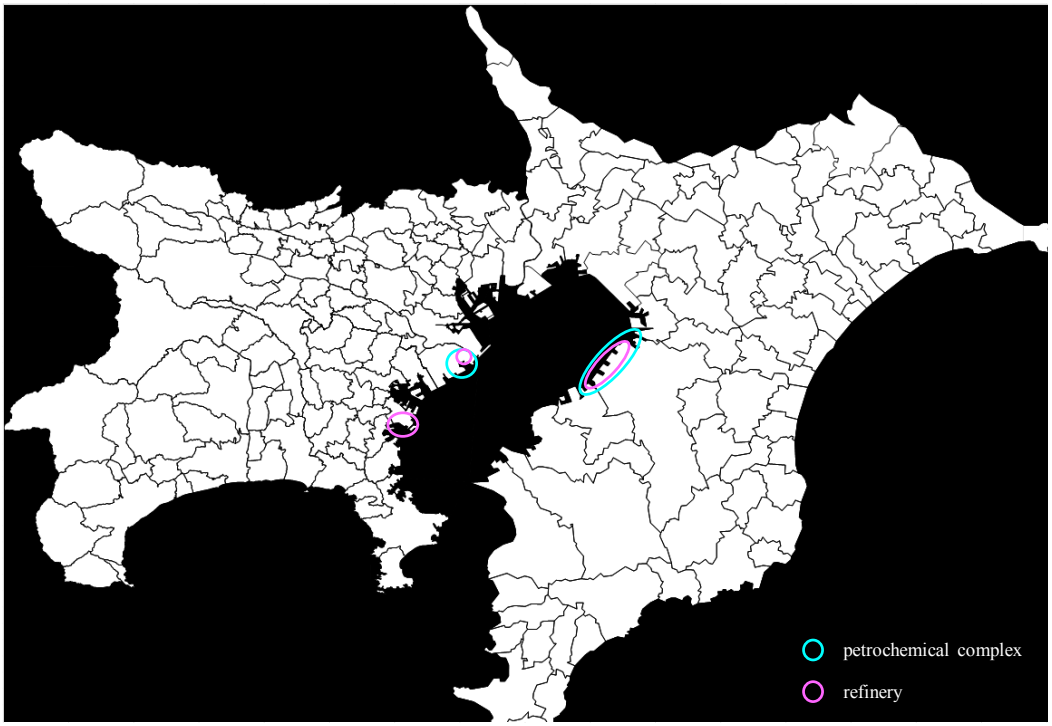

Figure 2-8. Location of petrochemical industrial facilities in the Tokyo Bay coastal area.

The sum (by month) of the number of hours during which NMHC concentrations exceeded the 90th percentile (calculated for ~35,000 data values between 2012 and 2015 for each of the four monitoring stations) is shown in Figure 2-9. It was found that NMHC concentrations are likely to be high in August at Honmoku and Ichihara, whereas in December this is more likely at Daishi and Higashikoujiya.

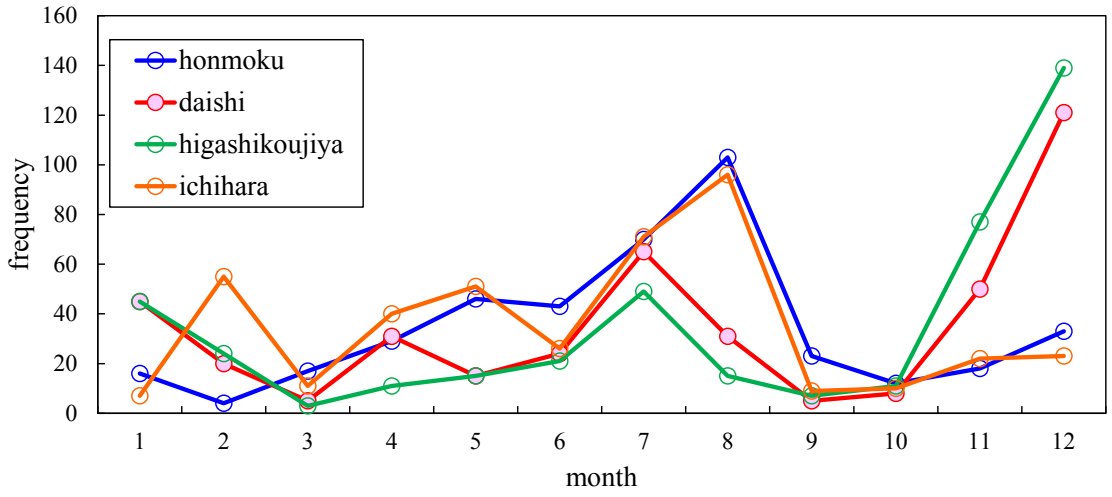

Figure 2-9. Frequency of NMHC concentrations greater than the 90th percentile (monthly).

This is presumably because meteorological conditions such as wind direction and temperature have a strong effect on VOC concentration and composition; the prevailing wind in summer is different from in winter, and volatility depends on temperature. In addition, Honmoku and Daishi show similar variation as well as Ichihara and Higashikoujiya, respectively, suggesting that the source area or source industry is the same for these two regions. There were increases from spring to summer in the number

of hours at Honmoku and Ichihara, and a second peak in July at Daishi and Higashikoujiya. It is speculated that the source emissions that affected VOC concentrations at Honmoku and Ichihara are dependent on temperature. It was further speculated that the sources that affected the first peak at Daishi and Higashikoujiya were different from those that affected the second peak due to the difference in wind direction.

2.3.2.3 VOC source determination by CPF analysis

To determine the major VOC source area, CPF analysis at each of four stations (Honmoku, Daishi, Higashikoujiya, and Ichihara) was conducted. The result is shown in Figure 2-10.

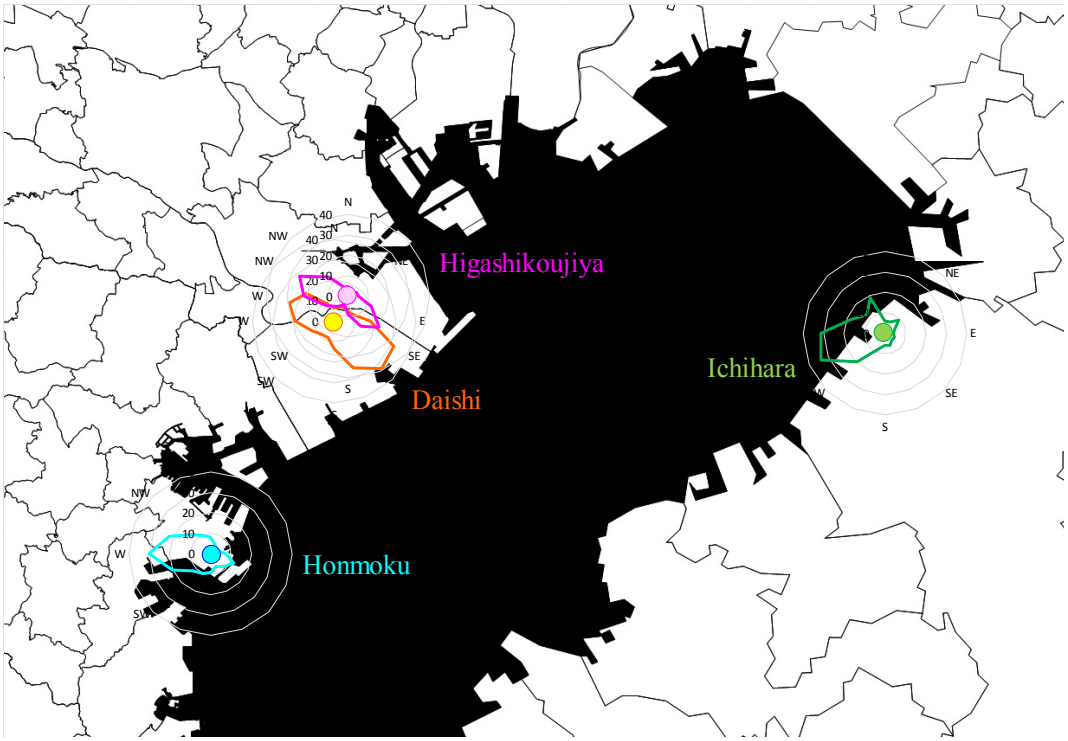

Figure 2-10. CPF results of NMHC at four stations.

The CPF results suggest that the main source originated to the W and WSW of Honmoku and Ichihara, respectively. On the other hand, the results imply that the source was derived from two directions, from the SE and WNW at Daishi and Higashikoujiya. The main source in summer was likely to be different from the main source in winter because the first and second peaks were in December and July, respectively. Consequently, CPF analysis of summer (July) and winter (December) was conducted separately. The result is shown in Table 2-1.

Table 2-1. CPF results for summer and winter (Daishi and Higashikoujiya).

	July	December
Daishi	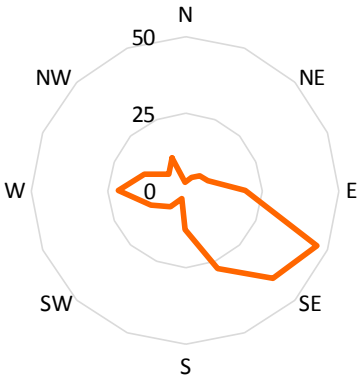	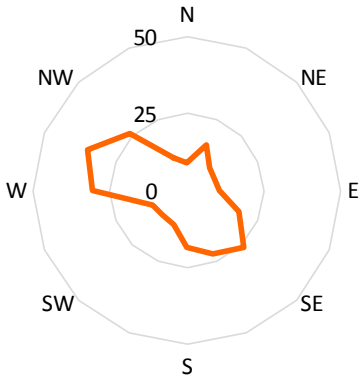
Higashikoujiya	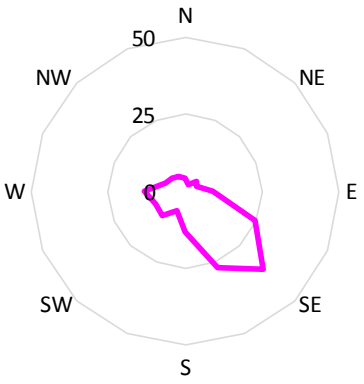	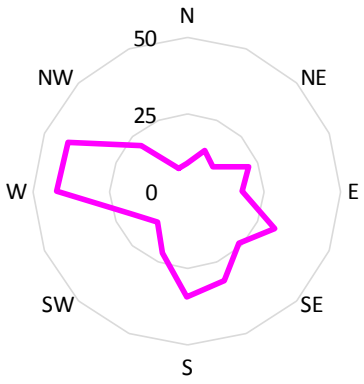

The CPF result in the summer was different from that in the winter. It was presumed that the main source in the summer originated from the ESE and SE at Daishi and Higashikoujiya, respectively. A common source located in the Kawasaki coastal area appears to influence both Daishi and Higashikoujiya in the summer (Figure 2-11).

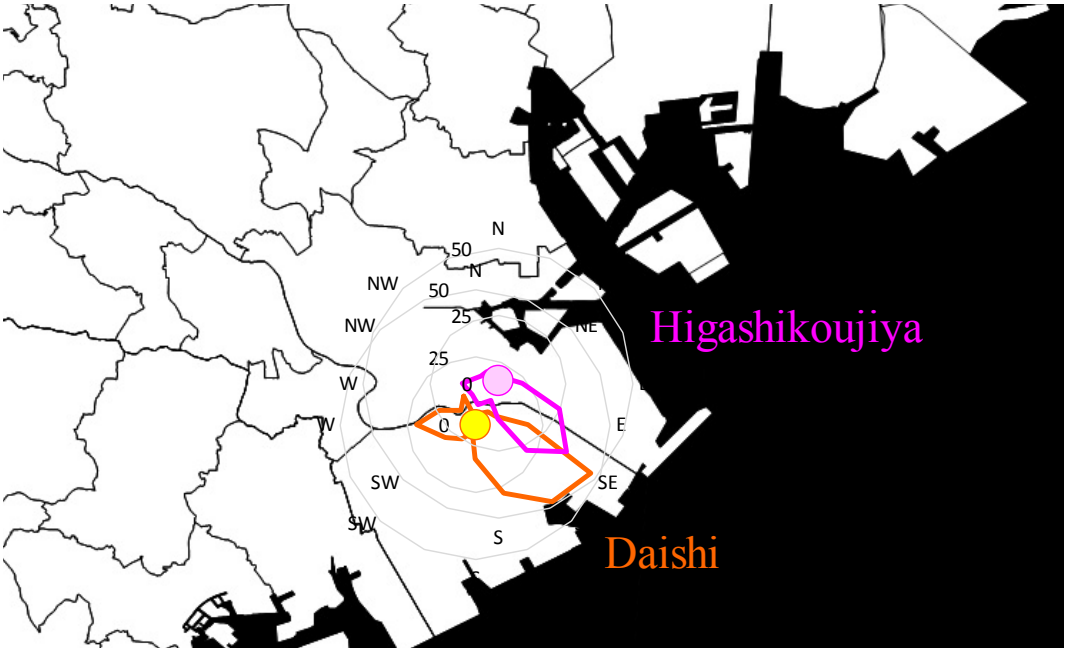

Figure 2-11. CPF results at Daishi and Higashikoujiya in July.

2.4 Conclusions

The fifty-four days on which the photochemical smog warnings were issued in Tokyo, Chiba, Kawasaki, and Yokohama during July and August (between 2012 and 2015) were categorized into three groups (SS, LSS, and LSW days) according to sea-breeze patterns. VOC-sensitivity in the South Kanto region was validated through the comparison of the number of hours on which Ox, NMHC, and NOx concentrations exceeded the criteria,

and finally, the location of major NMHC sources was estimated by Conditional Probability Function (CPF) analysis for NMHC concentrations at the monitoring stations.

The Ox and NMHC levels most frequently exceeded the respective criteria at the Kawasaki inland and coastal areas on LSW days, whereas the NOx level most frequently exceeded 60 ppb at the Tokyo coastal area on SS days. In comparing SS days with LSW days at all of areas (excluding the Tokyo area) the number of hours for Ox and NMHC on LSW days was higher than on SS days. However, NOx was nearly equal on LSW and SS days. This suggests the possibility that the increase in Ox comes from the increase in NMHC. The reason for the lack of difference between LSW and SS days in the Tokyo area is likely due to the lack of major NMHC sources.

The monitoring stations where NMHC concentration exceeded 0.40 ppm C more frequently at high Ox days were the Honmoku, Daishi, Higashikoujiya, and Ichihara stations. The locations of these monitoring stations accorded quite well with the locations of petrochemical industrial facilities in the Tokyo Bay coastal area. The CPF results in the summer implied that the major sources originated from the W, ESE, SE, and WSW directions of Honmoku, Daishi, Higashikoujiya, and Ichihara, respectively.

Based upon the above results, it was estimated that the major VOC sources in the Tokyo Bay coastal area were the Kawasaki and Ichihara coastal areas and around Honmoku. It is crucial to estimate which sources and which VOCs are being discharged and how strong an impact this has on Ox production.

References

Endo, F., Hayasaki, M., Kawamura, R. 2013. Diurnal variation of photochemical oxidants over central Japan during clear summer days and the associated thermally-induced local circulation. J. Jpn. Soc. Atmos. Environ. 48, 234-242 [in Japanese].

Iida, N., 2005. Relation between Formation and Transportation of Photochemical Oxidants High Concentrated Area and Wind at 850 hPa. Kanagawa Environmental Research Center Report. 28, 78-83 [in Japanese].

Inoue, T., 2008. The phenomena of high Ox level in 2008 in Chiba Prefecture. Chiba Environmental Research Center Report. 65-66 [in Japanese].

Yoshikado, H., 2015. Summertime behavior of the precursors (non-methane hydrocarbons and nitrogen oxides) related with high concentrations of ozone in the Tokyo metropolitan area. J. Jpn. Soc. Atmos. Environ. 50, 44-51 [in Japanese].

Yoshikado, H., 2016. How much did the VOC emission control executed since 2016 affect the high levels of local ozone formation-details of exclusion of meteorological effect-. J. Jpn. Soc. Atmos. Environ. 51, 230-237 [in Japanese].

Chapter 3

Source area identification of alkenes using alkene concentration ratios according to the 16 wind directions in the Tokyo Bay coastal area

Publication based on this chapter:

Fukusaki, Y., Kousa, Y., Asaki, M., Kobayashi, Y., Kokubu, Y., Hoshi, J., Sakamoto, H., Goto, A., Shima, M., Nakai, S., 2020. Estimation of Anthropogenic VOC source Area around Tokyo Bay: Results from the VOC Concentration Changes in Relation to Wind Direction. J. Jpn. Atmos. Environ. 55, 92-99.

Source area identification of alkenes using alkene concentration ratios according to the 16 wind directions in the Tokyo Bay coastal area

3.1 Introduction

VOC concentrations in the atmosphere vary under different meteorological conditions (Filella and Penuelas, 2006). Especially, because air pollution has a high correlation with wind direction (Chan et al., 2011; Liu et al., 2016), VOC concentrations and wind direction are both important predictors of air pollution. Chen et al (2019) clarified that the wind direction largely affected VOC concentrations using hourly VOC data for three years in west Taiwan. In addition, Buzcu-Guven and Fraser (2008) reported that the distance-weighted emissions of refineries and petrochemical facilities approximately accorded with CPF results using hourly VOC data at three sites in Houston. CPF analysis using source contribution coupled with wind direction data is extremely useful for determining the association between wind direction and pollution sources (Kim et al., 2003; Xie and Berkowitz, 2006). Although these previous studies validated the relationship between VOC concentration and wind direction using large volume of VOC data, this method could not be applied in this study due to a lack of data. However, there is a chance that combining a small number of high-resolution VOC data at multiple sites with the prevailing wind directions serves as a means to estimate major VOC source areas in the Tokyo Bay coastal area where the industrial sources were intensely clustered. This study aimed at testing the validity of the method combining VOC concentration ratios with the prevailing wind direction using a small number of VOC

datasets obtained in this investigation. This study further aimed to identify major alkene source area using the above method.

3.2 Methodology

3.2.1 Sampling

Figure 3-1 shows five sampling sites (Yokohama Port Symbol Tower, Morigasaki Water Reclamation Center, Central Breakwater Landfill Joint Office, Tokyo Metropolitan Research Institute for Environmental Protection, and Inage Seaside Park) and measurement points of wind direction and wind speed (Higashikoujiya, Daiba, and Masago Park).

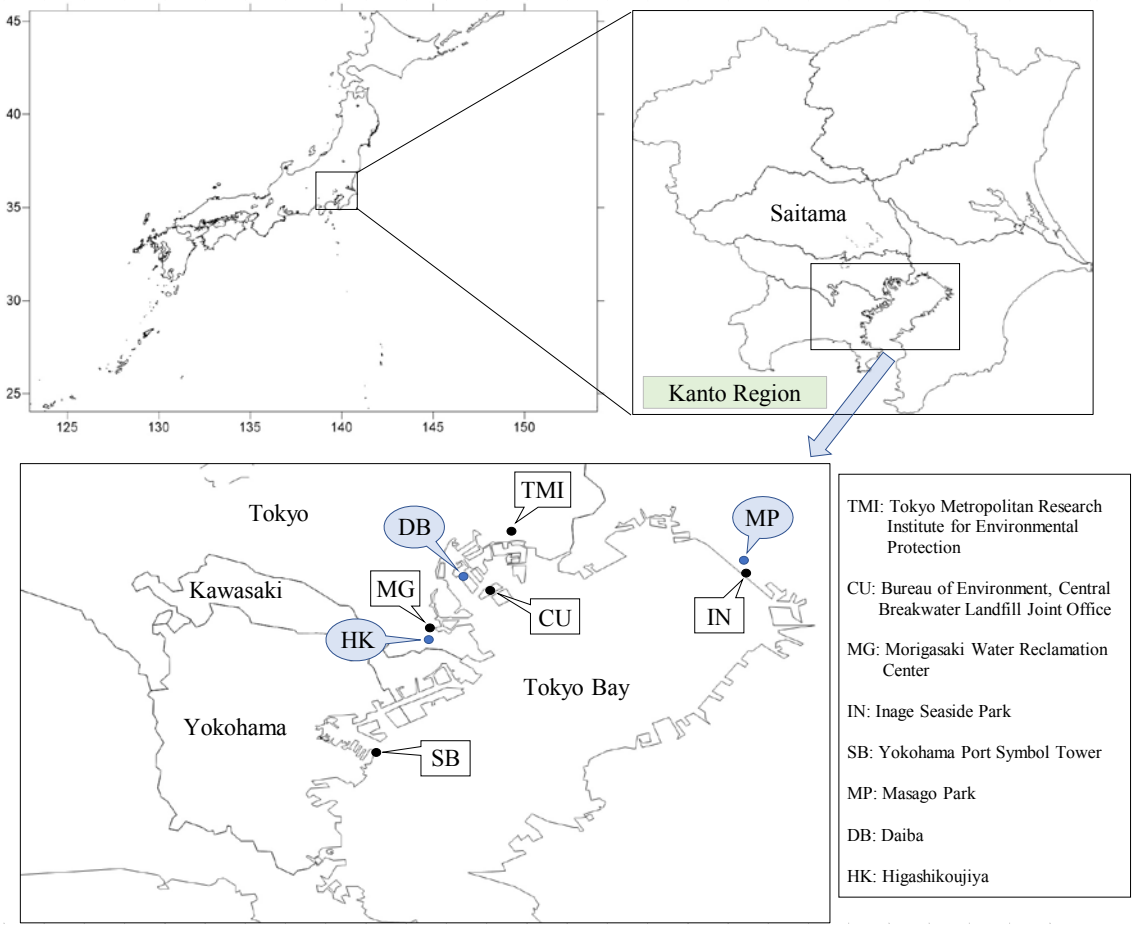

Figure 3-1. Sampling sites (squares) and measurement points of wind direction and speed (circles).

The sampling days were March 30, May 9, May 31, July 11, and August 1 in 2017, and March 28 and June 5 in 2018.

For VOCs other than aldehydes, 6.0-L canisters were heated, washed, and highly vacuumed, and thereafter air was sampled at a flow rate of 40 mL min^{-1} for 2 hours. Aldehydes were captured in a DNPH cartridge coupled with an ozone scrubber (BPE–DNPH, trans-1,2-bis(2-pyridyl)ethylene-2,4-dinitrophenylhydrazine) (Uchiyama et al.,

2011) at a flow rate of 1 L min^{-1} for 2 hours.

3.2.2 Analysis

After sampling, the canisters and cartridges were transported to the laboratory for analysis. 126 VOCs, including 28 alkanes, 23 alkenes, 18 aromatics, 3 biogenic compounds, 2 aldehydes, 3 ketones, 9 oxygenated compounds, and 40 other VOCs, were analyzed (Table 3-1). Because m-xylene + p-xylene and 2-ethyl-p-xylene and 4-ethyl-m-xylene were coeluted, we quantified them as m,p-xylene and 2,4-ethyl-m,p-xylene, respectively.

The Tokyo Metropolitan Institute for Environmental Protection (TMI), Morigasaki Water Reclamation Center, and Central Breakwater Landfill Joint Office samples were analyzed at the TMI while the Yokohama Port Symbol Tower and Inage Sea Park samples were analyzed at the Yokohama Environmental Science Research Institute (YEI).

The VOC analysis system at the TMI laboratory consisted of a gas chromatography (GC)/mass spectrometer (MS) (Agilent7890B/5977B) equipped with dual columns and a flame ionization detector (FID) coupled with a concentrator (Entech7200; Entech Instruments Inc., USA). H_2O and CO_2 were removed in the first two cryotraps using glass beads and Tenax-TA adsorbents, respectively. The VOCs were trapped at −180°C in the final stage. The trap was heated rapidly, and the VOCs were transferred into the GC-MS/FID for analysis. This system used a Deans Switch to introduce the effluent into a GS-GasPro column and a DB-1 column. The C2–C3 components, such as ethane, ethylene, propane, propylene, and acetylene, were separated in the GS-GasPro column (30 m × 0.32 mm, 4 μm) and quantified using the FID. The other components were

separated in the DB-1 column (60 m × 0.32 mm, 2 μm) and quantified using the quadrupole MS. The GC temperature program was the following: maintain at 35°C for 4 min; heat from 35°C to 140°C at a rate of 5°C min^{-1}; heat from 140°C to 240°C at a rate of 15°C min^{-1}; and maintain at 240°C for 8 min.

Dinitrophenylhydrazine (DNPH) derivatives for the aldehydes were eluted from the adsorbents by passing the solution through 25% dimethyl sulfoxide in an acetonitrile solution via a syringe and were analyzed using a high performance liquid chromatograph (HPLC) (1260 Infinity; Agilent Technologies, Inc., USA) equipped with a column (InfinityLab Poroshell 120 EC-C18; 2.1 × 100 mm; Agilent Technologies, Inc., USA). Solution A was a 5% acetonitrile solution, and solution B was 100% acetonitrile. Elution consisted of an A/B (80/20 (v/v)) mixture for 2 min, a linear gradient from A/B (80/20 (v/v)) to A/B (60/40 (v/v)) in 6 min, a linear gradient from A/B (60/40 (v/v)) to A/B (50/50 (v/v)) in 4 min, a linear gradient from A/B (50/50 (v/v)) to A/B (40/60 (v/v)) in 10 min, and then a linear gradient from A/B (40/60 (v/v)) to A/B (0/100 (v/v)) in 1 min. The flow rate was 0.4 mL min^{-1}, and the column temperature was 40°C. A VOC analysis was conducted in almost the same manner at the YEI laboratory.

Table 3-1. VOCs measured in this study

Group	VOC	Group	VOC	Group	VOC
alkane	Ethane	aromatic	Benzene	others	Acetylene
	Propane		Toluene		CFC-12
	Isobutane		Ethylbenzene		Chloromethane
	n-Butane		m-Xylene		CFC-114
	Isopentane		p-Xylene		Vinylchloride
	Pentane		Styrene		Bromomethane
	2,2-Dimethylbutane		o-Xylene		Ethylchloride
	Cyclopentane		Isopropylbenzene		CFC-11
	2,3-Dimethylbutane		Propylbenzne		Acrylonitrile
	2-Methylpentane		m-Ethyltoluene		1,1-Dichloroethene
	3-Methylpentane		p-Ethyltoluene		Dichloromethane
	Hexane		1,3,5-Trimethylbenzene		3-Chloro-1-propene
	Methylcyclopentane		2-Ethyltoluene		CFC-113
	2,4-Dimethylpentane		1,2,4-Trimethylbenzene		1,1-Dichloroethane
	Cyclohexane		1,2,3-Trimethylbenzene		cis-1,2-Dichloroethylene
	2-Methylhexane		m-Diethylbenzene		Chlorofolm
	2,3-Dimethylpentane		p-Diethylbenzene		1,2-Dichloroethane
	3-Methylhexane		2-Ethyl-p-Xylene		1,1,1,-Trichloroethane
	2,2,4-Trimethylpentane		4-Ethyl-m-Xylene		Carbontetrachloride
	Heptane		1,2,3,5-Tetramethylbenzene		1,2-Dichloropropane
	Methylcyclohexane	biogenic	Isoprene		Trichloroethylene
	2,3,4-Trimethylpentane		alpha-Pinene		cis-1,3-Dichloropropene
	2-Methylheptane		Camphene		trans-1,3-Dichloropropene
	3-Methylheptane		beta-Pinene		1,1,2-Trichloroethane
	Octane		Limonene		1,2-Dibromoethane
	Nonane	aldehyde	Formaldehyde		Tetrachloroethylene
	n-Decane		Acetaldehyde		Chlorobenzene
	n-Undecane	ketone	Acetone		1,1,2,2-Tetrachloroethane
alkene	Ethylene		Methylethylketone		m-Dichlorobenzene
	Propylene		Methyl-iso-butylketone		p-DiChlorobenzene
	trans-2-Butene	oxygenate	Isopropanol		o-Dichlorobenzene
	1-Butene		Methylacetate		1,2,4-Trichlorobenzene
	cis-2-Butene		n-Propanol		Hexachloro-1,3-butadiene
	1-Pentene		Methyl-t-butylether		
	trans-2-Pentene		Ethylacetate		
	cis-2-Pentene		Isobutanol		
	2-Methyl-1-pentene		n-Butanol		
	1,3-Butadiene		Butylacetate		
	Isobutene		ETBE		
	3-Methyl-1-butene				
	2-Methyl-1-butene				
	2-Methyl-2-butene				
	trans-1,3-Pentadiene				
	cis-1,3-Pendadiene				
	1-Hexene				
	cis-3-Hexene				
	trans-2-Hexene				
	cis-3-Methyl-2-pentene				
	cis-2-Hexene				
	trans-3-Methyl-2-pentene				
	1-Heptene				

3.2.3 Distance-weighted emissions based on PRTR data

To evaluate the validity of the method combining VOC concentration ratios with the prevailing wind directions as a means to estimate major VOC source areas, the distance-weighted emissions according to the 16 wind directions were compared with VOC concentration ratios according to the 16 wind directions. Emissions of toluene, 1,3,5-trimethylbenzene, and xylene as aromatic, and 1,3-butadiene as alkene from the PRTR database in 2016 were used to calculate the distance-weighted emissions according to the16 wind directions. This study targeted facilities within 30 km of the sampling site because the maximum distance between the sampling site and source was 28 km in a previous study (Buzcu-Guven and Fraser, 2008). The distance *D* between the sampling site and the facility was calculated using latitude and longitude data. The distance per second was unified as latitude 30.8 m and longitude 25.1 m (Science Chronology, 2014). Buzcu-Guven and Fraser (2008) used emissions from each production unit weighted by the inverse distance between the emission point and the receptor for calculating the ratio of the number of sources higher than a threshold criterion value. Therefore, the distance-weighted emissions (denoted as *X*) were calculated by dividing emissions of the facility by the distance *D*. The facilities were divided into the 16 wind directions centered on the sampling site, the distance-weighted emissions, *Xi*, were calculated using eq.3.1, and each of the distance-weighted emission ratios was calculated according to the 16 wind directions using eq.3.2:

$$X_i(\Delta\theta) = \sum_{k=1}^{\rho} \frac{G_{ik}(\Delta\theta)}{D_k} \qquad (3.1)$$

$$\gamma_i = \frac{X_i(\Delta\theta)}{X_i(360°)} \times 100 \qquad (3.2)$$

where D_k is the distance (km) between the facility k and the sampling site, G_{ik} is emissions (kg) of VOC species i at facility k based on PRTR data. Following these computations, the distance-weighted emission ratios were compared with VOC concentration ratios according to the 16 wind directions. Buzcu-Guven and Fraser (2008) compared the results using all data with those using only nighttime data in order to confirm the relationship between VOC concentration and wind direction. Although the results using only nighttime data accorded better with the distance-weighted emissions and the plots using all data showed greater range in direction. The direction of highest VOC concentration ratio corresponded with that in the highest distance-weighted emission ratio using all data. Therefore, this study attempted to calculate the VOC concentration ratios according to the 16 wind directions using all data, excluding the result if there was any missing component. The wind direction and wind speed data used for determining the prevailing wind direction every two hours were the 30-minute data of the Yokohama Port Symbol Tower, the 1-minute data of the Tokyo Metropolitan Research Institute for Environmental Protection, the 1-minute data of Higashikoujiya, the 1-minute data of Daiba, and the 5-minute data of the Masago Park. The wind direction and wind speed data at Higashikoujiya, Daiba, and Masago Park were used to estimate those variables for Morigasaki, Central Breakwater Landfill Joint Office, and Inage Seaside Park, respectively. The most frequent wind direction was used as the prevailing wind direction for that time. If two wind directions had the same frequency, the wind direction with the largest total wind speed for that time was used as the prevailing wind direction.

3.3 Results and discussion

3.3.1 Time series of VOC concentrations at the Yokohama Port Symbol Tower

The variation of VOC and Ox concentrations at the Yokohama Port Symbol Tower on March 30, 2017 and March 28, 2018, when the sea-land breeze blew, is shown in Figure 3-2.

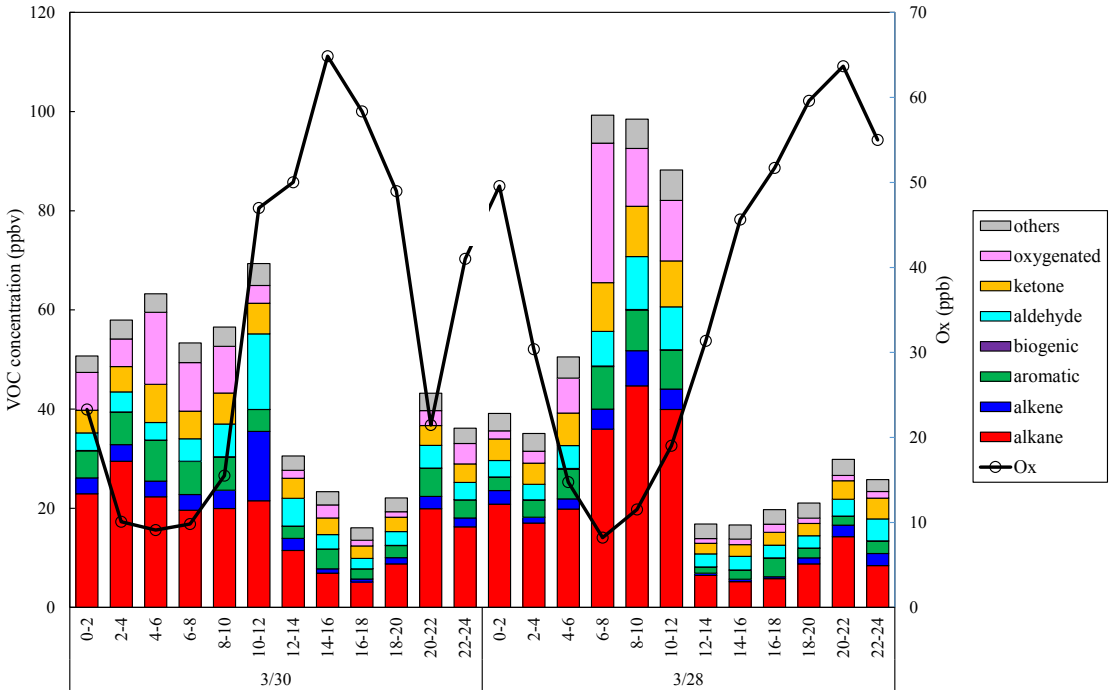

Figure 3-2. Variations of VOC and Ox concentrations at the Yokohama Port Symbol Tower on March 30, 2017 and March 28, 2018.

The time on which the land breeze changed to the sea breeze was around 9:30 and 11:00 on March 30, 2017, and March 28, 2018, respectively. The wind speed was calm from 8:30 to 10:30 on March 28, 2018. Ox concentrations began to rise when the sea breeze

began to blow. VOC concentration also increased immediately after the onset of the sea breeze, but then decreased sharply. In particular, this tendency was notable on March 30, 2017, when the largest VOC increases were noted for ethylene, followed by formaldehyde, acetaldehyde, and propylene.

From the above results, it was suggested that VOC accumulated over Tokyo Bay from night to dawn initiated photochemical reactions before penetrating to the inland area by the sea-breeze inflow.

3.3.2 Comparison of VOC concentration ratios with the distance-weighted emissions according to the 16 wind directions

The Yokohama Port Symbol Tower located in the Keihin industrial area, which has the largest number of samples, was selected as the representative site for validation, and VOC concentration ratios were compared with the distance-weighted emissions. The results are shown in Figure 3-3.

The concentration ratios of toluene were 12.4%, 8.7%, and 9.1% in the NNW, W, and S directions, respectively, while the distance-weighted emission ratios of toluene were 16.7%, 10.9%, and 21.5% in the N, WSW, and SSW directions, respectively. Both tended to be divided into the three directions N, W, and S. The concentration ratio of xylene was highest in the S direction (21.0%), while the distance-weighted emission ratio of toluene was highest in the SSW direction (35.4%), showing the tendency to be largely biased in only the south direction. The concentration ratios of 1,3,5-trimethylbenzene were 14.1%, 12.7%, and 14.3% in the NNW, W, and S directions,

respectively, while the distance-weighted emission ratios of 1,3,5-trimethylbenzene were 23.5%, 17.5%, 10.4%, and 12.0% in the NNW, W, and SSW directions, respectively. These results showed that both ratios were high in the NNW, W, and S directions. The distance-weighted emission ratio tended to be high in the ESE direction due to the impact of the source in Chiba Prefecture. It is speculated that VOC concentration ratios were not high in the ESE direction because the wind direction in Chiba Prefecture across Tokyo Bay was different from that in Kanagawa Prefecture. Concerning 1,3-butadiene, the NNE direction was highest in both VOC concentration ratio and distance-weighted emission ratio. Although the tendency of both results was roughly the same for all four species, there was an error of $\pm 22.5^{\circ}$ in the wind direction. The reason the wind direction did not completely match was presumably that the sampling time was two hours and that the wind direction data of the Yokohama Port Symbol Tower was 30-minute data. However, a certain tendency was obtained even with a small number of samples, suggesting that VOC concentration ratio is greatly affected by the fixed sources and wind direction. From these results, it is demonstrated that the method using VOC concentration ratios according to the 16 wind directions could serve as a means of VOC source area identification.

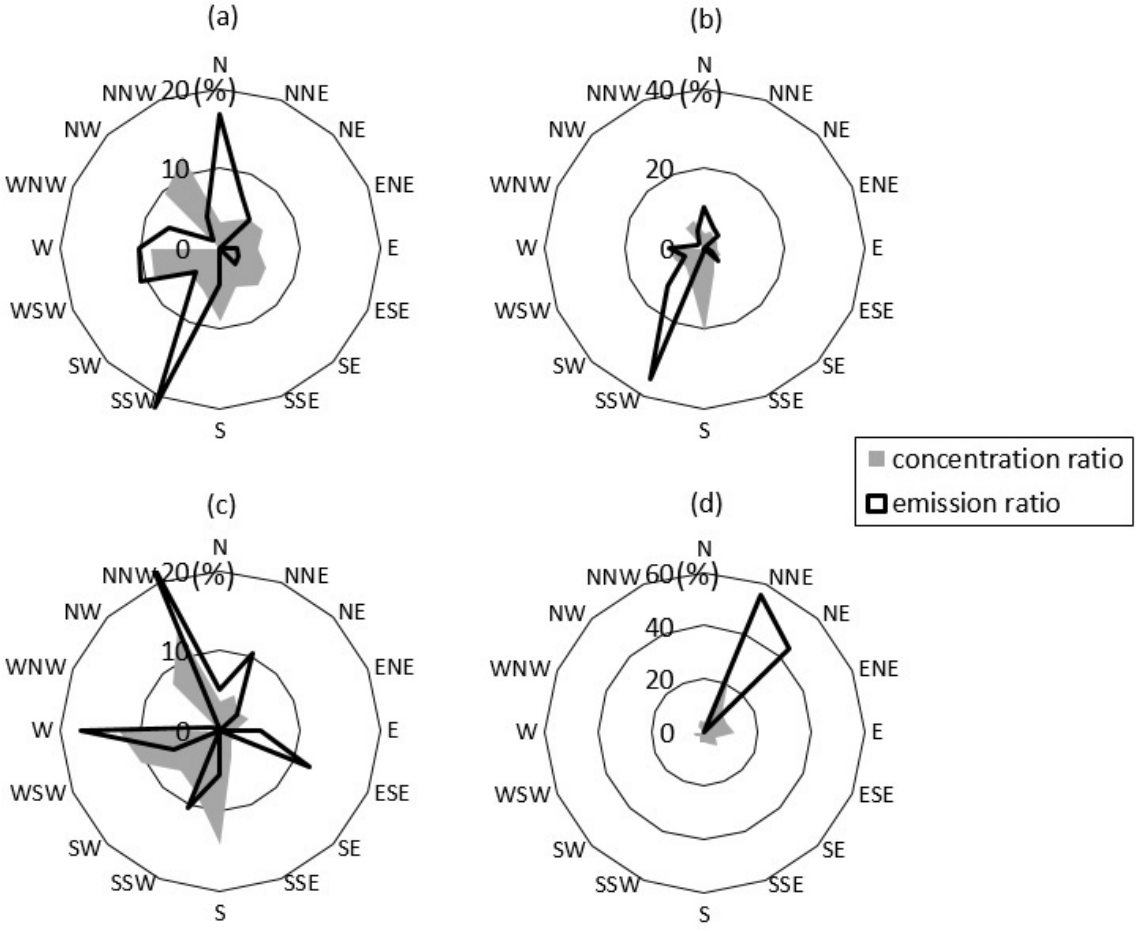

Figure 3-3. Polar plots of emission rate (%) (from PRTR data) and composition ratios (%) of VOC concentrations for (a) toluene, (b) xylenes, (c) 1,3,5-trimethylbenzene, and (d) 1,3-butadiene.

3.3.3 Source area identification of alkenes using alkene concentration ratios according to the 16 wind directions

The VOC concentration ratios according to the 16 wind directions at each sampling site are shown in Figure 3-4.

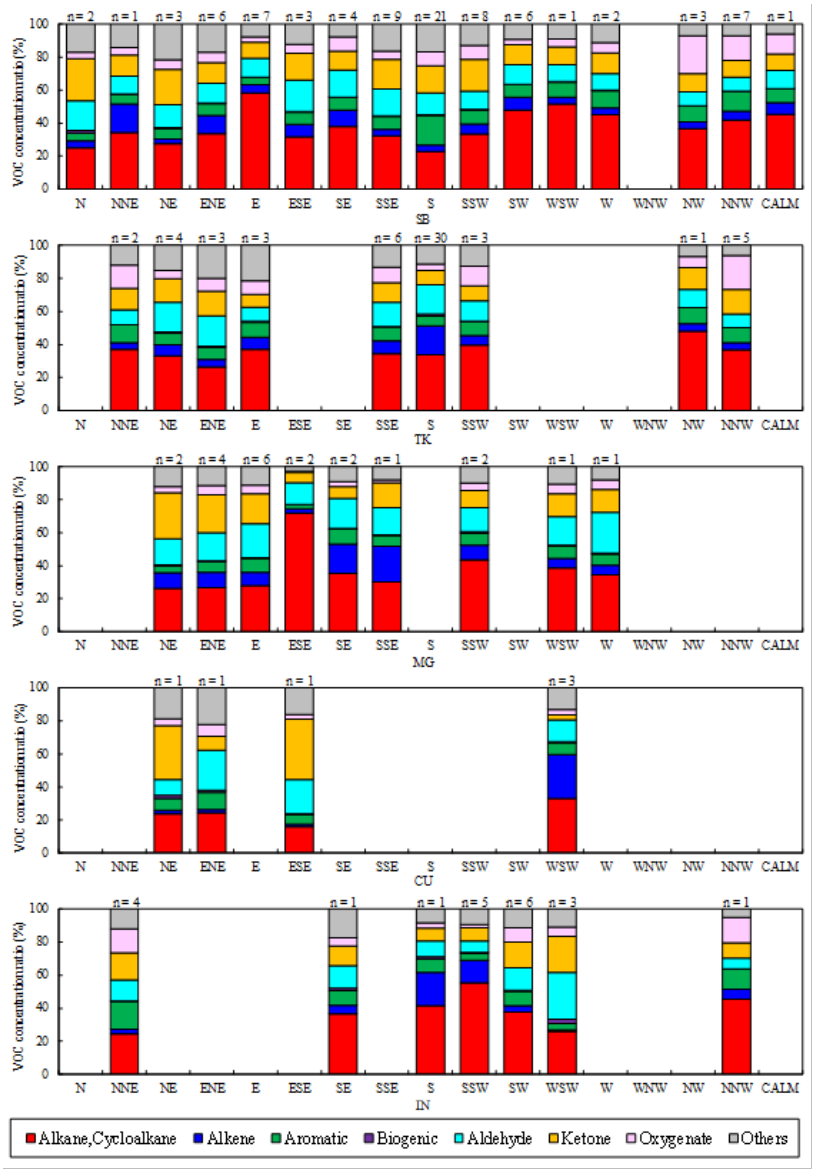

Figure 3-4. Comparisons of VOC concentration contributions by 16 wind directions at 5 points (SB: Yokohama Port Symbol Tower, TK: Tokyo Metropolitan Research Institute for Environmental Protection, MG: Morigasaki Water Reclamation Center, CU: Bureau of Environment, Central Breakwater Landfill Joint Office, and IN: Inage Seaside Park).

The concentration ratio of aromatics was highest in the S and NNE directions at the Yokohama Port Symbol Tower and Inage Seaside Park, respectively, while there was no noteworthy characteristics at the remaining sampling sites. The concentration ratio of alkene tended to be high in the NNE (17%), S (18%), SSE (22%), WSW (26%), and S (20%) directions at the Yokohama Port Symbol Tower, the Tokyo Metropolitan Research Institute for Environmental Protection, the Morigasaki Water Reclamation Center, the Central Breakwater Landfill Joint Office, and the Inage Seaside Park sites, respectively. The top two components among alkenes in the wind direction with the highest concentration ratio of alkene were: a) ethylene and propylene at the Yokohama Port Symbol Tower site, the Tokyo Metropolitan Research Institute for Environmental Protection, the Central Breakwater Landfill Joint Office, and the Inage Seaside Park sites, and b) ethylene and 1-butene at the Morigasaki Water Reclamation Center site. These species occupied 60–80% of total alkene concentration, with ethylene and propylene significantly contributing to specific directions of each sampling site.

The alkene concentration ratios of total alkenes according to the 16 wind directions and the locations and emissions of 1,3-butadiene by PRTR data are shown in Figure 3-5. The locations and emissions of 1,3-butadiene was described in Figure 3-5 as a reference because 1,3-butadiene is only major alkene included at PRTR data. The result of the Central Breakwater Landfill Joint Office site is excluded due to the lack of samples.

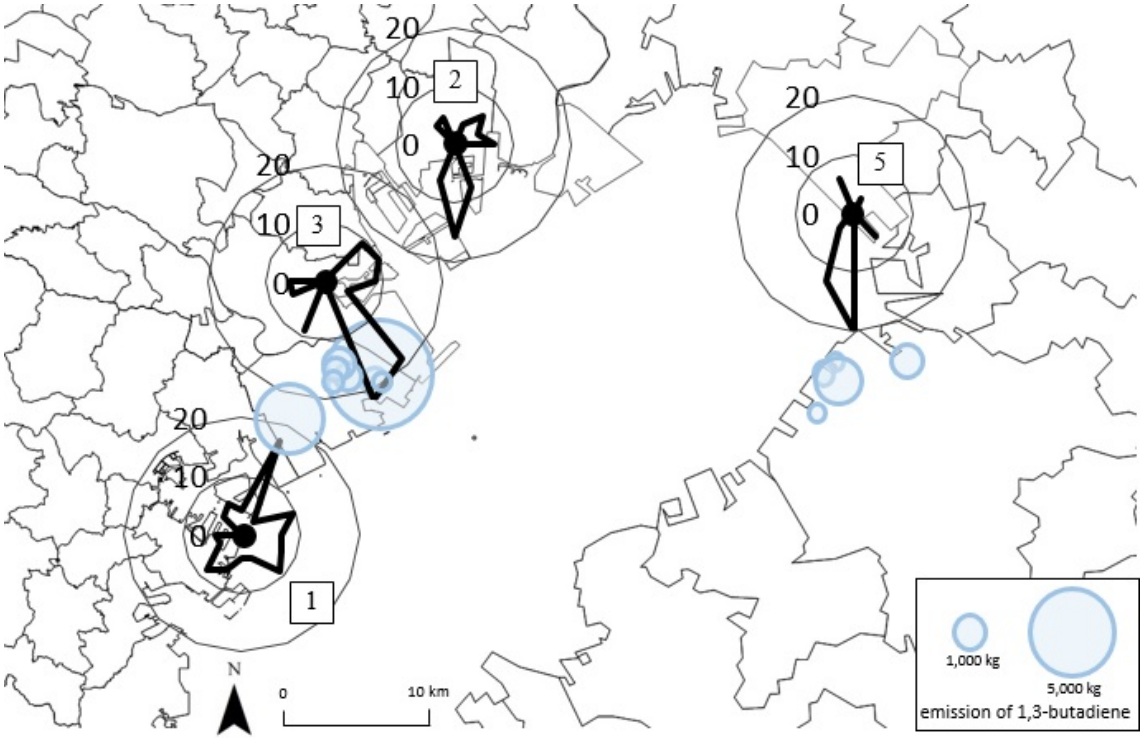

Figure 3-5. Comparisons of emission of 1,3-butadiene (from PRTR data) and composition ratio (%) of alkenes as a fraction of total VOC concentrations (1: Yokohama Port Symbol Tower, 2: Tokyo Metropolitan Research Institute for Environmental Protection, 3: Morigasaki Water Reclamation Center, and 4: Inage Seaside Park).

The wind direction with highest alkene concentration ratio at each sampling site was consistent with the direction of the facilities emitting 1,3-butadiene. The above results imply that the main alkene components, such as ethylene and propylene, were discharged from the same block as the facilities treating 1,3-butadiene.

3.4 Conclusions

Comparing VOC concentration ratios according to the 16 wind directions with the distance-weighted emission ratios from the PRTR data, the trends were almost the same. Since a similar tendency between VOC concentration ratios and distance-weighted emission ratios was obtained despite the small number of samples, this implies that VOC concentrations in the Tokyo Bay coastal area were affected by local industrial sources and wind direction. From this result, it is demonstrated that the method combining VOC concentration ratios with the prevailing wind direction was useful for VOC source area identification. Alkene concentration ratios were calculated according to the 16 wind directions in order to identify alkene source area. The wind direction with the highest alkene concentration ratio corresponded to the location of facilities treating 1,3-butadiene at all sampling sites except for the Central Breakwater Landfill Joint Office. From the above results, the main alkene source appears to be located in the same area as the facilities treating 1,3-butadiene.

In this study, it was demonstrated not only that VOC concentrations in the Tokyo Bay coastal area were significantly affected by the industrial VOC sources, but also that the method using VOC concentration ratios (calculated with a small dataset according the 16 wind directions) was useful for source area identification of VOCs. A high time resolution investigation at multiple sampling sites around the area near facilities treating 1,3-butadiene is needed for the source identification of alkenes because alkene sharply decline via photochemical reaction.

References

Buzcu-Guven, B., Fraser, M. P., 2008. Comparison of VOC emissions inventory data with source apportionment results for Houston, TX. Atmos. Environ. 42, 5032-5043.

Chan, Y. C., Hawas, O., Hawker, D., Vowles, P., Cohen, D. D., Stelcer, E., Simpson, R., Golding, G., Christensen, E., 2011. Using multiple type composition data and wind data in PMF analysis to apportion and locate sources of air pollutants. Atmos. Environ. 45, 439-449.

Chen, C., Chuang, Y., Hsieh, C., Lee, C., 2019. VOC characteristics and source apportionment at a PAMS site near an industrial complex in central Taiwan. Atmos. Pollut. Res. 10, 1060-1074.

Filella, I., Enuelas, J., 2006. Daily, weekly and seasonal relationships among VOCs, NOx and O_3 in a semi-urban area near Barcelona. J. Atmos. Chem. 54, 189-201.

Kim, E., Hopke, P. K., Edgerton, E. S., 2003. Source identification of Atlanta aerosol by positive matrix factorization. J. Air Waste Manag. Assoc. 53, 731-739.

Liu, C., Mu, Y., Liu, J., Zhang, C., Zhang, Y., Liu, P., Zhang, H., 2016. The levels, variation characteristics and sources of atmospheric nonmethane hydrocarbon compounds during wintertime in Beijing, China. Atmos. Chem. Phys. Discuss. https://doi.org/10.5194/acp-2016-783.

Uchiyama, S., Inaba, Y., Kunugita, N., 2011. A diffusive sampling device for simultaneous determination of ozone and carbonyls. Analy. Chi. Acta. 691, 119-124.

Xie, Y., Berkowitz, C. M., 2006. The use of positive matrix factorization with conditional probability functions in air quality studies: an application to hydrocarbon

emissions in Houston, Texas. Atmos. Environ. 40, 3070-3091.

Chapter 4

Source estimation of alkenes in the Tokyo Bay coastal area

Publication based on this chapter:

Fukusaki, Y., Kousa, Y., Umehara, M., Ishida, M., Sato, R., Otagiri, K., Hoshi, J., Nudejima, C., Takahashi, K., Nakai, S. 2021. Source region identification and source apportionment of volatile organic compounds in the Tokyo Bay coastal area, Japan. Atmos. Environ.: X. 9, 100103, 1-13.

Source estimation of alkenes in the Tokyo Bay coastal area

4.1 Introduction

Previous studies outside of Japan have shown that the major source of alkenes (including ethylene and propylene) was the petrochemical industry (Roberts et al., 2004; Zheng et al., 2020). Moreover, Ryerson et al. (2003) demonstrated that the bulk of initial VOC reactivity of petrochemical plumes was dominated for the first 50 km of transport (i.e., the first 2–3 hours after emission) by anthropogenic emissions of ethylene and propylene and by aldehyde photoproducts derived from these species in Houston. This clearly indicates that reducing emissions of these two alkenes was the most effective VOC-reduction strategy to minimize O_3 formation downwind of these sources. In Japan, there are 15 petrochemical complexes, 6 of which exist in the Tokyo Bay coastal area. Although alkenes emitted from these petrochemical complexes are assumed to significantly affect O_3 formation, to the best of our knowledge, few studies have attempted to identify alkene sources in the Tokyo Bay coastal area and estimate their impact on O_3 formation.

Several receptor models such as UNMIX, principal component analysis (PCA)/absolute principal component score (APCS), chemical mass balance (CMB), and positive matrix factorization (PMF) are known methods for VOC source apportionment. The receptor model is the multivariate statistical method determining the direct contributions of various air pollution sources to ambient concentrations measured at a receptor site. PMF has been most widely used among these receptor models. Outside of Tokyo, many studies involving VOC source apportionment by PMF have been reported, indicating that the main sources in urban and industrial areas were vehicular exhaust emissions and

industrial-related emissions, respectively (Lau et al., 2010; Song et al., 2008; Buzcu and Fraser, 2006; Dumanoglu et al., 2014).

The CMB method requires source profiles showing the compositions being emitted by sources. Although the source identification is not required, the CMB method is not capable of accurately estimating VOC source contributions for a VOC source without a profile. On the other hand, source profiles are not required for the PMF method, only the observed data. In addition, a PMF can weigh uncertainties in the individual observed data and introduce a non-negativity constraint for all factor matrices and elements to develop physically meaningful solutions. Therefore, with a PMF, the uncertainties of inaccurate source profiles can be excluded, and source apportionments can be more accurately evaluated when compared with the CMB (especially if the effect of a source without a profile could not be ignored). However, a shortcoming is that the assignment of source profiles tends to be subjective because the number of factors and factor identification resolved by a PMF must be arbitrarily determined.

In Japan, Morino et al. (2011) conducted a PMF analysis using the hourly concentrations of C2-C8 VOCs in Saitama, which is located 15–20 km north of Tokyo's urban center, resulting in source contributions of gasoline vapor, vehicle exhaust, evaporation sources, liquefied natural gas, and liquefied petroleum gas (LPG) that were 9%–16%, 14%–25%, 49%–71%, and 7%–10%, respectively. Furthermore, Ueno et al. (2015) estimated the source apportionment in different sites of Tokyo via a CMB analysis with consideration of the chemical loss and reported that the vehicle-related contribution was large in urban areas while the isoprene contribution was large in suburban areas. In the Tokyo Bay coastal area, where the industrial facilities are

intensely clustered, the source contributions were assumed to differ from those mentioned in the above studies because the VOC levels are significantly affected by pollutants freshly emitted from local sources. In the previous studies (Chen et al., 2019; Buzcu-Guven and Fraser, 2008), source area identification and source apportionment of VOCs were conducted combining PMF analysis with the conditional probability function (CPF). However, it was demonstrated in the previous chapter that VOC concentration ratios according to the 16 wind directions (calculated by small data sets in the area with the strongest impact of industrial sources) enable source area identification. Therefore, it was assumed that factor contributions (based on the 16 wind directions calculated by a PMF run using small data sets) also allow for alkene source identification. The objectives of this study are to apportion VOC sources by PMF analysis using the hourly ambient data at four sampling sites in the Tokyo Bay coastal area and to estimate major alkene sources through the comparison of alkene concentration ratios and factor contributions calculated from PMF results according to the 16 wind directions. We also aim to calculate the photochemical reactivity of the source factors resolved by PMF and identify the VOC source most significantly contributing to the photochemical reactions.

4.2 Methodology

4.2.1 Sampling

Figure 4-1 shows the locations of the four sampling sites, Higashikoujiya, Ushioda, the Yokohama Port Symbol Tower, and Honmoku. The Tokyo Bay coastal area, not inland, is suitable for the sampling sites because the wind direction in the coastal area tends to

be different from inland areas. Furthermore, if the investigation is conducted at the sampling sites located inland, air masses emitted from VOC sources cannot be distinguished from air masses accumulated above Tokyo Bay.

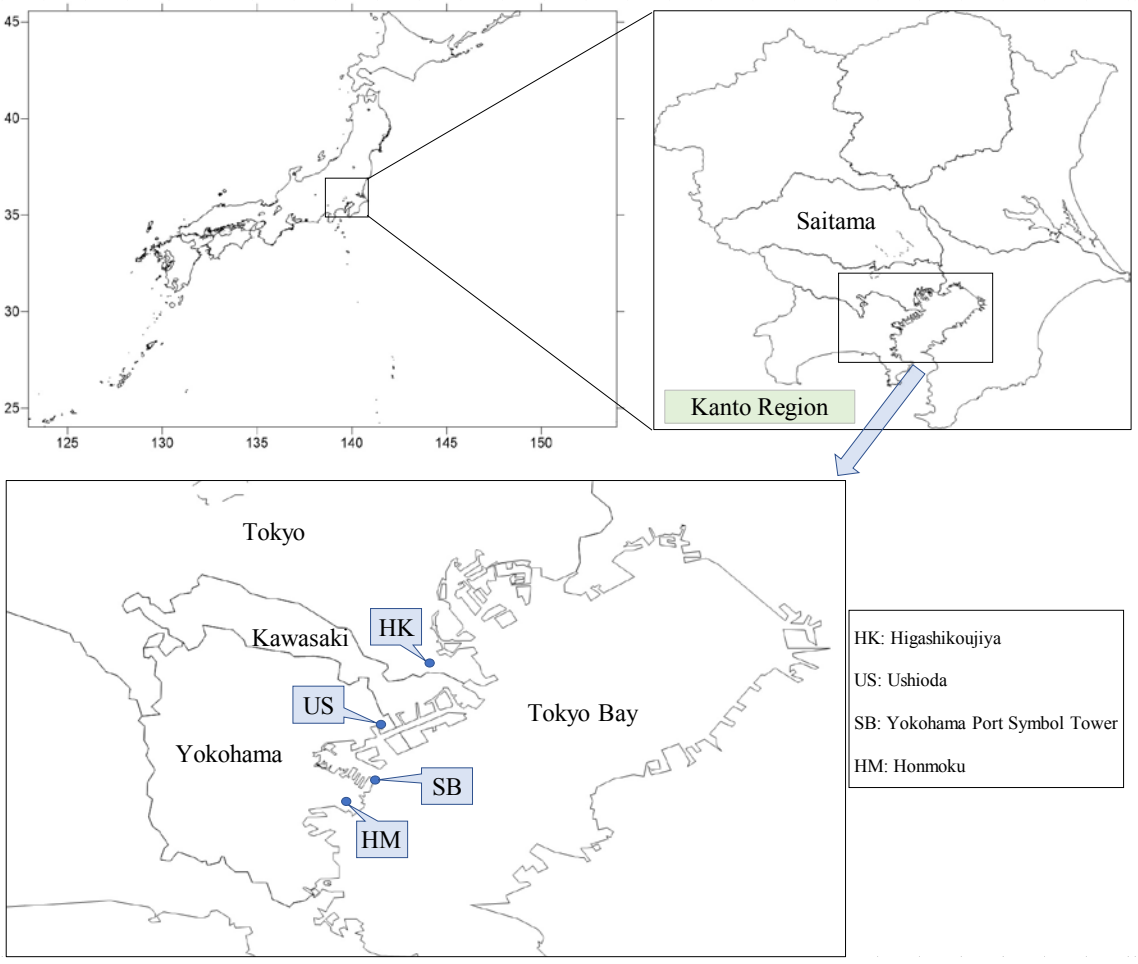

Figure 4-1. Map including the four sampling sites.

The small facilities are scattered around the Higashikoujiya site, which is situated approximately 3 km west of the Haneda Airport. The several industrial facilities such as glass manufacturing facilities, iron-steel plants, vessel manufacturing facility, and metal

manufacturing facilities are intensely clustered on the seaward side of the Ushioda site. The petrochemical complexes, power plants, and LNG storage facility exist in the Kawasaki coastal area between the Higashikoujiya and Ushioda sites. The Honmoku site is adjacent to a highway and surrounded by large petroleum-refining facilities from the southeast to the west. The Yokohama Port Symbol Tower site faces Tokyo Bay, ensuring that it is a good location to distinguish whether air pollutants were emitted from the petrochemical complexes or petroleum-refining facilities. VOC samples were obtained between 06:00 and 15:00 on six selected days (March 20, April 10, May 17, June 20, July 9, and August 29) in 2019. 216 samples were collected every hour using canisters (GL Science Inc., Japan) at a flow rate of 80 mL min^{-1}. Aldehydes were adsorbed in BPE–DNPH cartridges at a flow rate of 1 L min^{-1} using pumps (GSP-400FT; Gastec Inc., Japan).

4.2.2 Analysis

After sampling, we transported the canisters and BPE–DNPH cartridges to the laboratory for analysis. We analyzed 126 VOCs, including 28 alkanes, 23 alkenes, 18 aromatics, 3 biogenic compounds, 2 aldehydes, 3 ketones, 9 oxygenated compounds, and 40 other VOCs (Table 4-1). Because m-xylene + p-xylene and 2-ethyl-p-xylene + 4-ethyl-m-xylene were coeluted, we quantified them as m,p-xylene and 2,4-ethyl-m,p-xylene, respectively.

Table 4-1. List of the 126 VOC components.

Group	VOC	K_i^{OH} ※	PMF	Group	VOC	K_i^{OH} ※	PMF
alkane	Ethane	0.254	strong		1,2,4-Trimethylbenzene	32.5	strong
	Propane	1.11	strong		1,2,3-Trimethylbenzene	32.7	weak
	Isobutane	2.14	strong		m-Diethylbenzene	25.5	weak
	n-Butane	2.38	strong		p-Diethylbenzene	16.4	weak
	Isopentane	3.6	strong		2-Ethyl-p-xylene		weak
	n-Pentane	3.84	strong		4-Ethyl-m-xylene		
	2,2-Dimethylbutane	2.27	weak		1,2,3,5-Tetramethylbenzene		weak
	Cyclopentane	5.02	strong	biogenic	Isoprene	99.6	strong
	2,3-Dimethylbutane	5.79	strong		alpha-Pinene	51.8	strong
	2-Methylpentane	5.2	strong		beta-Pinene	73.5	weak
	3-Methylpentane	5.2	strong	aldehyde	Formaldehyde	8.47	strong
	Hexane	5.25	strong		Acetaldehyde	14.9	strong
	Methylcyclopentane	5.68	strong	ketone	Acetone	0.191	strong
	2,4-Dimethylpentane	4.77	weak		Methylethylketone	1.2	strong
	Cyclohexane	7.02	strong		Methyl-iso-butylketone	12.7	strong
	2-Methylhexane	6.89	strong	oxygenate	Isopropanol	5.09	weak
	2,3-Dimethylpentane	7.15	weak		Methylacetate	0.349	strong
	3-Methylhexane	7.17	strong		n-Propanol	5.81	weak
	2,2,4-Trimethylpentane	3.38	weak		Methyl-t-butylether	2.95	weak
	Heptane	6.81	strong		Ethylacetate	1.6	strong
	Methylcyclohexane	9.64	strong		Isobutanol	9.3	weak
	2,3,4-Trimethylpentane	6.6	weak		n-Butanol	8.45	strong
	2-Methylheptane	8.31	weak		Butylacetate	4.2	weak
	3-Methylheptane	8.59	weak		ETBE	8.68	weak
	n-Octane	8.16	strong	others	Acetylene	0.756	strong
	n-Nonane	9.75	strong		HCFC-22		strong
	n-Decane	11	strong		CFC-12		strong
	n-Undecane	12.3	weak		HCFC-142		strong
alkene	Ethylene	8.15	strong		Chloromethane	0.0448	strong
	Propylene	26	strong		CFC-114		weak
	trans-2-Butene	63.2	strong		Vinyl chloride	6.9	weak
	1-Butene	31.1	strong		Bromomethane	0.0412	weak
	cis-2-Butene	55.8	strong		Ethylchloride	0.418	weak
	1-Pentene	31.4	weak		HCFC-123		weak
	trans-2-Pentene	67	weak		CFC-11		strong
	cis-2-Pentene	65	weak		HCFC-141		strong
	2-Methyl-1-pentene	63	weak		Acrylonitrile	4.9	weak
	1,3-Butadiene	65.9	weak		HCFC-225ca		weak
	Isobutene	50.8	strong		1,1-Dichloroethylene	10.9	weak
	3-Methyl-1-butene	31.4	weak		Dichloromethane	0.145	strong
	2-Methyl-1-butene	61	weak		3-Chloro-1-propene	32	bad
	2-Methyl-2-butene	86	weak		HCFC-225cb		weak
	trans-1,3-Pentadiene	101	bad		CFC-113		strong
	cis-1,3-Pentadiene	101	bad		1,1-Dichloroethane	0.26	weak
	1-Hexene	37	weak		cis-1,2-Dichloroethylene		weak
	cis-3-Hexene	65.6	bad		Chloroform	0.106	strong
	trans-2-Hexene	66	weak		1,2-Dichloroethane	0.253	strong
	cis-3-Methyl-2-pentene	88.5	weak		1,1,1-Trichloroethane	0.0124	weak
	cis-2-Hexene	66	weak		Carbon tetrachloride		strong
	trans-3-Methyl-2-pentene	88.5	weak		1,2-Dichloropropane	0.45	weak
	1-Heptene	40	weak		Trichloroethylene	2.34	strong
aromatic	Benzene	1.22	strong		cis-1,3-Dichloropropene	8.45	weak
	Toluene	5.58	strong		trans-1,3-Dichloropropene	14.4	weak
	Ethylbenzene	7	strong		1,1,2-Trichloroethane	0.2	weak
	m-Xylene	23.1	strong		1,2-Dibromoethane	0.227	bad
	p-Xylene	14.3			Tetrachloroethylene	0.171	weak
	Styrene	58	weak		Chlorobenzene	0.77	weak
	o-Xylene	13.6	strong		1,1,2,2-Tetrachloroethane		bad
	Isopropylbenzene	6.3	weak		benzyl chloride		bad
	Propylbenzene	5.8	weak		m-Dichlorobenzene		bad
	m-Ethyltoluene	18.6	strong		p-Dichlorobenzene	0.555	weak
	p-Ethyltoluene	11.8	weak		o-Dichlorobenzene		bad
	1,3,5-Trimethylbenzene	56.7	weak		1,2,4-Trichlorobenzene		bad
	o-Ethyltoluene	11.9	strong		Hexachloro-1,3-butadiene		bad

※ Rate constant in 10^{-12} cm^3 $molecule^{-1}$ s^{-1}

The Higashikoujiya samples were analyzed at the Tokyo Metropolitan Research Institute of Environmental Protection (TMI) while the Ushioda, Yokohama Port Symbol Tower, and Honmoku samples were analyzed at the Yokohama Environmental Science Research Institute (YEI).

The VOC analysis system at YEI included two parts: a gas chromatography (GC)/flame ionization detector (FID) (Shimadzu Inc., Japan) coupled with a concentrator (GL Sciences Inc., Japan) for the C2–C4 components and a GC/mass spectrometer (MS) (Shimadzu Inc., Japan) coupled with a CC2110 concentrator (GL Sciences Inc., Japan) for the remaining components. A 400-mL aliquot of the air sample from each canister was concentrated in each concentrator. In the system for the C2–C4 component analysis, the VOCs were trapped in the pre-column at −100°C in the first stage. After the CO_2 was removed at −30°C, the trap was heated to 200°C and the C2–C4 components were transferred to the final cryotrap, which was set to −100°C. The C2–C4 components were rapidly heated to 200°C, transferred to a GC column (TC-BOND Alumina/KCl, 50 m × 0.53 mm) with the following GC temperature program: maintain at 40°C for 5 minutes; heat from 40°C to 130°C at a rate of 2.5°C min^{-1}; heat from 130°C to 200°C at a rate of 30°C min^{-1}; and maintain at 200°C for 11.5 minutes. Further quantification was performed using FID. The C2–C4 components detected by FID were ethane, ethylene, propane, acetylene, propylene, isobutane, isobutene, 1-butene, 1,3-butadiene, and butane. In the analysis system for the other components, the VOCs were trapped in two cryotraps; the first cryotrap was set at 40°C to trap VOCs with a high boiling point, and the second cryotrap was set at −100°C to trap CO_2, H_2O, and VOCs with a low boiling point. After CO_2 was removed, the two cryotraps were heated to 220°C and transferred to the final

cryotrap, which was set at −185°C. H_2O was removed at the moisture control system when transferring to the final cryotrap because the moisture control system was set to 10°C between the first and second cryotraps. The trap was rapidly heated to 200°C and transferred to a GC column (DB-1 column (60 m × 0.25 mm)) with the following GC temperature program: maintain at 40°C for 10 minutes; heat from 40°C to 60°C at a rate of 3.5°C min^{-1}; heat from 60°C to 120°C at a rate of 6°C min^{-1}; heat from 120°C to 200°C at a rate of 16°C min^{-1}; maintain at 200°C for 12 minutes; heat from 200°C to 250°C at a rate of 30°C min^{-1}; and maintain at 250°C for 8 minutes. Further, quantification was performed using MS. The carrier gas was pure helium (purity > 99.9999%). Each target compound was identified by the ratio of the identified ion to the check ion, its retention time, and the standard gases. Four types of mixed standard gases were used. Ten-point calibration curves including concentrations at 0, 0.02, 0.05, 0.1, 0.2, 0.5, 1, 2, 5, and 10 ppbv, were generated, yielding R2 values between 0.995 and 1.00 for the measured compounds. A gas standard (0.5 ppbv) was measured every day to confirm the stability of the system. The detection limits for various compounds were determined based on the gas standard (0.02 ppbv). To calculate the detection limits, the GC/MS and GC/FID analyses were repeated seven times.

The DNPH derivatives for the aldehydes were eluted from the adsorbents by passing the solution through 25% dimethyl sulfoxide in an acetonitrile solution containing 0.085% (v/v) phosphoric acid via a syringe and analyzed using an HPLC (1260 Infinity; Agilent Technologies, Inc., USA) equipped with a column (ZORBAX Eclipse Plus C18; 4.6 × 250 mm). The gradient program was operated first with acetonitrile/water (55/45 (v/v)) for 4 minutes, second at a linear gradient of acetonitrile/water (90/10 (v/v)) for 9 minutes,

and finally at acetonitrile/water (90/10 (v/v)) mixture for 5 minutes. The flow rate was 1 mL min^{-1}. The derivatives were detected at a single wavelength at 365 nm. The limited detections were calculated as being three times the standard deviation obtained from the data of eight replicate measurements. A VOC analysis was conducted in almost the same manner at the TMI laboratory.

4.2.3 PMF analysis

A PMF is one of several receptor models. A PMF run decomposes a large number of observation data sets into several factors, and factor contributions and factor profiles can be derived simultaneously. In this study, PMF 5.0 (developed by the US Environmental Protection Agency) was applied as a tool for VOC source apportionment analysis. The principles and procedures of the model are described in the user manual and in previous studies (Paatero and Tapper, 1994; Paatero, 1997).

PMF generally requires a large number of samples to make a stable and reliable source identification. Samples from multiple sites in close proximity having similar numbers of samples can potentially be used in a single PMF run to perform a simplified analysis (McCarthy et al., 2013). Therefore, the data collected at all sampling sites and campaigns were lumped together for the PMF source apportionment analysis. The input data were 216 samples with 116 VOC components. The concentrations of the components to be input into the PMF analysis must be preserved between the source and receptor site without chemical loss. Buzcu-Guven and Fraser (2008) showed that the emission inventory of the facilities within 28 km of the sampling site was approximately consistent with the PMF results using 54 VOC components containing

the components with high OH reactivity. In other words, the chemical loss of the component with high photochemical reactivity is not particularly important for a receptor site that is close to the industrial facilities. In this study, 116 VOC components were entered into a PMF run with the assumption that chemical loss is not important and VOC composition is preserved because the major industrial facilities are situated within 28 km from each sampling site.

The selection of the optimal number of factors in a PMF model was conducted on standard criteria, including the value of the minimized sum of squared residuals, the relative standard deviation (denoted as Q), the residual distribution, robustness, and the interpretability of the resulting profiles. Twenty base runs were performed, with different numbers of factors ranging from 4 to 9, to compare the results. The six-factor solution had a minimum relative standard deviation (Figure 4-2).

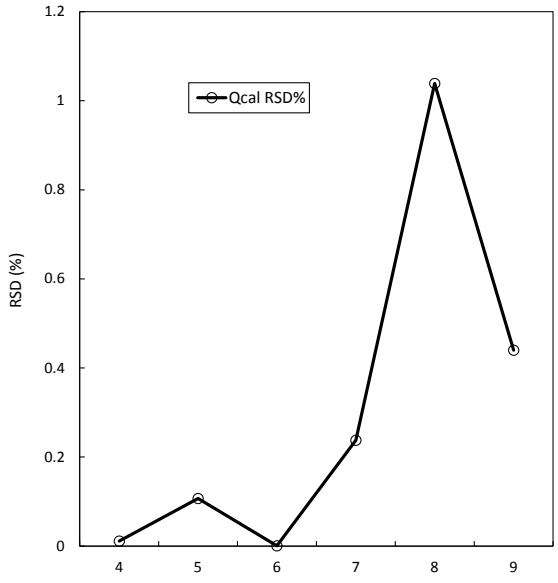

Figure 4-2. Relative standard deviations of Q with different numbers of factors ranging from 4 to 9.

The Q (robust) and Q (true) values were 15,407 and 15,452, respectively. The scaled residual distributions were approximately symmetrical and within the range of −3 to +3. From the result of 100 bootstrap runs, more than 80% of all of the bootstrapped factors were matched with the factors in the base run solution. From the above results, we decided that the six-factor solution was best based on the robustness, residual distribution, and interpretability of the resulting profiles. The F_{peak} value was selected as zero because changing it did not seem to improve the source profiles.

The profiles and contributions from the PMF result were used to reconstruct VOC concentrations of each of the six factors and examine the source orientation based on the result of the concentration ratios for each factor according to the 16 wind directions.

4.2.4 OH radical loss rate

VOCs react with OH radicals in the presence of solar radiation to generate photochemical oxidants. The photochemical reactivity of each factor resolved by PMF was examined to compare the potential photochemical reactivity with OH radicals. Ozone formation potential (OFP) and OH radical loss rate (L^{OH}) are widely used as indicators that represent the ozone production ability for each VOC component. OFP represents the maximum amount of ozone that can be generated by VOCs, whereas L^{OH} represents how quickly OH radicals react with VOCs. Therefore, OFP is likely to overestimate the VOC contribution to ozone production, whereas L^{OH} is likely to underestimate its contribution. In addition, the MIR values used for the calculation of OFP are not in accordance with the real atmosphere because they have been calculated under the NOx concentration at which the ozone concentration increased most

significantly. In this study, L^{OH} was selected as an indicator to accurately represent ozone production for 1–3 hours when the air mass emitted in the Tokyo Bay coastal area passes through Yokohama and Tokyo. The sum of the OH radical loss rate (L^{OH}) was calculated as follows (Hui et al., 2018; Wu et al., 2016):

$$L_i^{OH} = [VOC]_i \times K_i^{OH} \times N_A \times 10^{24} \Big/ Mw_i \quad (4.1)$$

where L_i^{OH} is the OH radical loss rate of VOC species i (s^{-1}), $[VOC]_i$ is the atmospheric concentration of VOC species i (μg m^{-3}), K_i^{OH} is a constant of the VOC species i reaction rate with OH radicals (10^{-12} cm^3 $molecule^{-1}$ s^{-1}), N_A is the Avogadro constant, and M_{w_i} is the molecular weight of VOC species i. The K_i^{OH} values were derived from Atkinson and Arey (2003) and are shown in Table 4-1. The mean concentrations of each component for each factor were calculated according to the factor contribution and profile to compare the integrated amounts of the OH radical loss rate for the PMF resolved factors. Assuming that O_3 production is in proportion to OH radical loss rate, the reduction rate of the O_3 concentration was estimated in the case of reducing each source emission.

OH radical loss rate (L^{OH}) at the facility k was calculated by a following equation:

$$L_{OH}(k) = L_{OH}(\Delta\theta) \times D_k$$

where $L_{OH}(\Delta\theta)$ is OH radical loss rate for $\Delta\theta$ direction within 30 km at the sampling site and D_k is distance between the sampling site and facility k.

4.3 Results and discussion

4.3.1 Characteristics of VOC concentrations at all sampling sites

Figure 4-4 shows the variations in the VOC concentrations at all sampling sites. The measured VOCs were classified into eight groups: alkanes, alkenes, aromatics, biogenic compounds, aldehydes, ketones, oxygenated compounds, and other VOCs.

Figure 4-4. Variation in the VOC concentrations (ppbv) at the (a) Higashikoujiya, (b) Ushioda, (c) Yokohama Port Symbol Tower, and (d) Honmoku sites in 2019.

At the Higashikoujiya site, the total VOC concentrations were in the range of 53–544 μg m^{-3} with a mean value of 152 μg m^{-3}. Alkanes (41 μg m^{-3}) were the predominant group, followed by aromatics (34 μg m^{-3}), ketones (22 μg m^{-3}), oxygenated compounds (21 μg m^{-3}), other (20 μg m^{-3}), aldehydes (7.3 μg m^{-3}), alkenes (6.2 μg m^{-3}), and biogenic compounds (0.56 μg m^{-3}). Acetone was found to be most abundant species, with a mean concentration of 19 μg m^{-3}, followed by isopropanol (12 μg m^{-3}), ethylbenzene (11 μg m^{-3}), isobutane (8.4 μg m^{-3}), toluene (8.1 μg m^{-3}), m,p-xylenes (6.9 μg m^{-3}), ethane (5.9 μg m^{-3}), propane (5.1 μg m^{-3}), n-butane (4.6 μg m^{-3}), and ethyl acetate (4.5 μg m^{-3}).

At the Ushioda site, the total VOC concentrations were in the range of 29–199 μg m^{-3} with a mean value of 86 μg m^{-3}. Alkanes (33 μg m^{-3}) were the predominant group, followed by other (13 μg m^{-3}), aromatics (11 μg m^{-3}), oxygenated compounds (9.0 μg m^{-3}), aldehydes (7.9 μg m^{-3}), ketones (7.3 μg m^{-3}), alkenes (5.2 μg m^{-3}), and biogenic compounds (0.35 μg m^{-3}). Propane was found to be the most abundant species, with a mean concentration of 6.9 μg m^{-3}, followed by ethyl acetate (6.0 μg m^{-3}), n-butane (5.2 μg m^{-3}), ethane (5.0 μg m^{-3}), acetone (4.8 μg m^{-3}), toluene (4.7 μg m^{-3}), acetaldehyde (4.3 μg m^{-3}), formaldehyde (3.7 μg m^{-3}), isopentane (3.4 μg m^{-3}), and isobutane (2.8 μg m^{-3}).

At the Yokohama Port Symbol Tower site, the total VOC concentrations were in the range of 20–255 μg m^{-3} with a mean value of 70 μg m^{-3}. Alkanes (25 μg m^{-3}) were the predominant group, followed by aromatics (11 μg m^{-3}), other (10 μg m^{-3}), oxygenated compounds (7.0 μg m^{-3}), alkenes (5.9 μg m^{-3}), ketones (5.7 μg m^{-3}), aldehydes (5.0 μg m^{-3}), and biogenic compounds (0.38 μg m^{-3}). Toluene was found to be the most abundant species, with a mean concentration of 5.1 μg m^{-3}, followed by propane (4.9 μg m^{-3}), ethyl

acetate (4.8 μg m^{-3}), acetone (3.8 μg m^{-3}), ethane (3.5 μg m^{-3}), isopentane (3.5 μg m^{-3}), n-butane (3.3 μg m^{-3}), formaldehyde (2.6 μg m^{-3}), acetaldehyde (2.5 μg m^{-3}), and ethylene (2.3 μg m^{-3}).

At the Honmoku site, the total VOC concentrations were in the range of 27–177 μg m^{-3} with a mean value of 79 μg m^{-3}. Alkanes (36 μg m^{-3}) were the predominant group, followed by other (11 μg m^{-3}), aromatics (8.8 μg m^{-3}), oxygenated compounds (7.3 μg m^{-3}), ketones (5.9 μg m^{-3}), alkenes (4.9 μg m^{-3}), aldehydes (4.1 μg m^{-3}), and biogenic compounds (1.2 μg m^{-3}). Butane was found to be the most abundant species with a mean concentration of 8.8 μg m^{-3}, followed by propane (5.1 μg m^{-3}), ethyl acetate (4.4 μg m^{-3}), isopentane (4.2 μg m^{-3}), acetone (4.1 μg m^{-3}), ethane (3.7 μg m^{-3}), pentane (3.5 μg m^{-3}), toluene (3.2 μg m^{-3}), isobutane (3.1 μg m^{-3}), and formaldehyde (2.3 μg m^{-3}).

The average mixing ratios were similar at all the sampling sites except Higashikoujiya, where aromatics, ketones, and oxygenated VOCs displayed higher mixing ratios than at the other sampling sites. The mixing ratios of ethane, propane, n-butane, acetone, and ethyl acetate were consistently high and similar for the Ushioda, Yokohama Port Symbol Tower, and Honmoku sites. This indicates that the same sources affect the air at these sites. Conversely, the mixing ratios of isopropanol, ethylbenzene, and m,p-xylene were only high at the Higashikoujiya site. The air at this site was likely strongly affected by sources different from those of the other three sampling sites.

Figure 4-5 shows the average concentrations of each VOC species.

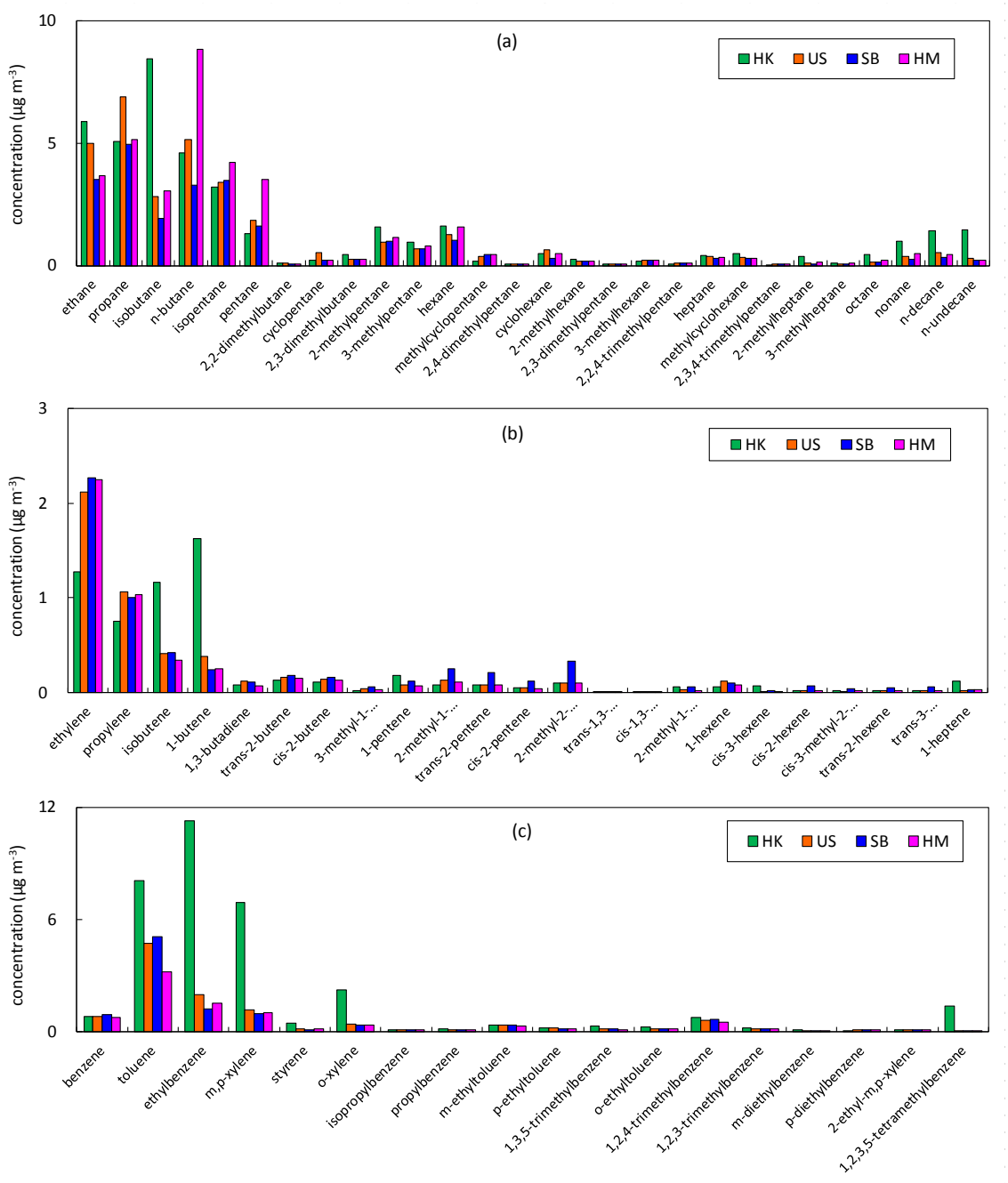

Figure 4-5. Average concentrations of each VOC species: (a) alkanes, (b) alkenes, and (c) aromatics (HK: Higashikoujiya, US: Ushioda, SB: Yokohama Port Symbol Tower, and HM: Honmoku).

As for alkanes, the concentrations of C2-C5 species such as ethane, propane, isobutene, and n-butane were higher than other compounds. Ethylene was highest in the sampling sites (excluding Higashikoujiya), followed by propylene. In the Higashikoujiya site, 1-butene was highest. Aromatics, especially ethylbenzene and m,p-xylene, were notable at the Higashikoujiya site, whereas toluene was highest in the remaining sites. In the Higashikoujiya site, nonane, n-decane, and n-undecane were higher than at the other sites. It has been known that these species were emitted from diesel vehicular exhaust emissions, indicating that the effect of vehicles was significant at the Higashikoujiya site.

4.3.2 Ratios of VOC species

Diagnostic ratios can be used to make simple identifications and assessments of VOC sources. The ratio of benzene to toluene (B/T) is widely used to differentiate vehicular emissions from other combustion sources (Perry and Gee, 1995). Mean B/T ratios of 0.2 and 0.6 are indicators of industrial and vehicular emissions, respectively (Barletta et al., 2005; Barletta et al., 2008), whereas a B/T ratio greater than 1 is an indicator of the burning of bio-fuel, charcoal, and coal (Andreae and Merlet, 2001; Moreira dos Santos et al., 2004). In addition, a B/T ratio of <0.4 and a ratio of xylenes to benzene (X/B) of >1.1 indicate a freshly emitted air mass (Hsu et al., 2018; Liu et al., 2008). The B/T ratios at the Higashikoujiya, Ushioda, Yokohama Port Symbol Tower, and Honmoku sites were 0.17, 0.26, 0.53, and 0.37, respectively, and the X/B ratios at these sites were 21, 2.5, 1.5, and 2.1, respectively. The B/T ratio at the Yokohama Port Symbol Tower site on May 17, 2019 (between 14:00 and 15:00) was 10.3; this was due to fugitive emissions. Except for

this event, the mean B/T ratio at the Yokohama Port Symbol Tower site remained below 0.4. This indicates that ambient air at each site was dominated by freshly emitted air from local VOC sources. These fresh VOCs were likely emitted from a nearby industrial area, where emissions are continuously or temporarily released.

The ethylene/acetylene (E/A) and propylene/acetylene (P/A) ratios are used as indicators to distinguish petrochemical emissions from non-petrochemical emissions. Higher E/A and P/A ratios are likely influenced by olefin-making processes because several petrochemical processes involving olefin processes have strong ethylene and propylene signatures compared to acetylene. Su et al. (2016) reported that the critical ratios distinguishing petrochemical from non-petrochemical emissions were 3.0 for E/A and 1.5 for P/A. The E/A ratios at the Higashikoujiya, Ushioda, Yokohama Port Symbol Tower, and Honmoku sites were 2.0, 4.3, 5.3, and 6.2, respectively, and the P/A ratios at these sites were 0.8, 1.4, 1.8, and 2.9, respectively. Therefore, it is likely that industrial emissions, especially petrochemical emissions, strongly affect the ambient air in the Tokyo Bay coastal area, except at the Higsahikoujiya site.

4.3.3 Estimation of alkene source area

Figure 4-6 shows 16wind-compass rose diagrams indicating the effect of the wind direction on the alkene concentration ratios with respect to the total VOCs.

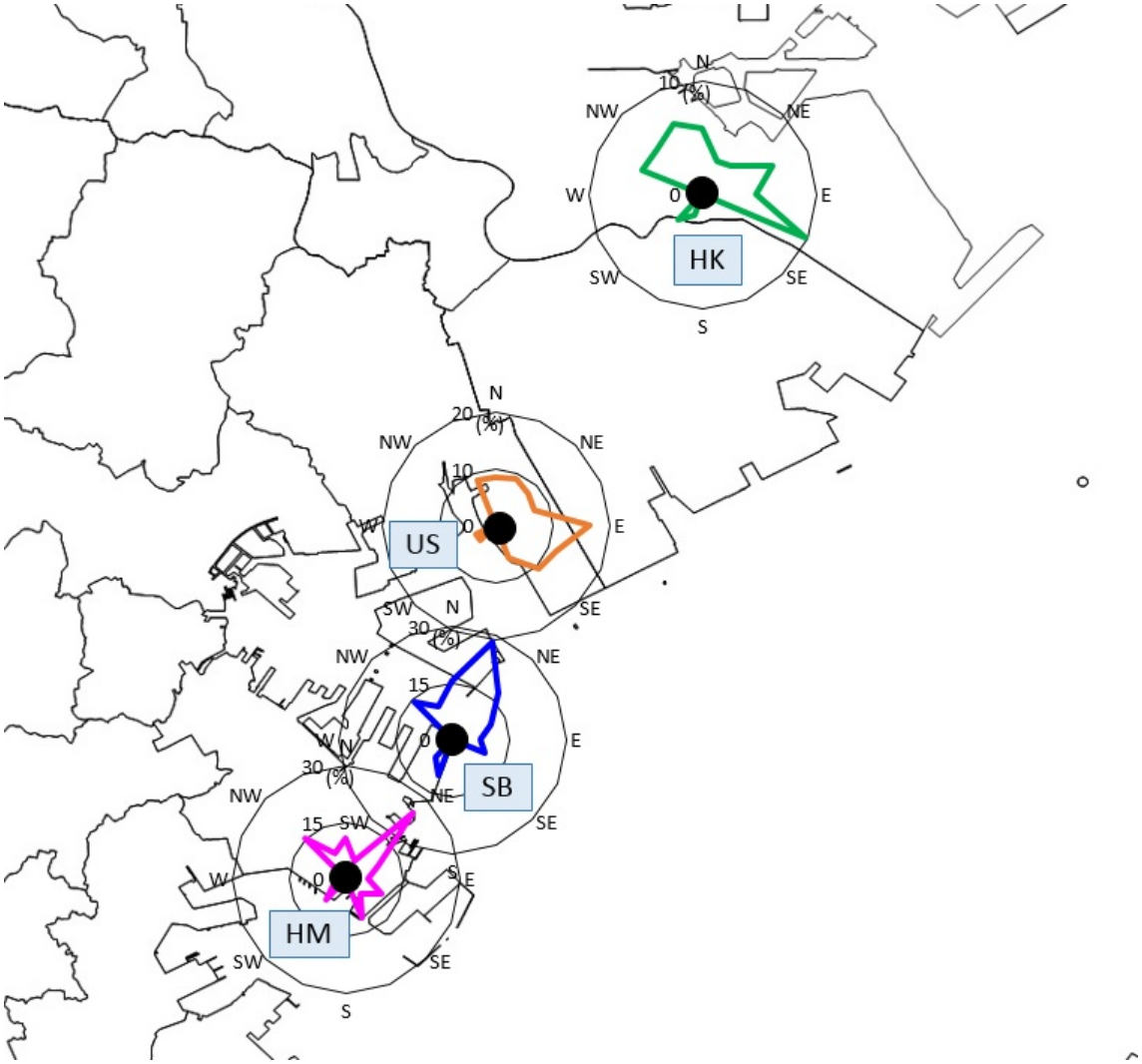

Figure 4-6. Alkene concentration ratios for the 16 wind directions at the four sampling sites (HK: Higashikoujiya, US: Ushioda, SB: Yokohama Port Symbol Tower, and HM: Honmoku).

These results are similar to those of a previous study (Fukusaki et al., 2020). The alkene ratios were obviously higher in the ESE, E, NNE, and NE directions at the Higashikoujiya, Ushioda, Yokohama Port Symbol Tower, and Honmoku sites, respectively. It appears that the impact of these wind directions is significantly stronger

with respect to the alkenes. Consequently, upwind industrial areas are likely to be the major alkene emission sources. It is speculated that the crucial upwind industrial area was the Kawasaki coastal area, located between the Higashikoujiya and Ushioda sites, where there are two petrochemical complexes.

4.3.4 Source apportionment of VOCs via PMF analysis

Six factors were identified via PMF analysis. The source profiles of these factors are shown in Figure 4-7.

The six sources identified were LPG + industry, aged air masses, fuel evaporation, the petrochemical industry, aromatics, and solvent usage. The mean contribution ratios of these six factors were 8.9%, 19.9%, 9.3%, 10.4%, 9.9%, and 14.0%, respectively, whereas that of the residual was 27.7%.

Figure 4-8 and 4-9 show the variations in the contributions of the factors and VOC concentration ratios of the factors according to the 16 wind directions, respectively. The graphs in Figure 4-8 are normalized so that the average of all the contributions for each factor is 1; this allows for a comparison of the temporal patterns of the source contributions.

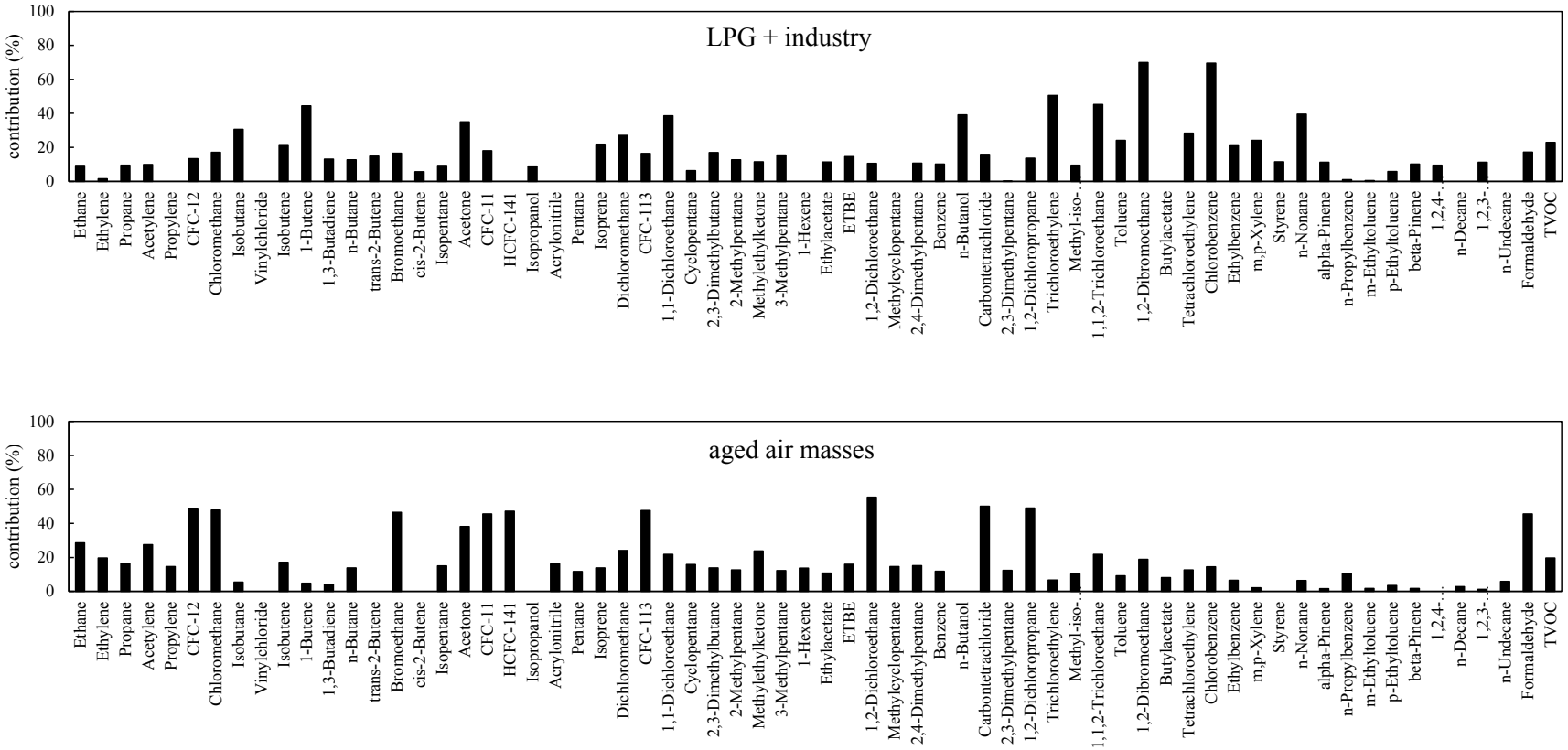
LPG + industry
aged air masses
contribution (%)
0
20
40
60
80
100
Ethane
Ethylene
Propane
Acetylene
Propylene
CFC-12
Chloromethane
Isobutane
Vinylchloride
Isobutene
1-Butene
1,3-Butadiene
n-Butane
trans-2-Butene
Bromoethane
cis-2-Butene
Isopentane
Acetone
CFC-11
HCFC-141
Isopropanol
Acrylonitrile
Pentane
Isoprene
Dichloromethane
CFC-113
1,1-Dichloroethane
Cyclopentane
2,3-Dimethylbutane
2-Methylpentane
Methylethylketone
3-Methylpentane
1-Hexene
Ethylacetate
ETBE
1,2-Dichloroethane
Methylcyclopentane
2,4-Dimethylpentane
Benzene
n-Butanol
Carbontetrachloride
2,3-Dimethylpentane
1,2-Dichloropropane
Trichloroethylene
Methyl-iso-...
1,1,2-Trichloroethane
Toluene
1,2-Dibromoethane
Butylacetate
Tetrachloroethylene
Chlorobenzene
Ethylbenzene
m,p-Xylene
Styrene
n-Nonane
alpha-Pinene
n-Propylbenzene
m-Ethyltoluene
p-Ethyltoluene
beta-Pinene
1,2,4-...
n-Decane
1,2,3-...
n-Undecane
Formaldehyde
TVOC

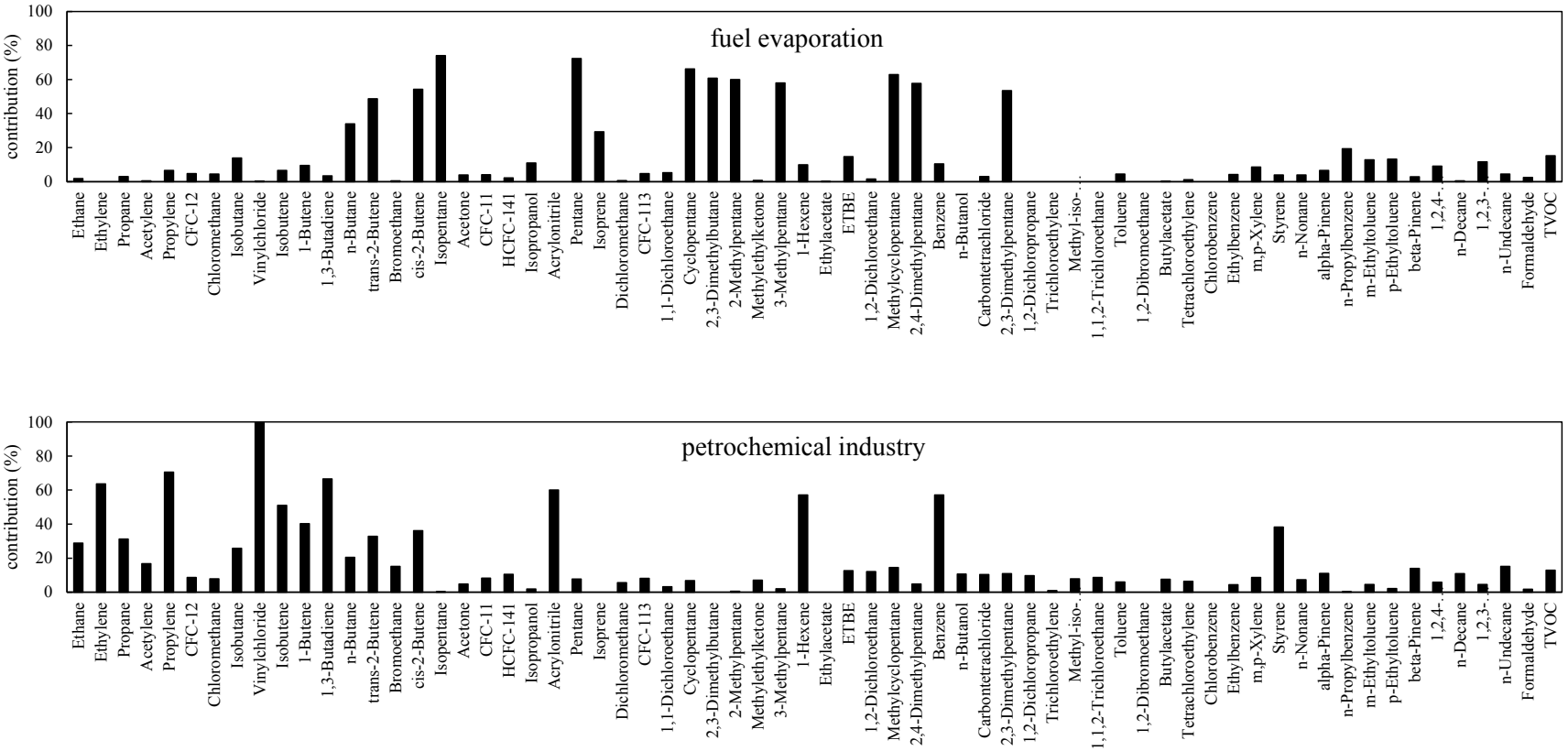
fuel evaporation
petrochemical industry
contribution (%)
0
20
40
60
80
100
Ethane
Ethylene
Propane
Acetylene
Propylene
CFC-12
Chloromethane
Isobutane
Vinylchloride
Isobutene
1-Butene
1,3-Butadiene
n-Butane
trans-2-Butene
Bromoethane
cis-2-Butene
Isopentane
Acetone
CFC-11
HCFC-141
Isopropanol
Acrylonitrile
Pentane
Isoprene
Dichloromethane
CFC-113
1,1-Dichloroethane
Cyclopentane
2,3-Dimethylbutane
2-Methylpentane
Methylethylketone
3-Methylpentane
1-Hexene
Ethylacetate
ETBE
1,2-Dichloroethane
Methylcyclopentane
2,4-Dimethylpentane
Benzene
n-Butanol
Carbontetrachloride
2,3-Dimethylpentane
1,2-Dichloropropane
Trichloroethylene
Methyl-iso-...
1,1,2-Trichloroethane
Toluene
1,2-Dibromoethane
Butylacetate
Tetrachloroethylene
Chlorobenzene
Ethylbenzene
m,p-Xylene
Styrene
n-Nonane
alpha-Pinene
n-Propylbenzene
m-Ethyltoluene
p-Ethyltoluene
beta-Pinene
1,2,4-...
n-Decane
1,2,3-...
n-Undecane
Formaldehyde
TVOC

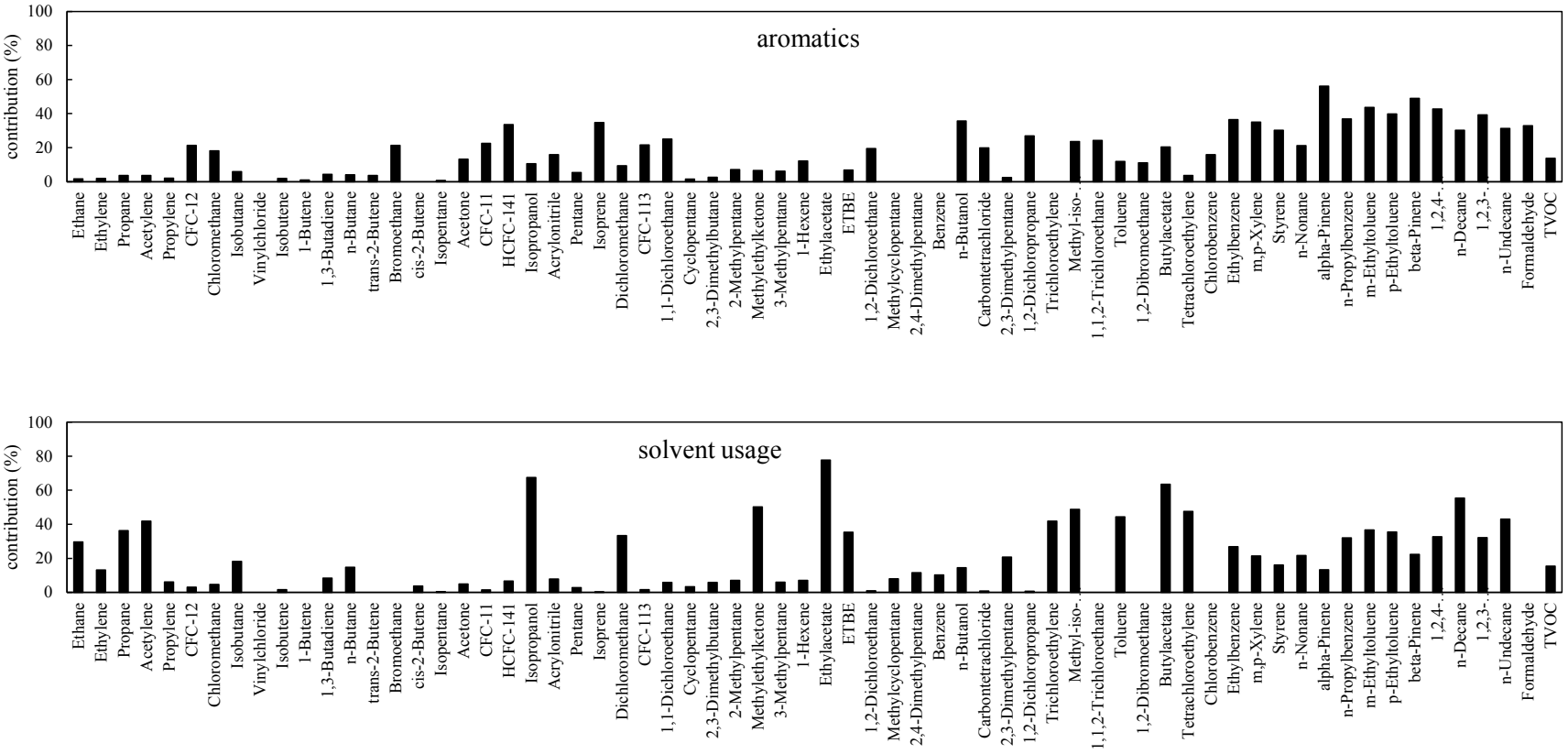

Figure 4-7. The six source profiles obtained via the PMF analysis for data collected at the four sampling sites

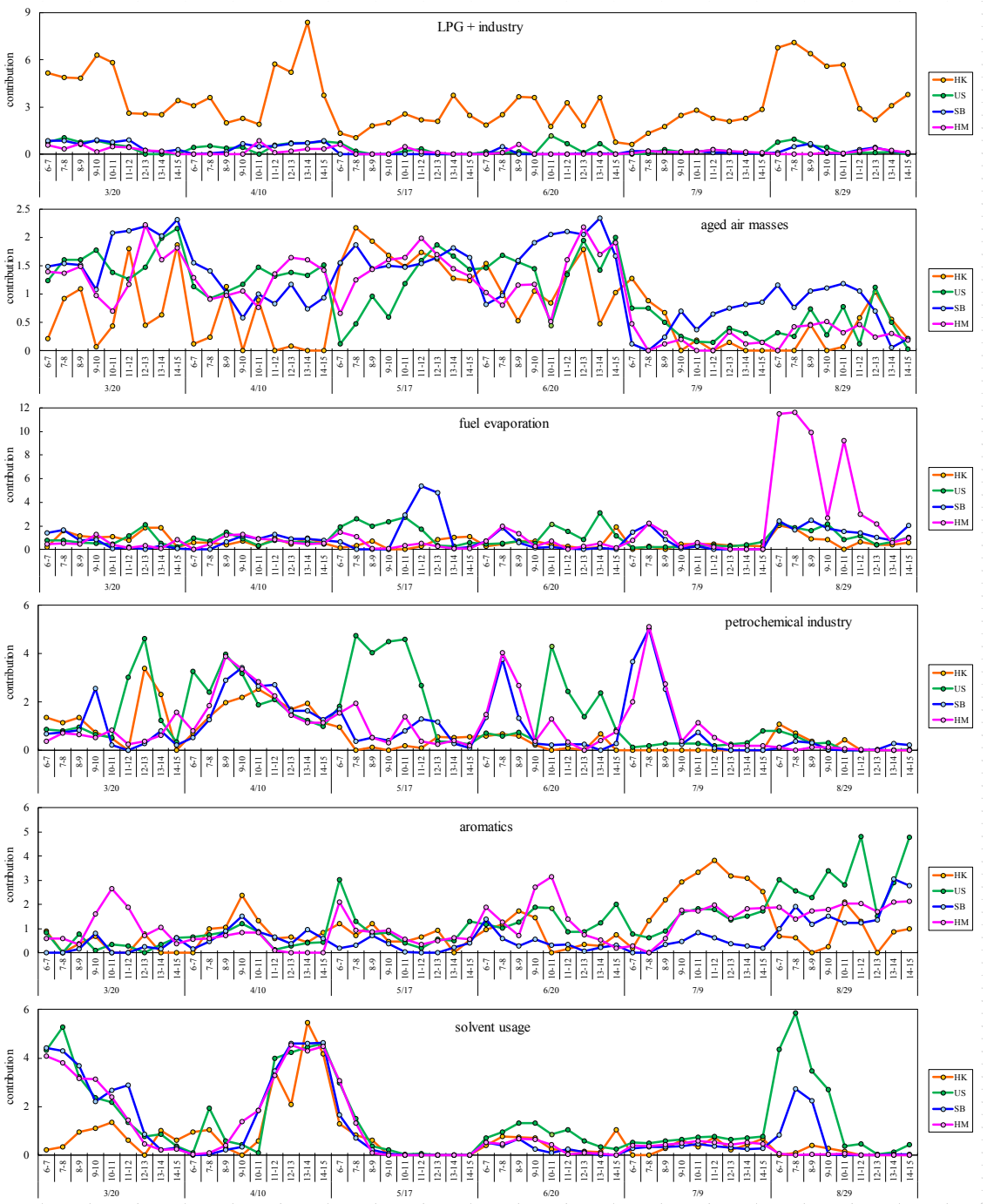

Figure 4-8. Time series of the contributions of the six factors given by the PMF analysis at the four sampling sites (HK: Higashikoujiya, US: Ushioda, SB: Yokohama Port Symbol Tower, and HM: Honmoku).

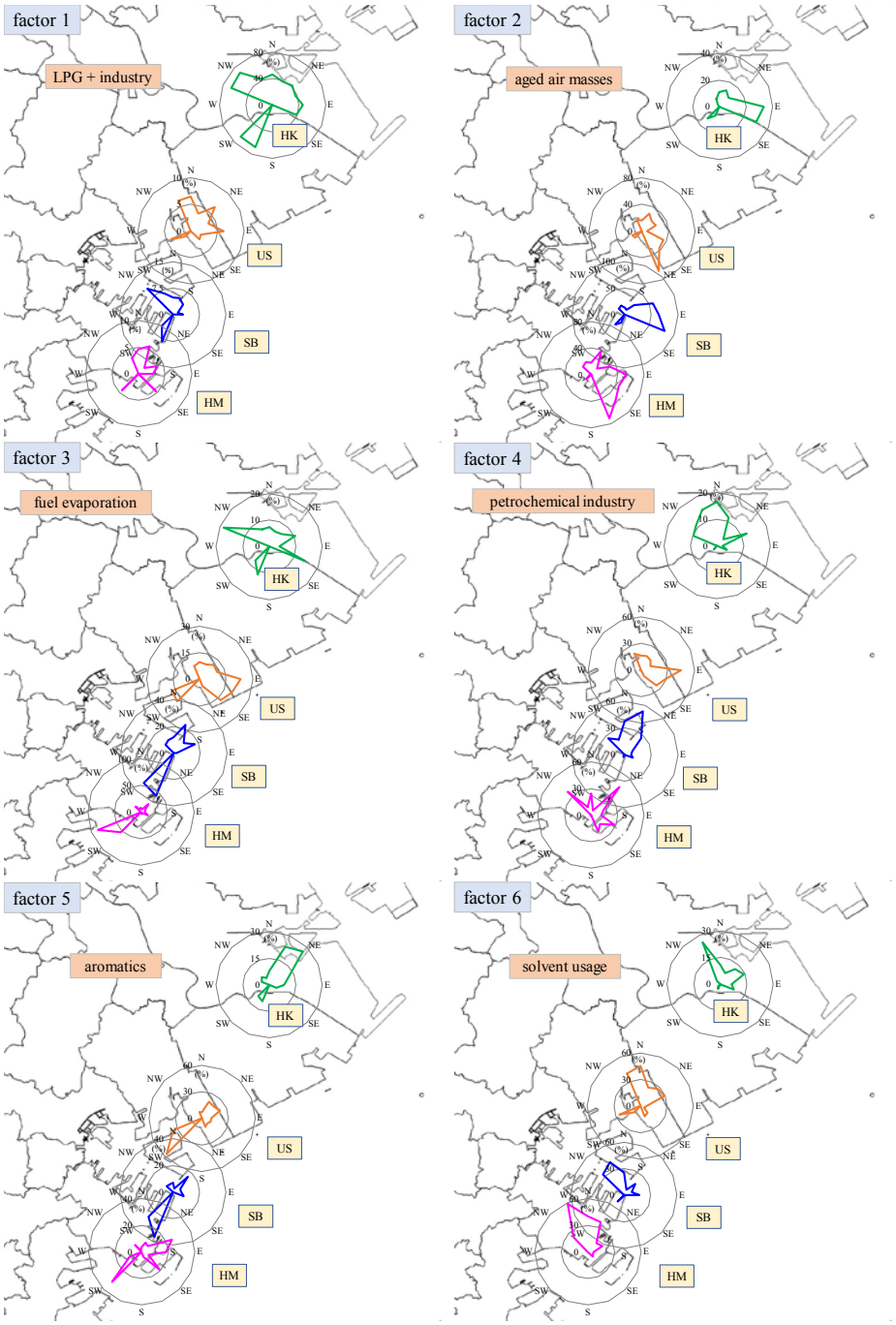

Figure 4-9. Concentration ratios of the six factors according to the 16 wind directions at the four sampling sites (HK: Higashikoujiya, US: Ushioda, SB: Yokohama Port Symbol Tower, and HM: Honmoku).

Factor 1 has a high loading of 1-butene, trichloroethylene, 1,2-dibromoethane, and chlorobenzene. Propylene, trans-2-butene, and 1-butene are likely released by the use of LPG because propane, isobutene, and n-butane are the main components of LPG (Hui et al., 2018; Lyu et al., 2016; Song et al., 2008; Yang et al., 2013). LPG is used as fuel for households, industries, and vehicles and as a raw chemical material. The time series of the contribution of factor 1 is shown in Figure 4-8. The contribution of factor 1 was highest at the Higashikoujiya site. LPG is frequently used in Tokyo, and there are three LPG stations around the Higashikoujiya site. 1-Butene was well correlated with isobutene ($r = 0.98$) and isobutene ($r = 0.99$), which are also associated with LPG usage (Zhang et al., 2018). However, the loadings of the remaining components, such as propylene and trans-2-butene, were not high. The low loadings of these components were due to their apportionment to other sources such as fuel evaporation and the petrochemical industry. Meanwhile, trichloroethylene is used in metal product manufacturing industries around the Higashikoujiya site. The factor loading of formaldehyde is also fairly high. It is assumed that formaldehyde was emitted via LPG combustion associated with households, industrial activities, and vehicles. Consequently, factor 1 was identified as LPG + industry. Factor 1 had high loadings of 1,2-dibromoethane and chlorobenzene as well as 1-butene and trichloroethylene. The sources of 1,2-dibromoethane and chlorobenzene were independent of the sources of 1-butene and trichloroethylene because the mixing ratios were not correlated to 1-butene and trichloroethylene. Aircraft may also affect the VOC mixing ratios at the Higashikoujiya site because of the vicinity of the Haneda Airport. Guo et al. (2007) reported that the impact of the airport on the VOC levels was insignificant at a sampling site located approximately 3 km south of the Hong Kong International Airport. The impact of emissions by aircraft at the Higashikoujiya site

(located approximately 2 km west of the Haneda Airport) awaits further investigation.

Factor 2 was identified as aged air masses. High percentages of halo hydrocarbons such as CFC-12 (49%), chloromethane (48%), CFC-113 (48%), 1,2-dichloroethane (55%), and carbon tetrachloride (50%), which have long atmospheric lifetimes, were observed in factor 2. Zheng et al. (2020) reported that freons, chloroform, chloromethane, dichloromethane, tetrachloroethylene, carbon tetrachloride, 1,2-dichloroethane, and 1,4-dichlorobenzene accounted for 43%–65% of the background source in Calgary, Alberta, Canada. However, another component with a high percentage in factor 2 was formaldehyde, which is not only emitted from industrial facilities but is also generated by photochemical reactions in the presence of solar radiation. We classified this factor as aged air masses and we considered formaldehyde to be a secondary product generated via photochemical reactions. The variations in the contributions of factor 2 were similar for all the sampling sites (Figure 4-8). This further implies that factor 2 was made up of aged air masses.

Factor 3 was identified as fuel evaporation because of its high percentages of trans-2-butene, cis-2-butene, isopentane, and n-pentane. Isopentane and n-pentane are typical tracers of volatile gasoline (Hui et al., 2018; Lau et al., 2010; Wang et al., 2013). Isobutane, n-butane, and trans-2-butene are also important species in volatile fuels. Most of these VOCs are the result of fuel evaporation, in particular that of gasoline (Guo et al., 2011). The process when fuel evaporation species are emitted is categorized into two patterns: fuel evaporation and exhaust gas. Exhaust gas includes not only fuel non-combustion components, but also combustion components such as ethylene and acetylene. However, ethylene, acetylene, and other combustion products were not included as contributors to

factor 3. Therefore, this factor was identified as fuel evaporation. The contribution of factor 3 was highest in May, June, and August. This indicates that the contribution level of factor 3 is dependent on the ambient temperature. At the Honmoku site, the contribution of factor 3 was highest in August when the mean temperature was the highest. VOC concentration ratios of factor 3 were most dominant for the WSW wind direction at the Honmoku site (Figure 4-9), suggesting that sources related to fuel evaporation exist in the WSW direction with respect to Honmoku.

Factor 4 was identified as the petrochemical industry. Factor 4 has high loadings of ethylene, propylene, vinyl chloride, 1,3-butadiene, acrylonitrile, 1-hexene, benzene, and styrene. Petrochemical sources are characterized by high percentages of ethylene and propylene (Chen et al., 2019), which are major raw materials for the petrochemical industry (Leuchner and Rappengluck, 2010). Alkenes and styrene are monomers used for the synthesis of various plastic materials, including polyethylene, polypropylene, and polystyrene (Ma et al., 2019; Whiteley et al., 2000). Vinyl chloride is a raw material used for the production of polyvinyl chloride (i.e., PVC) in the petrochemical industry (Na et al., 2001). 1,3-Butadiene is an important pyrolysis product of crude oil and gas (Morrow, 1990) and a raw material of synthetic rubber. Benzene is used to make chemicals such as plastics, paints, and dyes (ATSDR, 2007). Acrylonitrile is used as a raw material for acrylonitrile butadiene styrene (i.e., ABS) resin. All these species have been used in petrochemical industrial complexes. The contributions of factor 4 were higher at the Ushioda, Yokohama Port Symbol Tower, and Honmoku sites than at the Higashikoujiya site (Figure 4-8). The variation in the contribution of factor 4 at the Yokohama Port Symbol Tower site was consistent with that at the Honmoku site, whereas the contribution

at the Ushioda site was not consistent with those at the Yokohama Port Symbol Tower and Honmoku sites. The factor 4 concentration ratios according to the 16 wind directions agreed with both the location of the petrochemical industrial complexes in the Kawasaki coastal area and the alkene concentration ratios (Figure 4-9). We compared the time series of the alkene concentration ratios with that of the contribution of factor 4 to further verify the reliability of this estimated result. The correlation coefficients are good: 0.95 at Ushioda, 0.74 at the Yokohama Port Symbol Tower, 0.74 at Honmoku, and 0.48 at Higashikoujiya, indicating that Ushioda is in closest proximity to the alkene sources. The relative contributions of the factors with respect to the wind directions with the highest alkene ratios were 4.4, 3.7, and 2.7 at the Ushioda, Yokohama Port Symbol Tower, and Honmoku sites, respectively. This implies that Ushioda is the closest to the major alkene source, followed by the Yokohama Port Symbol Tower and Honmoku. This suggests that the alkene sources are primarily derived from the petrochemical industry and that the difference in the alkene contributions at the Ushioda site from those at the Yokohama Port Symbol Tower and Honmoku sites was caused by the wind direction.

Factor 5 was identified as aromatics, with high loadings of m-ethyltoluene, p-ethyltoluene, 1,2,4-trimethylbenzene, ethylbenzene, and m,p-xylene. Vehicle exhaust, combustion, and solvent usage are major sources of atmospheric aromatics (Ma et al., 2019). The low contribution of acetylene, which is a significant tracer of vehicle exhaust and combustion emissions, to factor 5 indicates that aromatics were not associated with vehicle exhaust or combustion emissions. In addition, aromatics were poorly correlated with ethylene and acetylene, suggesting that the sources of these emissions were related to solvent usage (e.g., textiles, furniture manufacturing, shoemaking, printing, and/or plastics (Selia et al.,

2001; Ling et al., 2011)). The high levels of m,p-xylene observed in factor 5 represent adhesives and sealants (Ma et al., 2019; Ling et al., 2011). Ethylbenzene is a major constituent of furniture-painting emissions (Li et al., 2018), while aromatics such as m,p-xylene are compounds characteristic of architectural coatings (Liu et al., 2008). The major sources of these aromatic species (ethylbenzene, xylene, 1,3,5-trimethylbenzene, and 1,2,4-trimethylbenzene) around the sampling sites have been identified by the PRTR data as the painting industry, especially of ships and vehicles. Therefore, the factor contribution ratios were compared with the distance-weighted emission ratios obtained based on the PRTR data by considering 16 wind directions (Fukusaki et al., 2020) (Figure 4-10).

The factor contribution ratios were approximately consistent with the distance-weighted emission ratios, with the exception of Higashikoujiya. It is assumed that there was no effect from the large painting facilities of ships and vehicles located in the SSE direction in Ushioda and the S direction in Honmoku, respectively, during the six field campaigns. These results imply that factor 5 was related to solvent usage. Factor 5 had a high loading of pinenes and formaldehyde. Pinenes are not only primarily emitted from conifers, but they are also raw materials for fragrances and medicines. Because the concentration variations of the pinenes were not correlated with those of the aromatics, pinenes did not come from the same sources as aromatics. Formaldehyde is emitted from large facilities that utilize paint containing aromatics and that have introduced combustion treatment equipment as a measure against exhaust gas. The variations in the contribution of factor 5 exhibited no obvious characteristics (Figure 4-8). This indicates that the aromatic sources were unevenly distributed and/or emitted temporarily.

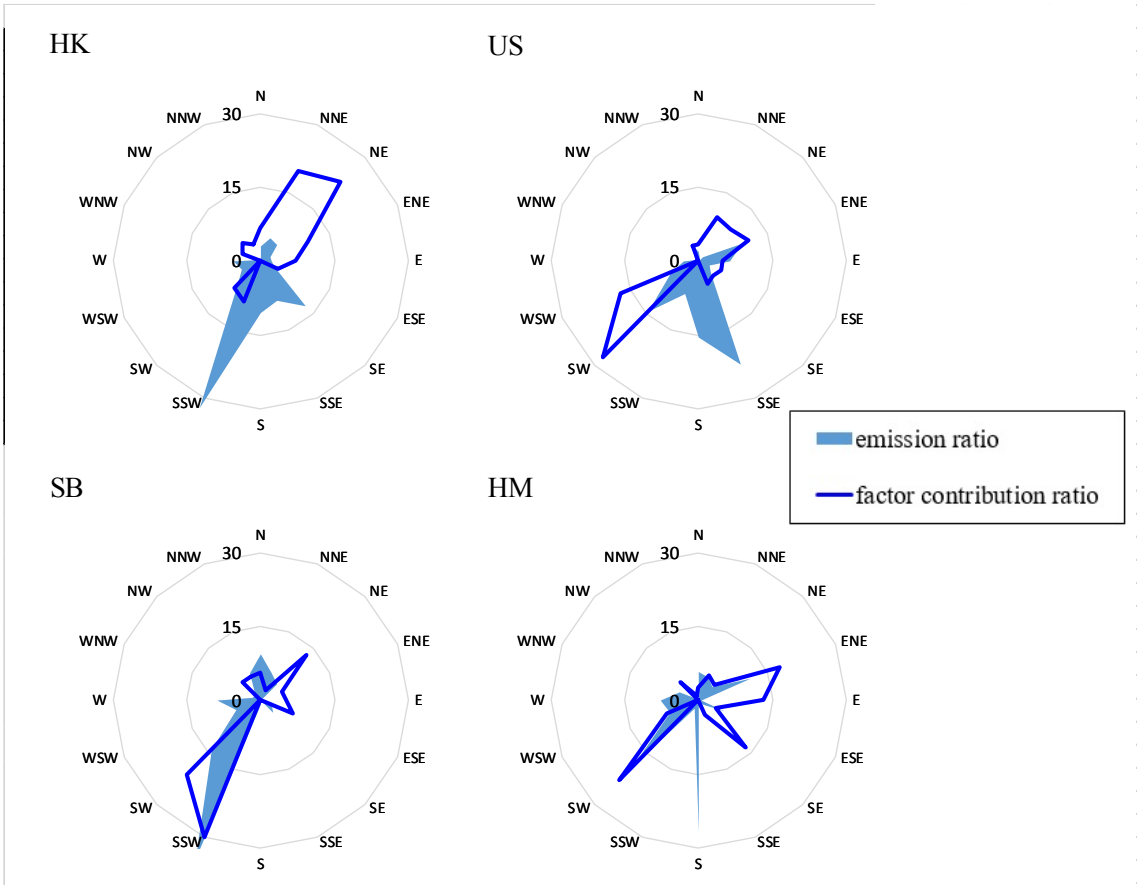

Figure 4-10. Comparison of the factor contribution ratios of the aromatics (xylene, ethylbenzene, 1,3,5-trimethylbenzene, and 1,2,4-trimethylbenzene) with the distance-weighted emission ratios at each site (HK: Higashikoujiya, US: Ushioda, SB: Yokohama Port Symbol Tower, and HM: Honmoku).

Factor 6 was identified as solvent usage. Ethyl acetate is dominant in factor 6, followed by isopropanol, butyl acetate, n-decane, methylethylketone, tetrachloroethylene, and toluene. These are common organic species in solvents. Ethyl acetate is used in paints and adhesives. Tetrachloroethylene is widely used as a dry-cleaning agent, in printed circuit boards, and in precision metal parts cleaning (Zhou et al., 2011). Methylethylketone and

toluene are frequently used as solvents for painting. The variations in the contributions of factor 6 at the four sampling sites were similar (Figure 4-8). This indicates that many sources of solvent usage ubiquitously exist around all the sampling sites and that they were emitted uniformly during the sampling period. VOC concentration ratios of factor 6 according to the 16 wind directions indicate that these are inland sources (Figure 4-9).

The source apportionment in the Tokyo Bay coastal area differed significantly compared to those resolved in other countries. It is notable that coal and biomass combustion and vehicular exhaust emissions were not identified in this study. This result agrees with the source assessment from the VOC ratios. Figure 4-11 shows the factor contributions at the sampling sites.

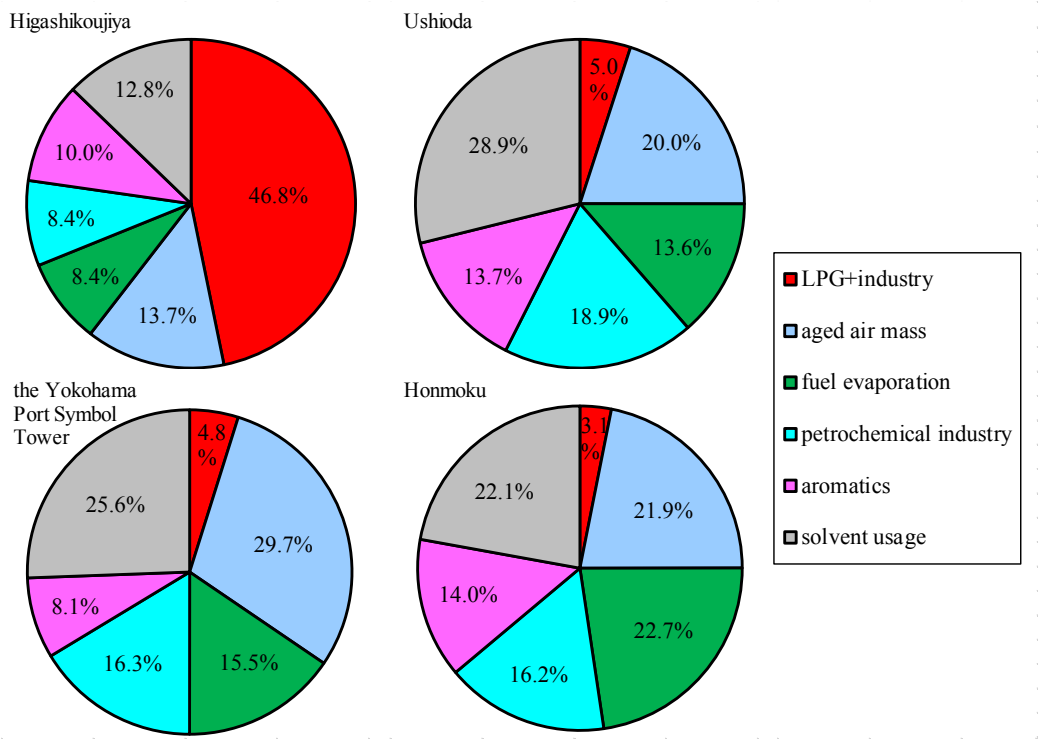

Figure 4-11. Factor contributions at all sampling sites.

At the Higashikoujiya site, the contribution of LPG + industry to the total VOC concentrations was dominant at 46.8%, followed by aged air masses at 13.7% and solvent usage at 12.8%. This suggests the strong impact of ubiquitous sources such as LPG usage and the manufacturing industries around the Higashikoujiya site.

At the Ushioda site, solvent usage largely contributed to the total VOC concentrations at 28.9%, followed by aged air masses at 20.0% and the petrochemical industry at 18.9%. The strongest impact on solvent usage is ascribed to manufacturing facilities, which treat paints, adhesives, and sealants, around the Ushioda site, especially metal manufacturing facilities. Effect of vessel and glass manufacturing facility, power plants, and LPG storage facility was not nearly found in this study. Moreover, this site is also susceptible to petrochemical industrial emissions because of its comparatively closer position to the petrochemical industrial complexes compared to the other sampling sites.

At the Yokohama Port Symbol Tower site, the contribution of aged air masses to the total VOC concentration was 29.7%, followed by solvent usage at 25.6% and the petrochemical industry at 16.3%. The Yokohama Port Symbol Tower site is located at the edge of Yokohama City, facing Tokyo Bay, and it is also located between the petrochemical complexes and the Honmoku site. The frequent southerly wind along with the enhancement of VOC loss via photochemical reactions and the development of a mixing layer in the summer result in clean and/or aged air at the Yokohama Port Symbol Tower site.

At the Honmoku site, the contribution of fuel evaporation to the total VOC concentrations was most significant at 22.7%, followed by solvent usage at 22.1% and aged air masses at 21.9%. The contribution of fuel evaporation was highest in August at the Honmoku

site, which is adjacent to petroleum refineries. This reason is primarily due to the fact that the high temperature in August promoted fuel evaporation.

The source contributions showed significant spatial variations across all sampling sites, with the exception of the Higashikoujiya site. These results indicate that meteorological parameters and location are the factors affecting the source contributions in the Tokyo Bay coastal area. Higashikoujiya showed different VOC apportionments when compared with those observed at the other sites. If Higashikoujiya's data are excluded, the five factors, excluding LPG + industry, were resolved by PMF, with the result being that the correlation coefficient between the observed and predicted values of the total VOC increased from 0.38 to 0.79 (Figure 4-12), while the mean contribution ratios of the residual decreased from 27.7% to 22.9%.

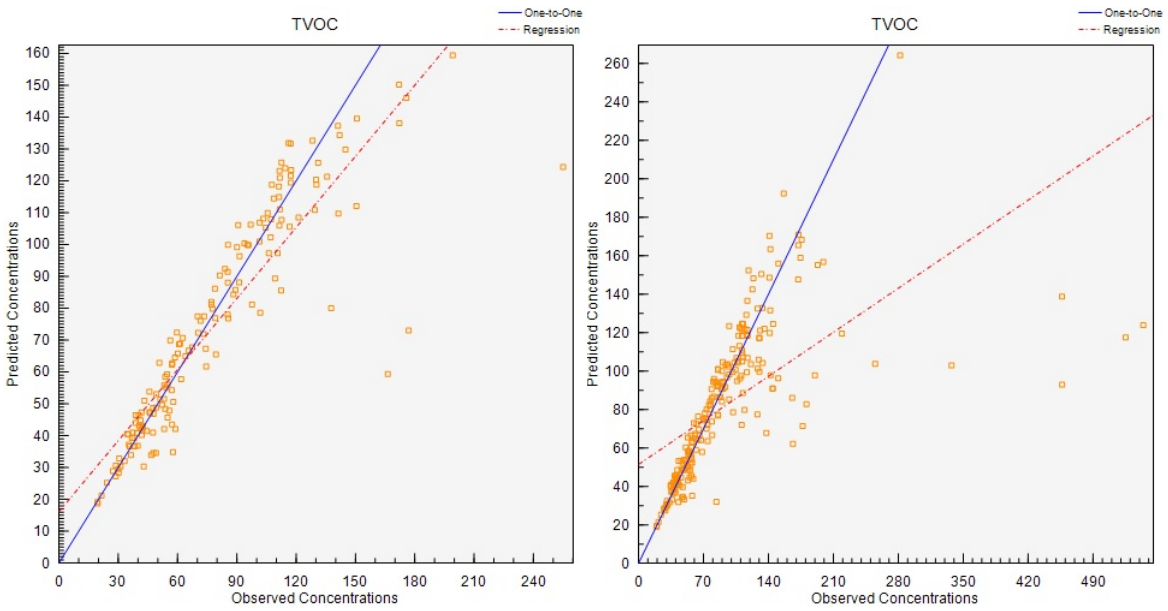

Figure 4-12. Correlations between the observed and predicted concentrations (left: all sampling sites, right: three of the four sites, excluding the Higashikoujiya site).

These results imply that Ushioda, the Yokohama Port Symbol Tower, and Honmoku were strongly affected by the fixed VOC sources in the vicinity, whereas Higashikoujiya was strongly affected by other VOC sources such as vehicular exhaust emissions. The mean contribution ratio of the residual could be explained by other VOC sources such as vehicular exhaust emissions, the Haneda airport, and vessels which were not separated by PMF because of the strength of the industrial VOC source emissions. It suggests that vehicular exhaust emissions, the Haneda airport, and vessel exhaust emissions do not strongly affect VOC composition in the Tokyo Bay coastal area.

4.3.5 Estimation of major alkene sources

The six major VOC sources were determined by PMF analysis. Figure 4-13 shows the average VOC concentration and the percent contribution for each factor, which were reconstructed by multiplying the source profile with the factor contribution.

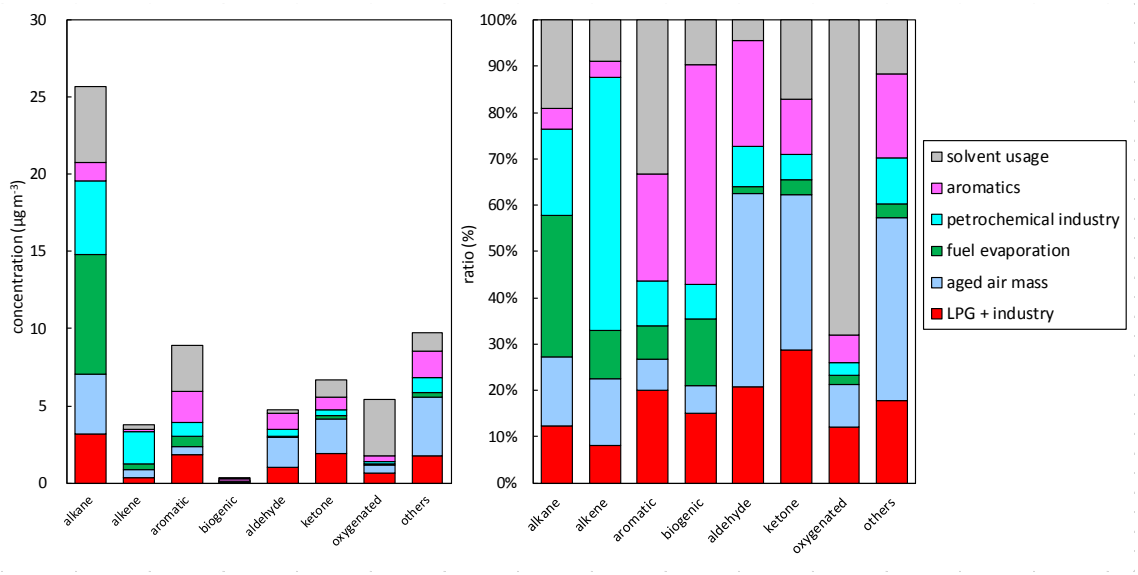

Figure 4-13. Average VOC concentrations for different compound classes and the percent contribution of each source factor resolved by PMF.

Percentage of alkenes was overwhelmingly highest in the petrochemical industry. Furthermore, the petrochemical industry contribution ratios were most consistent with the alkene concentration ratios according to the 16 wind directions (Figure 4-14).

The above results suggested that the petrochemical complexes in the Kawasaki coastal area was the main alkene source.

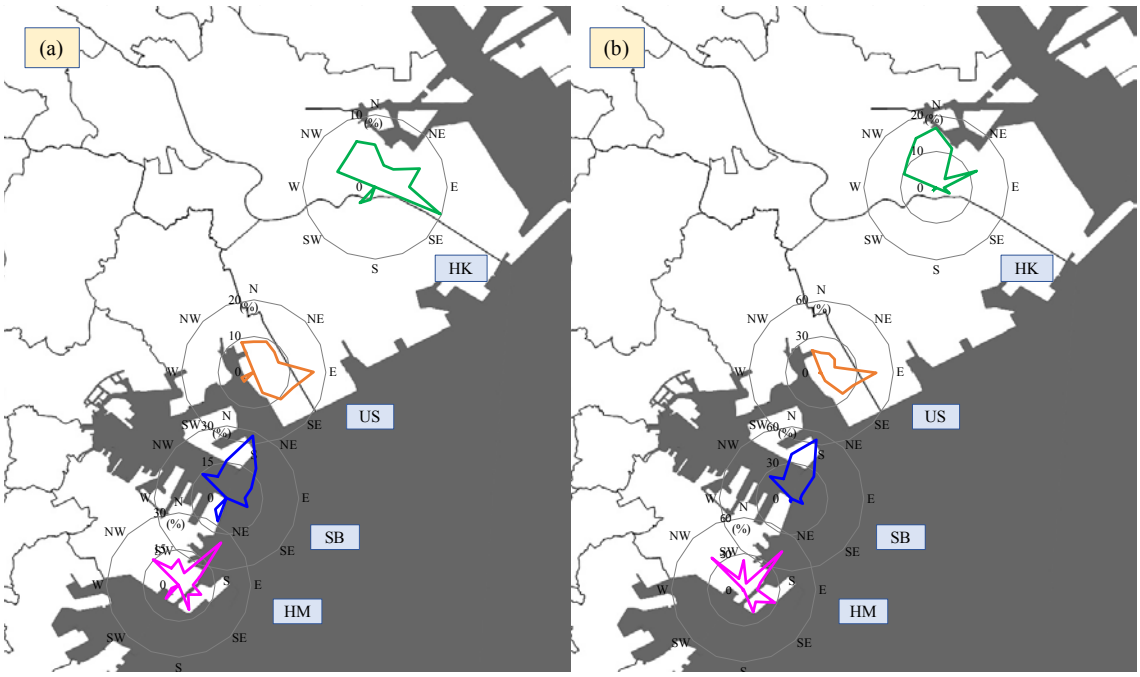

Figure 4-14. (a) Alkene concentration ratios and (b) Petrochemical industry contribution ratios according to the 16 wind directions at the four sampling sites (HK: Higashikoujiya, US: Ushioda, SB: Yokohama Port Symbol Tower, and HM: Honmoku).

4.3.6 Comparison of OH radical loss rates among factors resolved by PMF

A comparison of the average L^{OH} values for the six factors at all sampling sites is shown in Figure 4-15.

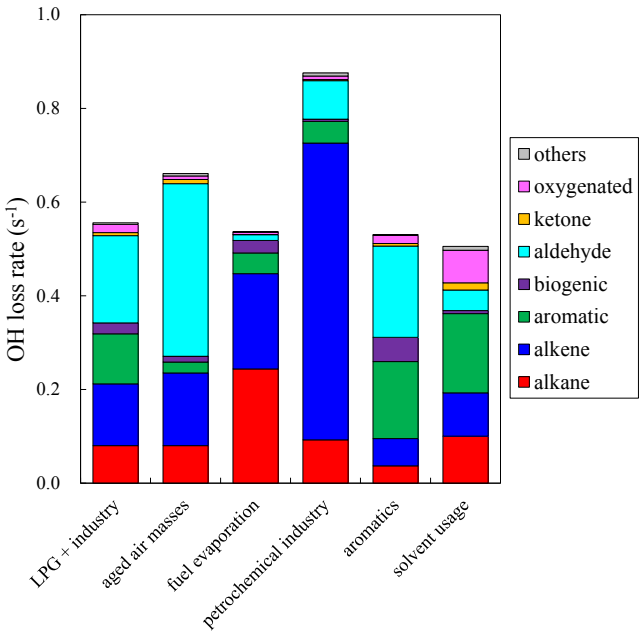

Figure 4-15. Comparison of the OH radical loss rates for the six factors.

The most significant L^{OH} source was the petrochemical industry (accounting for 29.1% of the total L^{OH}, excluding the L^{OH} of the aged air masses), followed by LPG + industry (18.5%), fuel evaporation (17.9%), aromatics (17.7%), and solvents (16.8%). This suggests that Ox concentrations can be reduced by up to about 30% by controlling emissions from the petrochemical industry. In particular, alkenes with high OH reactive rate constants are major components in the petrochemical industry, which has a higher fraction of alkenes to total L^{OH} compared to other sources. Table 4-2 shows the contribution to total OH radical loss rate excluding aged air masses, and Table 4-3 shows the top 10 components contributing to OH radical loss rates for 5 of the factors. Alkenes of the petrochemical industry most significantly contributed to total OH radical loss rate, followed by alkanes of the petrochemical industry, and alkenes of fuel evaporation. With respect to individual components, propylene from the petrochemical industry contributed

most significantly to the total OH radical loss rate, followed by ethylene of the petrochemical industry.

Table 4-2. Contribution to total OH radical loss rate

	LPG+industry	fuel evaporation	petrochemical industry	aromatics	solvent usage
alkane	2.7	8.1	3.1	1.2	3.3
alkene	4.4	6.8	21.1	1.9	3.1
aromatic	3.6	1.5	1.5	5.5	5.6
biogenic	0.8	0.9	0.2	1.7	0.2
aldehyde	6.2	0.4	2.7	6.5	1.5
ketone	0.2	0.0	0.1	0.2	0.5
oxygenated	0.6	0.2	0.2	0.6	2.3
others	0.1	0.0	0.2	0.1	0.3

Table 4-3. The top 10 components contributing to the OH radical loss rate for 5 factors resolved by PMF.

LPG+industry		aged air masses		fuel evaporation	
component	L^{OH}	component	L^{OH}	component	L^{OH}
Acetaldehyde	0.119	Acetaldehyde	0.192	Isopentane	0.072
Formaldehyde	0.067	Formaldehyde	0.176	trans-2-Butene	0.036
1-Butene	0.045	Ethylene	0.055	n-Butane	0.033
Isobutene	0.044	Propylene	0.041	Pentane	0.032
Toluene	0.034	Isobutene	0.035	cis-2-Butene	0.031
mp-Xylene	0.026	Isopentane	0.015	2-methyl-2-butene	0.025
Isoprene	0.018	n-Butane	0.014	Isoprene	0.024
Isobutane	0.017	Toluene	0.013	2-Methylpentane	0.021
n-Butane	0.013	Propane	0.012	Propylene	0.019
Ethylbenzene	0.012	Isoprene	0.012	Hexane	0.018

petrochemical industry		aromatics		solvent usage	
component	L^{OH}	component	L^{OH}	component	L^{OH}
Propylene	0.200	Formaldehyde	0.128	Toluene	0.063
Ethylene	0.179	Acetaldehyde	0.067	Acetaldehyde	0.044
Isobutene	0.104	mp-Xylene	0.038	Ethylene	0.037
Acetaldehyde	0.075	124-Trimethylbenzene	0.033	Ethylacetate	0.031
1-Butene	0.040	Isoprene	0.029	Propane	0.028
13-Butadiene	0.028	Ethylbenzene	0.020	124-Trimethylbenzene	0.025
trans-2-Butene	0.024	alpha-Pinene	0.017	mp-Xylene	0.023
Propane	0.024	Toluene	0.017	Isopropanol	0.023
cis-2-Butene	0.021	135-Trimethylbenzene	0.011	Propylene	0.017
n-Butane	0.020	2-methyl-2-butene	0.011	Ethylbenzene	0.015

Previous studies considering the photochemical reactivity of VOC species (Shao et al., 2016; Mo et al., 2017; Xue et al., 2017) have also reported that alkenes were dominant contributors to ozone photochemical production and that the most significant OFP source was the petrochemical industry. Highly reactive species, such as ethylene and propylene, are known to be primarily emitted from petrochemical industry facilities (Su et al., 2016). This result is in good agreement with these previous studies, suggesting that emissions from the petrochemical industry are also a significant contributor to ozone production in the Kanto region.

We attempted to calculate the OH radical loss rate for each of the industrial VOC sources. We confined the analysis to factor 3 (fuel evaporation), factor 4 (the petrochemical industry), and factor 5 (aromatics) because it was shown that the main sources for these factors were located in the Tokyo Bay coastal area. The Higashikoujiya site was excluded from this analysis due to its limited impact upon industrial VOC sources. First, the strength of the OH radical loss rate for the petrochemical complexes and refineries was calculated using the OH radical loss rate for the Ushioda, Yokohama Port Symbol Tower, and Honmoku sites. The distance between the petrochemical complex and the Ushioda, Yokohama Port Symbol Tower, and Honmoku sites were set as 9.5, 14.2, and 16.4 km, respectively, and the distance between the refinery and the Ushioda, Yokohama Port Symbol Tower, and Honmoku sites were set as 0.3, 2.5, and 10.0 km, respectively (Figure 4-16).

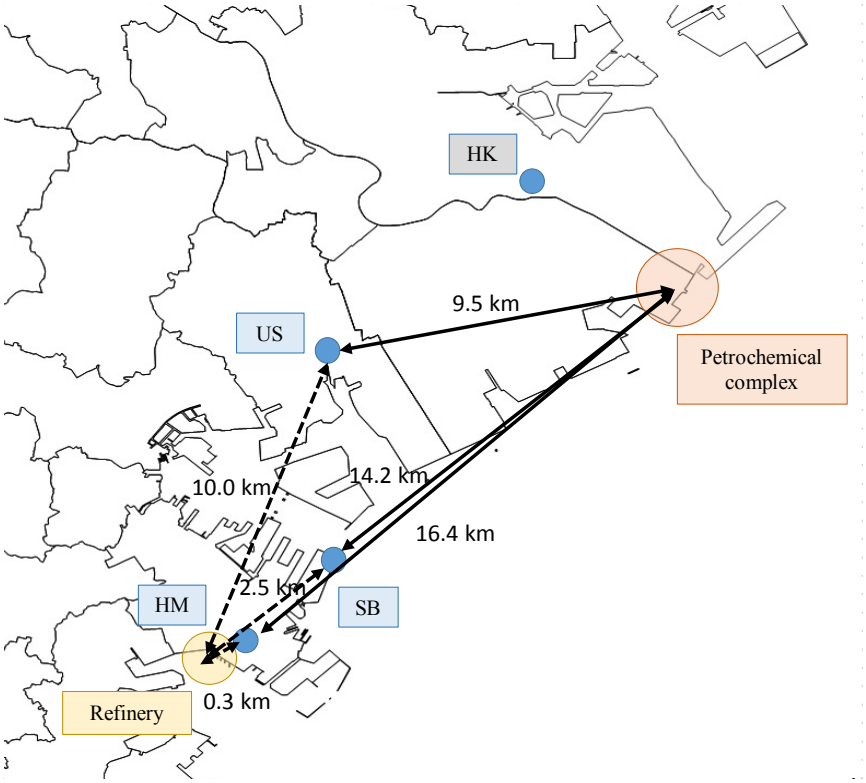

Figure 4-16. Locations of petrochemical complex and refinery.

The wind directions in which the petrochemical complexes affect the Ushioda, Yokohama Port Symbol Tower, and Honmoku sites were set as E, NNE, and NE, respectively, and the wind directions in which the refineries affect the Ushioda, Yokohama Port Symbol Tower, and Honmoku sites were set as SW to WSW, SSW to SW, and SW to SSW, respectively. The OH radical loss rates for the petrochemical complex and refinery for factors 3 and 4 are shown in Table 4-4.

Table 4-4. OH radical loss rate for the petrochemical complex and refinery for factor 3 and 4 (US: Ushioda, SB: Yokohama Port Symbol Tower, and HM: Honmoku).

	factor3		factor4	
	petrochemical complexes	refineries	petrochemical complexes	refineries
US	1.2	1.2	3.8	0.14
SB	0.87	1.7	3.2	0.23
HM	0.65	8.3	2.3	0.10

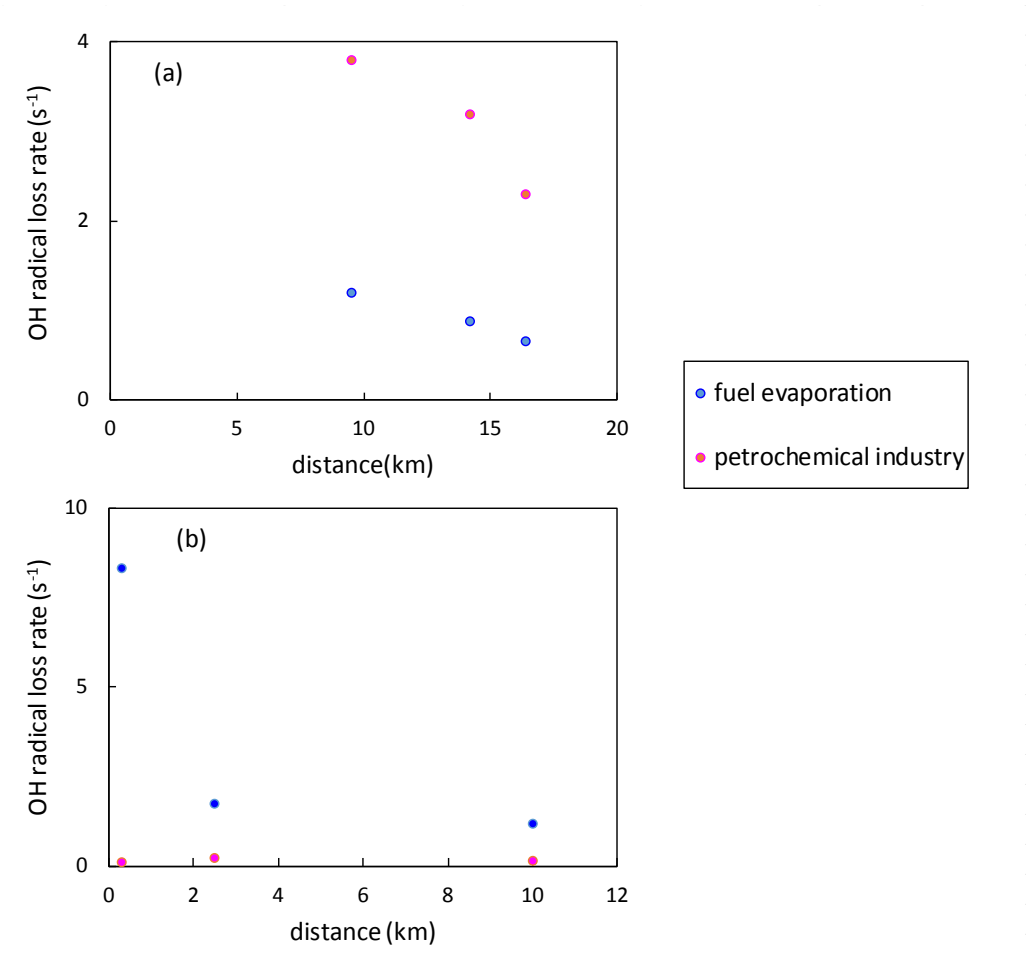

Figure 4-17. Correlation of OH radical loss rates for the sampling sites to distance from (a) petrochemical complex and (b) refinery.

It was assumed that the OH radical loss rate was not changed if the distance between the VOC source and the sampling site was within 1 km. The impact of the petrochemical complex on each sampling site was nearly in inverse proportion to the distance (Figure 4-17). As a result, it was estimated that the OH radical loss rate of the petrochemical complexes and the refineries for factor 3 were 10 and 3 s^{-1}, respectively. For factor 4 these loss rates were 35 and 0.5 s^{-1}. Ultimately, the OH radical loss rate for the petrochemical complex was more than 10 times higher than for refinery. In the same way, the OH radical loss rate of the main aromatic sources for factor 5 was calculated. Six major sources for aromatics situated in the coastal area were employed for calculation (Figure 4-18). The distance-weighted emissions for these sources exceeded 1,000 kg km^{-1} at three sampling sites. Table 4-5 shows the distance between each sampling site and source and wind direction from each sampling site. If there are two sources in the same direction, OH radical loss rate affected by a source at the sampling site was calculated in dividing by the proportion of distance-weighted emissions for two sources. There was not data for US in S and SSW direction where sources (e) and (f) affect.

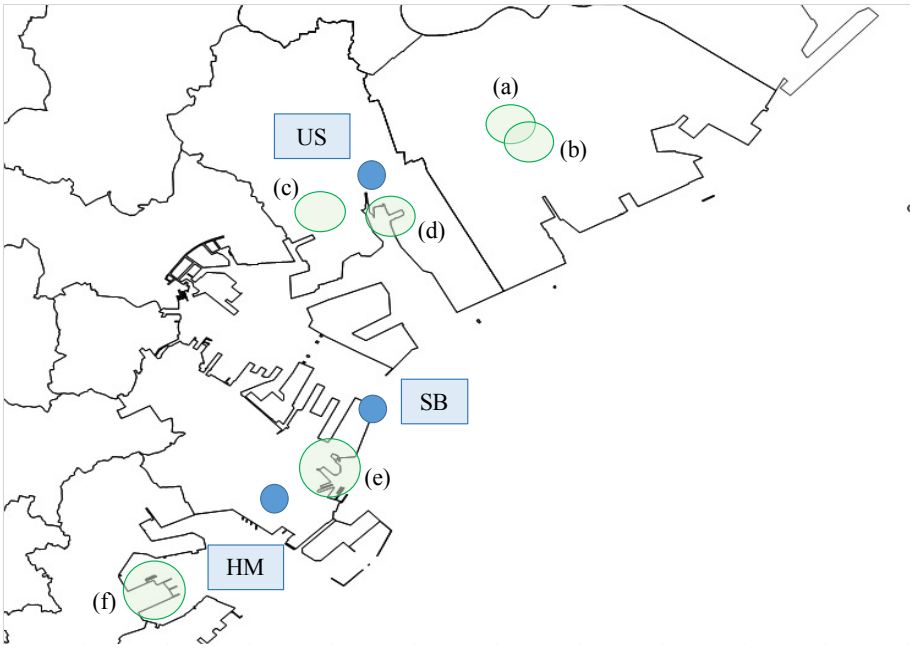

Figure 4-18. Locations of major six sources for aromatics.

Table 4-5. OH radical loss rate for the petrochemical complex and refinery for factor 3 and 4 (US: Ushioda, SB: Yokohama Port Symbol Tower, and HM: Honmoku).

	US		SB		HM	
	distance (km)	WD	distance (km)	WD	distance (km)	WD
a	5.98	ENE	11.1	NNE	14.6	NNE
b	9.22	ENE	12.7	NE	16.5	NE
c	1.75	SW	5.65	NNW	8.23	N
d	0.80	SSE	6.12	N	9.20	NNE
e	9.26	S	2.82	SSW	1.09	ENE
f	13.3	SSW	7.83	SW	4.12	SW

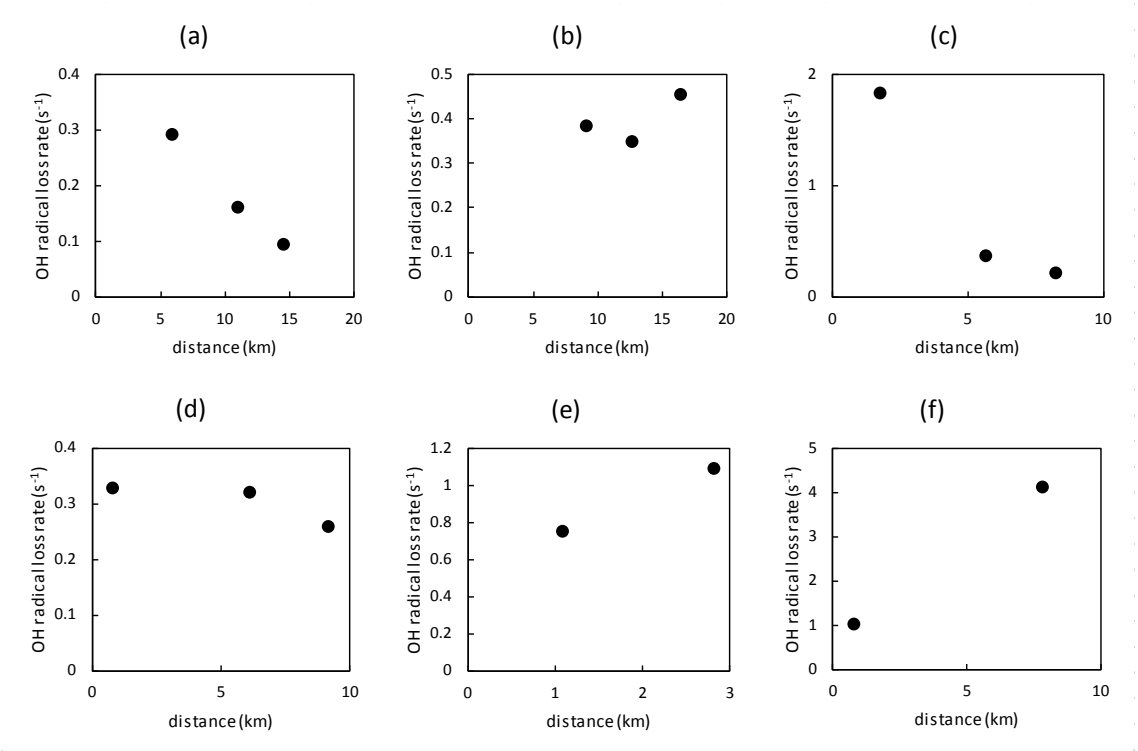

Figure 4-19. Correlation of OH radical loss rates for the sampling sites to distance from six sources for aromatics.

The impact of sources (b), (e), and (f) was not in inverse proportion to the distance (Figure 4-19). It is likely because these sources did not influence during the campaigns, or emission processes were different from other sources. Total OH radical loss rate of six major sources for aromatics was calculated as 10 s^{-1}.

From the above results, it was shown that the petrochemical complexes accounted for 67% of total OH radical loss rate for the main industrial VOC sources in the Yokohama and Kawasaki coastal areas. It was demonstrated that, in order to reduce the level of photochemical oxidants, it is crucial to control emissions from the petrochemical industry.

4.4 Conclusions

We estimated the source area and major sources of alkenes in the Tokyo Bay coastal area. The ratios of VOCs indicated that the ambient air in this area is strongly affected by the local fixed sources. The alkene concentration ratios according to the 16 wind directions revealed that major alkene sources exist in the Kawasaki coastal area. A PMF analysis resolved six factors which were identified as LPG + industry, aged air masses, fuel evaporation, the petrochemical industry, aromatics, and solvent usage. The contribution ratios for the petrochemical industry according to the 16 wind directions were most consistent with the alkene concentration ratios according to the 16 wind directions. This corresponded to the location of the petrochemical industrial complexes in the Kawasaki coastal area and indicated that the petrochemical industry was the main alkene source in this area.

The source contributions showed significant spatial variations across the sampling sites. The contribution ratio for the petrochemical industry at each sampling site tended to gradually decrease with increasing distance from the Kawasaki coastal area to the Ushioda (18.9%), Yokohama Port Symbol Tower (16.3%), and Honmoku (16.2%) sites. At the Honmoku site, which is adjacent to petroleum refineries, fuel evaporation was the major source of VOCs. The local LPG + industry effect was overwhelmingly dominant at the Higashikoujiya site.

The petrochemical industry was the most significant contributor to ozone production according to a comparison of the L^{OH} values of the sources. It was estimated that Ox concentration could be reduced by up to about 30% by controlling emissions from the petrochemical industry.

The L^{OH} values for the petrochemical complexes in the Kawasaki coastal area and refineries around the Honmoku site were 45 and 3.5, respectively. This suggests that the photochemical reactivity for petrochemical complex was more than 10 times higher than for the refinery. Further considering the major aromatic sources, it was shown that the petrochemical complexes accounted for 67% of total L^{OH} for the main industrial VOC sources in the Yokohama and Kawasaki coastal areas.

The above results indicate that, in order to effectively reduce levels of photochemical oxidants, it is crucial to control the level of alkenes emitted by the petrochemical industry.

References

Andreae, M. O., Merlet, P., 2001. Emissions of trace gases and aerosols from biomass burning. Glob. Biogeochem. Cycles 15, 955-966. https://doi.org/10.1029/2000GB001382.

Atkinson, R., Arey, J., 2003. Atmospheric Degradation of volatile organic compounds. Chem. Rev. 103, 4605-4638. https://doi.org/10.1021/cr0206420.

ATSDR (Agency for Toxic Substances and Disease Registry), 2007. Toxicological Profile for Benzene. U.S. Department of Health and Human Services, Public Health Service, Atlanta, GA.

Barletta, B., Meinardi, S., Rowland, F. S., Chan, C. Y., Wang, X., Zou, S., et al., 2005. Volatile organic compounds in 43 Chinese cities. Atmos. Environ. 39, 5979-5990. https://doi.org/10.1016/j.atmosenv.2005.06.029.

Barletta, B., Meinardi, S., Simpson, I. J., Zou, S., Sherwood Rowland, F., Blake, D. R., 2008. Ambient mixing ratios of nonmethane hydrocarbons (NMHCs) in two major urban centers of the Pearl River Delta (PRD) region: Guangzhou and Dongguan. Atmos. Environ. 42, 4393-4408. https://doi.org/10.1016/j.atmosenv.2008.01.028.

Buzcu, B., Fraser, M. P., 2006. Source identification and apportionment of volatile organic compounds in Houston, TX. Atmos. Environ. 40, 2385-2400. https://doi.org/10.1016/j.atmosenv.2005.12.020.

Buzcu-Guven, B., Fraser, M. P., 2008. Comparison of VOC emissions inventory data with source apportionment results for Houston, TX. Atmos. Environ. 42, 5032-5043. https://doi.org/10.1016/j.atmosenv.2008.02.025.

Chen, C.-H., Chuang, Y.-C., Hsieh, C.-C., Lee, C.-S., 2019. VOC characteristics and

source apportionment at a PAMS site near an industrial complex in central Taiwan. Atmos. Pol. Res. 10, 1060-1074. https://doi.org/10.1016/j.apr.2019.01.014.

Dumanoglu, Y., Kara, M., Altiok, H., Odabasi, M., Elbir, T., Bayram, A., 2014. Spatial and seasonal variation and source apportionment of volatile organic compounds (VOCs) in a heavily industrialized region. Atmos. Environ. 98, 168-178. https://doi.org/10.1016/j.atmosenv.2014.08.048.

Fukusaki, Y., Kousa, Y., Asaki, M., Kobayashi, Y., Takahashi, K., Kokubu, Y., Hoshi, J., Sakamoto, H., Goto, Y., Shima, M., Nakai, S., 2020. Estimation of Anthropogenic VOC source area around Tokyo Bay: Results from the VOC Concentration Changes in Relation to Wind Direction, J. Jpn. Soc. Atmos. Environ. 55, 92-99.

Guo, H., So, K. L., Simpson, I. J., Barletta, B., Meinardi, S., Blake D. R., 2007. C_1-C_8 volatile organic compounds in the atmosphere of Hong Kong: Overview of atmospheric processing and source apportionment, Atmos. Environ. 41, 1456-1472. https://doi.org/10.1016/j.atmosenv.2006.10.011.

Guo, H., Cheng, H. R., Ling, Z. H., Louie, P. K. K., Ayoko, G. A., 2011. Which emission sources are responsible for the volatile organic compounds in the atmosphere of Pearl River Delta? J. Hazard. Mater. 188, 116-124. https://doi.org/10.1016/j.jhazmat.2011.01.081.

Hsu, C.-Y., Chiang, H.-C., Shie, R.-H., Ku, C.-H., Lin, T.-Y., Chen, M.-J., Chen, N.-T., Chen, Y.-C., 2018. Ambient VOCs in residential areas near a large-scale petrochemical complex: Spatiotemporal variation, source apportionment and health risk. Environ. Pol. 240, 95-104. https://doi.org/10.1016/j.envpol.2018.04.076.

Hui, L., Liu, X., Tan, Q., Feng, M., An, J., Qu, Y., Zhang, Y., Jiang, M., 2018. Characteristics, source apportionment and contribution of VOCs to ozone formation in Wuhan, Central China. Atmos. Environ. 192, 55-71. https://doi.org/10.1016/j.atmosenv.2018.08.042.

Lau, A. K. H., Yuan, Z., Yu, J. Z., Louie, P. K. K., 2010. Source apportionment of ambient volatile organic compounds in Hong Kong. Sci. Total Environ. 408, 4138-4149. https://doi.org/10.1016/j.scitotenv.2010.05.025.

Leuchner M., Rappengluck, B., 2010. VOC source-receptor relationships in Houston during TexAQS- Ⅱ. Atmos. Environ. 44, 4056-4067. https://doi.org/10.1016/j.atmosenv.2009.02.029.

Li, G. H., Wei, W., Shao, X., Nie, L., Wang, H. L., Yan, X., Zhang, R., 2018. A comprehensive classification method for VOC emission sources to tackle air pollution based on VOC species reactivity and emission amounts. J. Environ. Sci. 67, 78-88. https://doi.org/10.1016/j.jes.2017.08.003.

Ling, Z. H., Guo, H., Cheng, H. R., Yu, Y. F., 2011. Sources of ambient volatile organic compounds and their contributions to photochemical ozone formation at a site in the Pearl River Delta, southern China. Environ. Pol. 159, 2310-2319. https://doi.org/10.1016/j.envpol.2011.05.001.

Liu, Y., Shao, M., Fu, L., Lu, S., Zeng, L., Tang, D., 2008. Source profiles of volatile organic compounds (VOCs) measured in China: Part Ⅰ. Atmos. Environ. 42, 6247-6260. https://doi.org/10.1016/j.atmosenv.2008.01.070.

Lyu, X. P., Chen, N., Guo, H., Zhang, W. H., Wang, N., Wang, Y., Liu, M., 2016. Ambient

volatile organic compounds their effect on ozone production in Wuhan, central China. Sci. Total. Environ. 541, 200-209. https://doi.org/10.1016/j.scitotenv.2015.09.093.

Ma, Z., Liu, C., Zhang, C., Liu, P., Ye, C., Xue, C., Zhao, D., Sun, J., Du, Y., Chai, F., Mu, Y., 2019. The levels, sources and reactivity of volatile organic compounds in a typical urban area of Northeast China. J. Environ. Sci. 79, 121-134. https://doi.org/10.1016/j.jes.2018.11.015.

McCarthy, M. C., Aklilu, Y.-A., Brown, S. G., Lyder, D. A., 2013. Source apportionment of volatile organic compounds measured in Edmonton, Alberta. Atmos. Environ. 81, 504-516. https://doi.org/10.1016/j.atmosenv.2013.09.016.

Mo, Z., Shao, M., Lu, S., Niu, H, Zhou, M., Sun, J., 2017. Characterization of non-methane hydrocarbons and their sources in an industrialized coastal city, Yangtze River Delta, China. Sci. Total. Environ. 593-594, 641-653. https://doi.org/10.1016/j.scitotenv.2017.03.123.

Moreira Dos Santos, C. Y., Azevedo, D. A., Aquino Neto, F. R., 2004. Atmospheric distribution of organic compounds from urban areas near a coal-fired power station. Atmos. Environ. 38, 1247-1257. https://doi.org/10.1016/j.atmosenv.2003.11.026.

Morino, Y., Ohara, T., Yokouchi, Y., Ooki, A., 2011. Comprehensive source apportionment of volatile organic compounds using observational data, two receptor models, and an emission inventory in Tokyo metropolitan area. J. Geophy. Res. 116, https://doi.org/10.1029/2010JD014762.

Morrow, N. L., 1990. The industrial production and use of 1,3-butadiene. Environ. Health Perspect. 86, 7-8. https://doi.org/10.1289/ehp.90867.

Na, K., Kim, Y. P., Moon, K. C., Moon, I., Fung, K., 2001. Concentrations of volatile organic compounds in an industrial area of Korea. Atmos. Environ. 35, 2747-2756. https://doi.org/10.1016/S1352-2310(00)00313-7.

Paatero, P., Tapper, U., 1994. Positive matrix factorization: a non-negative factor model with optimal utilization of error estimates of data values. Environmetrics 5, 111-126. https://doi.org/10.1002/env.3170050203.

Paatero, P., 1997. Least squares formulation of robust nonnegative factor analysis. Chemom. Intell. Lab. Syst. 37, 23-35. https://doi.org/10.1016/S0169-7439(96)00044-5.

Perry, R., Gee, I. L., 1995. Vehicle emissions in relation to fuel composition. Transp. Air Pollut. 169, 149-156. https://doi.org/10.1016/0048-9697(95)04643-F.

Roberts, P. T., Brown, S. G., Reid, S. B., Buhr, M. P., Funk, T. H., Stiefer, P. S., 2004. Emission Inventory Evaluation and Reconciliation in the Houston-Galveston Area. STI-903640-2490-FR.

Ryerson, T. B., Trainer, M., Angevine, W. M., Brock, C. A., Dissly, R. W., Fehsenfeld, F. C., Frost, G. J., Goldan, P. D., Holloway, J. S., Hubler, G., Jakoubek, R. O., Kuster, W. C., Neuman, J. A., Nicks Jr., D. K., Parrish, D. D., Roberts, J. M., Sueper, D. T., 2003. Effect of petrochemical industrial emissions of reactive alkenes and NOx on tropospheric ozone formation in Houston, Texas. J. Geophy. Res. 108, NO.D8, 4249, doi:10.1029/2002JD003070.

Selia, R. L., Main, H. H., Arriaga, J. L., Martinez, G. V., Ramadan, A. B., 2001. Atmospheric volatile organic compounds measurements during the 1996 Paso del Norte ozone study. Science of the Total Environment 276, 153-169.

https://doi.org/10.1016/S0048-9697(01)00777-X.

Shao, P., An, J., Xin, J., Wu, F., Wang, J., Ji, D., Wang, Y., 2016. Source apportionment of VOCs and the contribution to photochemical ozone formation during summer in the typical industrial area in the Yangtze River Delta, China. Atmos. Res. 176-177, 64-74. https://doi.org/10.1016/j.atmosres.2016.02.015.

Song, Y., Dai, W., Shao, M., Liu, Y., Lu, S., Kuster, W., Goldan, P., 2008. Comparison of receptor models for source apportionment of volatile organic compounds in Beijing, China. Environ. Pollut. 156, 174-183. https://doi.org/10.1016/j.envpol.2007.12.014.

Su, Y,-C., Chen, S.-P., Tong, Y.-H., Fan, C.-L., Chen, W.-H., Wang, J.-L., Chang, J. S., 2016. Assessment of regional influence from a petrochemical complex by modeling and fingerprint analysis of volatile organic compounds (VOCs). Atmos. Environ. 141, 394-407. https://doi.org/10.1016/j.atmosenv.2016.07.006.

Ueno, H., Uchida, Y., Ishii, K., Saito, S., Akiyama, K., Yokota, H., 2015. Composition of VOCs and Source Apportionment by CMB Considering Photochemical Reaction Losses with OH Radical in Tokyo. J. Jpn. Soc. Atmos. Environ. 50, 207-225 [in Japanese].

Wang, Q., Chen, C. H., Wang, H. L., Zhou, M., Lou, S. R., Qiao, L. P., Huang, C., Li, L., Su, L. Y., Mu, Y. Y., Chen, Y. R., Chen, M. H., 2013. Forming potential of secondary organic aerosols and sources apportionment of VOCs in autumn of Shanghai, China. Environ. Sci. 34, 424-433.

Whiteley, K. S., Heggs, T. G., Koch, H., Mawer, R. L., Immel, W., 2000. Polyolefins. Ullmanns Encycl. Ind. Chem. Wiley-VCH Verlag GmbH & Co. KGaA A21, 487-578. https://doi.org/10.1002/14356007.a21_487.

Wu, F., Yu, Y., Sun, J., Zhang, J., Wang, J, Tang, G., Wang, Y., 2016. Characteristics, source apportionment and reactivity of ambient volatile organic compounds at Dinghu Mountain in Guangdong Province China. Sci. Total Environ. 548-549, 347-359. https://doi.org/10.1016/j.scitotenv.2015.11.069.

Xue, Y., Ho, S. S. H., Huang, Y., Li, B., Wang, L., Dai, W., Cao, J., Lee, S., 2017. Source apportionment of VOCs and their impacts on surface ozone in an industry city of Baoji, Northwestern China, Sci. Rep. https://doi.org/10.1038/s41598-017-10631-4.

Yang, H., Zhu, B., Gao, J., Li, Y., Xia, L., 2013. Source apportionment of VOCs in the northern suburb of Nanjing in summer. Environ. Sci. 34, 4519-4528.

Zhang, Y., Li, R., Fu, H., Zhou, D., Chen, J., 2018. Observation and analysis of atmospheric volatile organic compounds in a typical petrochemical area in Yangtze River Delta, China. J. Environ. Sci. 71, 233-248. https://doi.org/10.1016/j.jes.2018.05.027.

Zheng, H., Kong, S., Yan, Y., Chen, N., Yao, L., Liu, X., Wu, F., Cheng, Y., Niu, Z., Zheng, S., Zeng, X., Yan, Q., Wu, J., Zheng, M., Liu, D., Zhao, D., Qi, S., 2020. Compositions, sources and health risks of ambient volatile organic compounds (VOCs) at a petrochemical industrial park along the Yangtze River. Sci. Total. Environ. 703, 135505. https://doi.org/10.1016/j.scitotenv.2019.135505.

Zhou, Y., Hao, Z., Wang, H., 2011. Pollution and source of atmospheric volatile organic compounds in urban-rural juncture belt area in Beijing. Environ. Sci. 32, 3560-3565.

Chapter 5

Conclusions

Conclusions

This study demonstrated that the petrochemical industry is a major alkene emission source in the Tokyo Bay coastal area and most significantly contributes to Ox production. The development of the land-sea breeze causes photochemical smog. For the purpose of this investigation, fifty-four days were investigated on which photochemical smog warnings were issued in Tokyo, Chiba, Kawasaki, and/or Yokohama during July and August (between 2012 and 2015), and each day was categorized according to the sea-breeze patterns. VOC-sensitivity in the South Kanto region was validated through a comparison of the number of hours on which Ox, NMHC, and NOx concentration exceeded the criteria. Finally, the locations of major NMHC sources were estimated by Conditional Probability Function (CPF) analysis for NMHC concentrations at the four monitoring stations where NMHC concentration exceeded 0.40 ppm C most frequently. The Ox and NMHC levels most frequently exceeded the criteria at the Kawasaki inland and coastal areas on LSW days, respectively, whereas the NOx levels most frequently exceeded 60 ppb at the Tokyo coastal area on SS days. In comparing SS days at all areas excluding the Tokyo area, the number of hours for Ox and NMHC on LSW days was greater than on SS days, although NOx on LSW days was nearly equal to that on SS days. This suggests the possibility that the increase in Ox comes from an increase in NMHC, namely the VOC-sensitive process. The reason for the lack of difference between LSW and SS days in the Tokyo area is likely that there are no major NMHC sources in this region. The top four atmospheric environmental monitoring stations where NMHC concentration exceeded 0.40 ppm C during the targeted fifty-four days were the Honmoku, Daishi,

Higashikoujiya, and Ichihara stations. The locations of these monitoring stations accorded quite well with the locations of petrochemical industrial facilities. The CPF analysis indicated that major source regions of VOCs exist in the W, ESE, SE, and WSW directions of Honmoku, Daishi, Higashikoujiya, and Ichihara, respectively.

To test the validity of the method combining VOC concentration ratios to total VOC concentration according to the 16 wind directions with the prevailing wind direction as a means of identifying the source area, VOC concentration ratios according to the 16 wind directions were compared with the distance-weighted emissions based on PRTR data. The tendency of both results was roughly the same for all four species within an error of $\pm 22.5^{\circ}$ in the wind direction. This suggests that VOC concentrations depend greatly upon wind direction and were significantly affected by the industrial VOC sources. From this result, it was demonstrated that this method was useful for source area identification of VOCs. The wind direction with highest alkene concentration ratios agreed with the wind direction of the area with the facilities treating 1,3-butadiene at all sampling sites. The major alkene source is likely to be located in the same area as the facilities treating 1,3-butadiene.

In order to identify the major alkene sources, PMF analysis was run to apportion VOC sources. PMF analysis resolved six factors, which are identified as LPG + industry, aged air masses, fuel evaporation, the petrochemical industry, aromatics, and solvent usage. The percentage of alkenes was overwhelmingly highest in the petrochemical industry. Furthermore, the petrochemical industry contribution ratios were most consistent with the alkene concentration ratios according to the 16 wind directions. The above result implies that the major alkene source is the petrochemical complex. Comparing OH radical loss

rates, the petrochemical industry most significantly contributed to OH radical loss rate. In addition, it was estimated that Ox concentrations could be reduced by up to about 30% by controlling emissions from the petrochemical industry. The L^{OH} values for the petrochemical complex in the Kawasaki coastal area and refinery around the Honmoku site were 45 and 3.5, respectively, suggesting that the photochemical reactivity for petrochemical complex was more than 10 times higher than for the refinery. Further considering the main aromatic sources, it was shown that the petrochemical complex accounted for 67% of total L^{OH} for the main industrial VOC sources in the Yokohama and Kawasaki coastal areas. It was concluded that controlling the level of alkenes emitted by the petrochemical complex was the most effective means to mitigate Ox levels. This results are useful for the strategy for controlling Ox levels in the future. Furthermore, this results demonstrated that even small dataset enable to estimate the major source in area like the Tokyo Bay coastal area which is strongly affected by local industrial VOC sources, although large volume of VOC data was used in the previous studies. This opened up the possibility of identifying more simply and economically major sources of air pollutants.

Bibliography

Peer-Reviewed Journal Papers

1. **Yukiko Fukusaki**, Yuka Kousa, Maiko Asaki, Yoshihisa Kobayashi, Yutaka Kokubu, Junya Hoshi, Hironari Sakamoto, Arisa Goto, Mirin Shima, Satoshi Nakai, 2020. Estimation of Anthropogenic VOC source Area around Tokyo Bay: Results from the VOC Concentration Changes in Relation to Wind Direction. J. Jpn. Atmos. Environ. 55, 92-99.

2. **Yukiko Fukusaki**, Yuka Kousa, Masataka Umehara, Maiko Ishida, Reiko Sato, Kouji Otagiri, Junya Hoshi, Chieko Nudejima, Kazukiyo Takahashi, Satoshi Nakai, 2021. Source region identification and source apportionment of volatile organic compounds in the Tokyo Bay coastal area, Japan. Atmos. Environ.: X. 9, 100103, 1-13.

Acknowledgments

I sincerely thank everyone at the Yokohama Environmental Science Research Institute, the Tokyo Metropolitan Research Institute for Environmental Protection, the Chiba City Institute of Health and Environment Research, and Nakai Labortory, Graduate School of Environment and Information Sciences, Yokohama National University.

I would like to acknowledge Professor Akihiro Iijima from Takasaki City University of Economics with advice about PMF analysis and Professor Hideo Takahashi from Tokyo Metropolitan University for offering data on wind direction and wind speed.

I would like to thank Enago (www.enago.jp) for the English language review.

I appreciate the valuable comments on my doctoral thesis from Professor Takashi Amemiya, Professor Hiroki Hondo, Professor Takashi Kameya, and Professor Takeshi Kobayashi.

Finally, I would like to thank my supervisor, Professor Satoshi Nakai, for accepting me as a doctoral student and giving me valuable advice to complete my doctoral thesis.